

Sheffield Hallam University

Heat transfer during the transformation of steels.

VASQUEZ CEDENO, Jose Luis.

Available from the Sheffield Hallam University Research Archive (SHURA) at:

<http://shura.shu.ac.uk/20474/>

A Sheffield Hallam University thesis

This thesis is protected by copyright which belongs to the author.

The content must not be changed in any way or sold commercially in any format or medium without the formal permission of the author.

When referring to this work, full bibliographic details including the author, title, awarding institution and date of the thesis must be given.

Please visit <http://shura.shu.ac.uk/20474/> and <http://shura.shu.ac.uk/information.html> for further details about copyright and re-use permissions.

Sheffield City Polytechnic Library

REFERENCE ONLY

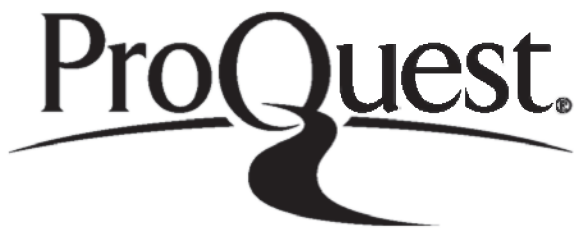
ProQuest Number: 10701121

All rights reserved

INFORMATION TO ALL USERS

The quality of this reproduction is dependent upon the quality of the copy submitted.

In the unlikely event that the author did not send a complete manuscript and there are missing pages, these will be noted. Also, if material had to be removed, a note will indicate the deletion.



ProQuest 10701121

Published by ProQuest LLC (2017). Copyright of the Dissertation is held by the Author.

All rights reserved.

This work is protected against unauthorized copying under Title 17, United States Code
Microform Edition © ProQuest LLC.

ProQuest LLC.
789 East Eisenhower Parkway
P.O. Box 1346
Ann Arbor, MI 48106 – 1346

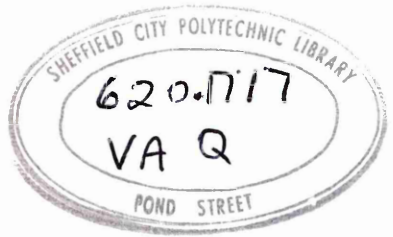


HEAT TRANSFER DURING THE
TRANSFORMATION OF STEELS

Jose Luis Vasquez Cedeno

This thesis is submitted
in part fulfilment of the requirements
for the degree of Doctor of Philosophy
of the
Council for National Academic Awards.
The work was carried out at
Sheffield City Polytechnic
Department of Metals and Materials Engineering.
Collaborating Establishment:- British Steel Corporation.

APRIL 1986



heat transfer during one dimensional transformation

ABSTRACT

by

Jose Luis Vasquez Cedeno

The extent to which heat conduction within large steel samples (billets) influences and is influenced by solid state transformation reactions has been studied under conditions of one dimensional heat flow with heat removed by convection with a constant heat transfer coefficient. Values of the heat transfer coefficient in the range $130-220$ ($\text{W}/\text{m}^{20}\text{C}$) has been used. These values were independently measured using steady state heat transfer and mass transfer analogy techniques which gave results in fair agreement. The progress of transformation front was followed using thermal analysis technique.

The effects of different values of the heat transfer coefficient during transformation were investigated. The principal purpose of this investigation was to try to discover whether the assumptions made in establishing the theoretical method provided a basis for predicting the rates at which steel transformation reactions took place. The theoretical method assumed that the rate of the transformation was controlled by the rate of cooling and hence by the rates at which heat was transferred from the cooling steel component. The rate of transformation could thus be predicted by solving the heat transfer equation. The theory developed ignored any interaction between the kinetics of the transformation and the heat transfer process. The reaction was assumed to take place over so narrow a range of temperature that the latent heat of the reaction could be assumed to be liberated at a single unique temperature. The method used to solve the heat transfer equation, and hence to predict the transformation rates was the integral profile method. This is an approximate method that uses assumed quadratic temperature profiles within the transformed and untransformed steel in order to obtain average solutions to the heat transfer equation in the two regions.

The experimental results obtained are relevant to cooling rates significantly lower than those involved in most previous investigations and extend our current knowledge concerning heat transfer during transformation in large steel components.

PREFACE

This thesis is submitted in part fulfilment of the requirements for the Degree of Doctor of Philosophy of the Council for National Academic Awards. The research described was carried out during the period from October 1981 to February 1986 in the Department of Metals and Materials Engineering (formerly Department of Metallurgy) at the Sheffield City Polytechnic. No part of this dissertation has been submitted for a degree at any other University or College.

During the period of this work the author attended the following lectures which constituted part of the MSc in Metallurgical Process Management at the Sheffield City Polytechnic.

Module I: Process Metallurgy.

Advanced Thermodynamics.

Module II: Computational Methods and Numerical Analysis.

Module III: Heat treatment and Transformations.

Secondary Steelmaking.

Metals and Competitive Materials.

Arc Furnace Steelmaking.

Continuous Casting.

Corrosion Resistant and High Temperature

Metals and Alloys.

Stainless Steels.

ACKNOWLEDGEMENTS

Sincere appreciation is extented to Dr. A.W.D. Hills for supervision and assistance given during the course of this work.

Special thanks to Dr. G. Briggs, Dr. A. J. Fletcher, Dr. R. Acheson, Mr. D. Latimer, Mr. R. Day, Mr. J. Bradshaw, Mr. B. Dodds, Mr. R. Grant, Mr. G. Gregory, Mr. R. Dimberline, Mr. P. Slingsby, Mr. B. Palmer, Mr. B. Taylor, Mr. J. Evans for their help and friendship. The assistance of Dr. E. Wilson, Dr. B. Lewis and Dr. J. Cawley is also gratefully acknowledged.

I would like to acknowledge my sister Gladys and my sons for their moral support during the course of this work, and my fellow students Mr. A. Basilius, Mr. J. Duncombe, Mr. J. Soady, Mr. M. Simon for their encouragement and friendship.

I would also like to acknowledge Mrs. R. Barker for her help in typing this work.

The author is indebted to the Polytechnic de Guayana for its support and The Fundacion Gran Mariscal de Ayacucho for the financial assistance given in support of this work.

ABSTRACT

by

Jose Luis Vasquez Cedeno

The extent to which heat conduction within large steel samples (billets) influences and is influenced by solid state transformation reactions has been studied under conditions of one dimensional heat flow with heat removed by convection with a constant heat transfer coefficient. Values of the heat transfer coefficient in the range 130-220 ($\text{W}/\text{m}^{20}\text{C}$) has been used. These values were independently measured using steady state heat transfer and mass transfer analogy techniques which gave results in fair agreement. The progress of transformation front was followed using thermal analysis technique.

The effects of different values of the heat transfer coefficient during transformation were investigated. The principal purpose of this investigation was to try to discover whether the assumptions made in establishing the theoretical method provided a basis for predicting the rates at which steel transformation reactions took place. The theoretical method assumed that the rate of the transformation was controlled by the rate of cooling and hence by the rates at which heat was transferred from the cooling steel component. The rate of transformation could thus be predicted by solving the heat transfer equation. The theory developed ignored any interaction between the kinetics of the transformation and the heat transfer process. The reaction was assumed to take place over so narrow a range of temperature that the latent heat of the reaction could be assumed to be liberated at a single unique temperature. The method used to solve the heat transfer equation, and hence to predict the transformation rates was the integral profile method. This is an approximate method that uses assumed quadratic temperature profiles within the transformed and untransformed steel in order to obtain average solutions to the heat transfer equation in the two regions.

The experimental results obtained are relevant to cooling rates significantly lower than those involved in most previous investigations and extend our current knowledge concerning heat transfer during transformation in large steel components.

TABLE OF CONTENTS

	<u>PAGE NUMBER</u>
Preface	i
Acknowledgements	ii
Abstract	iii
List of Symbols	iv
List of Figures	viii
List of Tables	xii
<u>CHAPTER 1</u>	
<u>Introduction</u>	1/1 to 1/2
<u>CHAPTER 2</u>	
<u>Literature Survey</u>	2/1 to 2/43
2.1 The integral profile method	2/1
2.2 The formation of pearlite	2/5
2.3 Effect of cooling rate on pearlite transition	2/14
2.4 The Interlamella spacing of pearlite	2/24
2.5 Effect of temperature variation and of heat transfer processes	2/33
<u>CHAPTER 3</u>	
<u>Theoretical Treatment</u>	3/1 to 3/44
3.1 Heat transfer during solid state transformation	3/1
3.2 Equation for the transformed layer	3/7
3.3 The equation for the cooled layer	3/15
3.4 The semi-infinite cooling mode	3/21
3.5 Finite cooling mode	3/25

/Continued.....

<u>CHAPTER 3</u> (continued)	<u>PAGE NUMBER</u>
3.6 Transformation delay	3/27
3.7 Semi-infinite transformation mode	3/28
3.8 The finite transformation mode	3/29
3.9 Computer programme	3/30

CHAPTER 4

<u>Experimental Treatment</u>	<u>PAGE NUMBER</u>
4.1 Design of the apparatus	4/1
4.2 Cooling system	4/3
4.3 Measurement of the heat transfer coefficient by a mass transfer analogy	4/10
4.4 Measurement of the heat transfer coefficient by steady state heat transfer	4/15
4.5 Profile of temperature in the sample of steel at 500°C, 600°C, 700°C and 800°C without air cooling	4/16
4.6 Profile of temperature in the sample of steel at 850°C with air cooling	4/18
4.7 Chemical composition of the steel used	4/19

CHAPTER 5

<u>Results</u>	<u>PAGE NUMBER</u>
5.1 Heat transfer coefficient measured by the mass transfer analogy	5/1
5.2 Heat transfer coefficient measured by steady state heat transfer	5/13

/Continued.....

CHAPTER 5 (continued)PAGE NUMBER

5.3 Profile of temperature in the sample of steel at 500°C, 600°C, 700°C and 800°C without air cooling	5/17
5.4 Profile of temperature in the sample of steel at 850°C with air cooling	5/22
5.5 Temperature of transformation	5/41
5.6 Progress of transformation front	5/43
5.7 Heat balance on the billet in the absence of transformation	5/52
5.8 Interlamella spacing of pearlite	5/57
5.9 Computer results	5/62

CHAPTER 6

<u>Discussion</u>	6/1 to 6/43
6.1 Heat transfer measurements	6/1
6.2 Performance of the transformation apparatus	6/8
6.3 Transformation experiments	6/17
6.4 Comparison between theoretical and experimental results	6/26
6.5 Comparisons with other workers	6/40

CHAPTER 7

<u>Conclusions and Further Work</u>	7/1 to 7/3
7.1 Conclusions	7/1
7.2 Further work	7/2

REFERENCES

R/1 to R/6

APPENDICES

1. <u>Property Values used in this work</u>	A1/ to A1/3
---	-------------

/Continued.....

Table A1: Densities, conductivities and thermal capacities		A1/1
2.	<u>Basic Computer Programmes used in Heat Balance Calculations</u>	A2/1 to A2/4
A2.1	Overall heat balance in the absence of transformation	A2/1
A2.2	Dynamic heat balance during transformation	A2/2

LIST OF SYMBOLS

Roman Symbols

- a Amperage.
- a_0, a_1, a_2 } Coefficients in polynomial series used to describe temperature profile in transformed metal layer.
- A Cross sectional area over which heat transfer is occurring.
- A_f Ratio of the total area of the nozzle holes to the area of the heat transfer surface, as a percentage.
- A_0 Cross sectional area of the orifice plate.
- B Characteristic length.
- b Constant in experimental heat flux correlation.
- C Specific heat.
- D_N Diffusivity.
- D Diameter of multiple nozzle holes.
- g Acceleration due to gravity.
- H Latent heat of transformation.
- H_0 Manometric height.
- h Overall heat transfer coefficient from surface of steel billet to cooling air.
- h_c Convective heat transfer coefficient.
- $[h_M]_N$ Mass transfer coefficient.
- K Thermal conductivity.
- K_f The flow coefficient.
- L Thickness of the billet.
- m Constant used in the dimensionless relationship used to describe forced convection heat and mass transfer.

n	Constant used in the dimensionless relationship used to describe forced convection heat and mass transfer.
N	Spacing between nozzle and heat transfer surface.
\dot{n}''	Number of moles of naphthalene lost in unit time from unit area of the sublimating surface.
$[P_{eq}]_N$	Equilibrium evaporation pressure of naphthalene.
\dot{q}	Heat conducted through the copper disc.
\dot{q}''_o	Surface heat flux from transformed layer.
\dot{q}''_t	Heat received at the transformation front from the cooled layer of steel.
R	Gas content.
t	Thickness of transformed layer.
t_c	Thickness of the cooled layer.
u	Velocity.
V	Voltage.
\bar{V}_o	Flow velocity at the orifice plate.
∇	Volumetric flow rate.
X	Distance coordinate.
Y	Spacing between nozzle holes.

Greek Symbols

α	Constant used in dimensionless relationships used to describe forced convection heat and mass transfer.
θ	Temperature.
θ_a	Temperature of the cooling air.

θ_I	Temperature of the insulated surface.
θ_o	Temperature of the cooled surface.
θ_s	Average temperature of the copper disc
θ_t	Temperature at the boundaries of the cooled layer.
θ_T	Transformation temperature.
θ_1	Initial temperature of the uncooled billet.
ϵ	Emissivity.
ρ	Density.
σ	Stefan's Boltzman Constant.
μ	Viscosity.
t	Time.
Ω	Coefficient function.
Γ	Coefficient function.
Δ	Coefficient function.

Dimensionless Groups

H^*	Dimensionless latent heat of transformation = $H/(C\theta_T)$.
L^*	Dimensionless thickness of the billet (56).
q^*	Dimensionless heat flow from cooled metal = $q \cdot \frac{t}{\tau} / (-h\theta_T)$.
q_t^*	Dimensionless heat received at the transformation front from the cooled steel layer (44).
t^*	Dimensionless thickness = $h\tau/K$.
t_c^*	Dimensionless thickness of the cooled layer (42).
θ^*	Dimensionless temperature of cooled surface = θ_o/θ_T .

θ^*_1	Dimensionless initial temperature of the uncooled billet (45).
θ^*_I	Dimensionless temperature of the insulate surface (58).
θ^*_t	Dimensionless temperature at the boundaries of the cooled layer (42).
$\bar{\gamma}$	Dimensionless time = $h^2 \tau / (\rho CK)$.
$\bar{\gamma}_1$) Dimensionless duration of the semi-infinite
$\bar{\gamma}_2$) cooling mode (55,57).
$\bar{\gamma}_3$	Dimensionless duration of the finite cooling mode (65).
$\bar{\gamma}_{\text{Delay}}$	Dimensionless transformation delay (66,67).
Nu	Nusselt number = hB/K .
Pr	Prandtl number = uc/K .
Re	Reynolds number = $uB\rho/\mu$.
Sh	Sherwood number = $h_M B/D$.
Sc	Schmidt number = $u/\rho D$.

LIST OF FIGURES

<u>FIGURE NO.</u>	<u>TITLE</u>	<u>PAGE NO.</u>
1	Cooling modes in the transformation of a steel billet.	3/2
2	Cooling/transformation algorithm.	3/6
3	Generalised schematic diagram of the cooled layer.	3/19
4	Diagram of apparatus.	4/2
5	Multiple air jet nozzle.	4/7
6	Plate.	4/13
7	Perspex plate.	4/14
8	Thermocouple positions in the copper disc.	4/17
9	Thermocouple positions in the steel billet sample.	4/20
10	Mass transfer coefficients plotted against air flow rate (together with Moore's results).	5/12
11	Temperature distribution in the uncooled billet.	5/19
12	Temperature variation with radius at 2 and 8 cm from the base.	5/21A
13	Temperature changes with time during air cooling at 37.4 litres/s (incomplete insulation during preheat).	5/24
14	Temperature changes with time during air cooling at 32.3 litres/s (incomplete insulation during preheat).	5/26

<u>FIGURE NO.</u>	<u>TITLE</u>	<u>PAGE NO.</u>
15	Temperature changes with time during air cooling at 26.4 litres/s (incomplete insulation during preheat).	5/28
16	Temperature changes with time during air cooling at 18.7 litres/s (incomplete insulation during preheat).	5/30
17	Temperature changes with time during air cooling at 37.4 litres/s (complete insulation during preheat).	5/32
18	Temperature changes with time during air cooling at 37.4 litres/s (complete insulation during preheat).	5/34
19	Temperature changes with time during air cooling at 37.4 litres/s (complete insulation during preheat).	5/36
20	Temperature changes with time during air cooling at 18.7 litres/s (complete insulation during preheat).	5/38
21	Temperature changes with time during air cooling at 13.2 litres/s (complete insulation during preheat).	5/40
22	Progress of the transition front with air cooling at 37.4 litres/s (incomplete insulation during preheat).	5/45
23	Progress of the transition front with air cooling at 32.3 litres/s (incomplete insulation during preheat).	5/46
24	Progress of the transition front with air cooling at 26.4 litres/s (incomplete insulation during preheat).	5/47
25	Progress of the transition front with air cooling at 18.7 litres/s (incomplete insulation during preheat).	5/48

<u>FIGURE NO.</u>	<u>TITLE</u>	<u>PAGE NO.</u>
26	Progress of the transition front with air cooling at 37.4 litres/s (incomplete insulation during preheat).	5/49
27.	Progress of the transition front with air cooling at 18.7 litres/s (incomplete insulation during preheat).	5/50
28	Progress of the transition front with air cooling at 13.2 litres/s (incomplete insulation during preheat).	5/51
29	Temperature distribution in the billet at the start and finish of the cooling experiment in the absence of transformation.	5/53
30	Micrograph of pearlite taken 12 cm from the cooled base.	5/59
31	Micrograph of pearlite taken 10 cm from the cooled base.	5/59
32	Micrograph of pearlite taken 8 cm from the cooled base.	5/60
33	Micrograph of pearlite taken 6 cm from the cooled base.	5/60
34	Micrograph of pearlite taken 4 cm from the cooled base.	5/61
35	Micrograph of pearlite taken 2 cm from the cooled base.	5/61
36	Heat transfer coefficients measured in the steady state heat flow experiments plotted against the radiation contribution.	6/3

<u>FIGURE NO.</u>	<u>TITLE</u>	<u>PAGE NO.</u>
37	Values of the convective heat transfer coefficient from the heat transfer and mass transfer experiments plotted against the air flow rate to the 0.8 power (also with results obtained by Moore).	6/6
38	Theoretical and experimental positions of the transformation front - cooling air flow = 37.4 litres/s.	6/28
39	Theoretical and experimental temperature distributions at different times - cooling air flow is 37.4 litres/s.	6/29
40	Theoretical and experimental positions of the transformation front - cooling air flow = 18.7 litres/s.	6/30
41	Theoretical and experimental temperature distributions at different times - cooling air flow is 18.7 litres/s.	6/31
42	Theoretical and experimental positions of the transformation front - cooling air flow - 13.2 litres/s.	6/32
43	Theoretical and experimental temperature distributions at different times - cooling air flow is 13.2 litres/s.	6/33
44	Isothermal transformation diagram taken from the work of Razik, Lorimer and Ridley.	6/43

LIST OF TABLES

<u>TABLE NO.</u>	<u>TITLE</u>	<u>PAGE NO.</u>
1	Calculated air flow rates against manometric height.	4/8
2	Measured manometric flow against orifice manometer reading.	4/9
3	Naphthalene removal at maximum air flow and 6 cm separation.	5/2
4	Naphthalene removal at '3/4' air flow and 6 cm separation.	5/3
5	Naphthalene removal at '1/2' air flow and 6 cm separation.	5/4
6	Naphthalene removal at '1/4' air flow and 6 cm separation.	5/5
7	Naphthalene removal at maximum air flow and 8.5 cm separation.	5/6
8	Naphthalene removal at maximum air flow and 9.6 cm separation.	5/7
9	Heat transfer coefficient values obtained from mass transfer experiments.	5/11
10	Voltages and amperages obtained during steady state heat transfer method.	5/14
11	Heat transfer coefficients obtained during the steady state heat transfer experiments.	5/15
12	Temperatures at different distances from the bottom of the sample.	5/18
13	Temperatures at different radii and 2 cm from the bottom.	5/20

<u>TABLE NO.</u>	<u>TITLE</u>	<u>PAGE NO.</u>
14	Temperatures at different radii and 8 cm from the bottom.	5/20
15	Temperatures of axial thermocouples at different times with air cooling at 37.4 litres/s (incomplete insulation during preheat).	5/23
16	Temperatures of axial thermocouples at different times with air cooling at 32.3 litres/s (incomplete insulation during preheat).	5/25
17	Temperatures of axial thermocouples at different times with air cooling at 26.4 litres/s (incomplete insulation during preheat).	5/27
18	Temperatures of axial thermocouples at different times with air cooling at 18.7 litres/s (incomplete insulation during preheat).	5/29
19	Temperatures of axial thermocouples at different times with air cooling at 37.4 litres/s (complete insulation during preheat).	5/31
20	Temperatures of axial thermocouples at different times with air cooling at 37.4 litres/s (complete insulation during preheat).	5/33
21	Temperatures of axial thermocouples at different times with air cooling at 37.4 litres/s (complete insulation during preheat).	5/35
22	Temperatures of axial thermocouples at different times with air cooling at 18.7 litres/s (complete insulation during preheat).	5/37
23	Temperatures of axial thermocouples at different times with air cooling at 13.2 litres/s (complete insulation during preheat).	5/39

<u>TABLE NO.</u>	<u>TITLE</u>	<u>PAGE NO.</u>
24	Temperature of transformation at different air cooling rates.	5/41
25	Transformation times at different thermocouple positions.	5/44
26	Temperatures within the sample billet at the start of the cooling experiment in the absence of transformation.	5/54
27	Temperatures within the sample billet at the finish of the cooling experiment in the absence of transformation.	5/54
28	Surface temperatures and heat removal rates from the billet base during the cooling experiment in the absence of transformation.	5/56
29	Interlamella spacing of pearlite as a function of distance from the cooled base.	5/58
30	Theoretical computer results for conditions specified as run 53 - predicted thicknesses.	5/64
31	Theoretical computer results for conditions specified as run 53 - predicted temperatures.	5/65
32	Theoretical computer results for conditions specified as run 54 - predicted thicknesses.	5/66
33	Theoretical computer results for conditions specified as run 63 - predicted thicknesses.	5/67
34	Theoretical computer results for conditions specified as run 63 - predicted temperatures.	5/68

<u>TABLE NO.</u>	<u>TITLE</u>	<u>PAGE NO.</u>
35	Theoretical computer results for conditions specified as run 73 - predicted thicknesses.	5/69
36	Theoretical computer results for conditions specified as run 73 - predicted temperatures.	5/70
37	Heat transfer coefficient obtained by extrapolation from the steady state heat flow experiments.	6/4
38	Dynamic heat balance on billet heated above the transition temperature - Run 53.	6/23
39	Dynamic heat balance on billet heated above the transition temperature - Run 63.	6/24
40	Dynamic heat balance on billet heated above the transition temperature - Run 73.	6/25

The heat transfer during solid state transformation reactions are normally studied using samples that are small enough for temperature variations within the sample to be ignored.

The present work studied the extent to which heat conduction within large steel samples (billets) influences and is influenced by, solid state transformation reactions. The method used was the thermal analysis technique, which consists of placing thermocouples at various positions in the steel sample and recording the cooling curves given by these thermocouples as transformation occurs. The progress of transformation could be followed from these cooling curves. The method basically depends on three factors: accurate positioning of the thermocouples, accurate temperature measurement by the thermocouples, and rapid response of the thermocouples to changes in temperature. In addition to the experimental work, a theoretical method has been developed from the integral-profile method capable of predicting the progress of the transformation front and of predicting temperature histories throughout the sample. A computer programme has been produced from this method and used to obtain theoretical results. In order to compare the predictions of the integral profile theories with the experimental results, a value was needed for the heat transfer coefficient from the surface of the solid steel to the cooling air and in order to get a reliable

value for this important quantity two independent methods were used to evaluate this factor. One of these methods depended on steady state heat transfer and the other method was a mass transfer analogy.

The second chapter of this thesis contains a survey of studies related to integral profile method (heat balance integral), eutectoid transformation, interlamella spacing and predictions in solid state transformation.

The next chapter develops the theoretical treatment of heat transfer during solid state transformations following the integral profile method for the prediction of solidification rates and also the computer programme produced from this method.

Chapter Four describes the experimental work that was carried out during the development of this thesis.

The results are presented in Chapter Five and discussed in Chapter Six.

Finally, the conclusions and propositions for further work are presented in Chapter Seven.

2.1 THE INTEGRAL PROFILE METHOD (HEAT BALANCE INTEGRAL)

The integral profile method is analogous to the momentum integral used by Von Karmann and Pohlhausen⁽¹⁾ to solve boundary layer problems in fluid Mechanics. Further details of the approach are given in standard works on boundary layers.^{(2) and (3)}

The application of the method to the solid state transformation problem is complicated by two effects which do not arise in fluid flow boundary layers. At the outer surface of the cooled solid the temperature may be a constant or a variable, but is never zero. In fluid flow the velocity at the corresponding boundary is always zero. At the transformation front a source of heat is always present but in fluid flow a source of momentum is rarely present at the analogous surface, the surface of the boundary layer.

A layer of transformed material is assumed to exist between the transformation front and the outer cooled surface of the solid steel. In the simplest application of the integral profile method, temperature gradients are assumed to exist only within this transformed layer. Beyond the transformation front the temperature falls rapidly to the transformation temperature and remains there until passage of the transformation front.

Further assumptions made are that the steel has a unique transformation point and that heat conduction occurs in one dimension only. The principle of the conservation of thermal energy is then applied using solid steel layer as a macroscopic control volume. This leads to the conservation equation which is analogous to the unsteady state heat conduction equation, which is obtained by a rigorous statement of the problem. The conservation equation contains the integral of the temperature profile across the solid steel layer, hence the name of the technique.

In order to evaluate this integral, it is assumed that the temperature profile can be represented as a function of the space variable only. The function most used is a polynomial series, the coefficients of which are not functions of the space variable but are functions of time. The coefficients are determined from the boundary conditions of the problem.

In effect, the use of the boundary conditions ensures that the assumed profile is correct near the two boundaries (the outer surface and the transformation front) and the use of the integral of the assumed profile in the conservation equation ensures that it is correct, on average, across the solid steel layer. If the integral of the temperature profile is obtained in this way and substituted in the conservation equation, an ordinary differential equation can be obtained for the

rate of advance of the transformation front. This equation can be solved analytically in many cases, but if it is non-linear it can be solved by a simple numerical technique. Detailed application of the method to solid state transformation is presented in Chapter 3.

Assumptions made in applying the integral profile method to solid state transformation problems

The basic assumption which must be made in using the integral profile method is that of one dimensional heat conduction, as the method can only be applied to this case.

In order to simplify the application of the integral profile method to solid state transformation one other assumption has been made, that is, that the steel has a unique transformation point (eutectoid temperature).

The accuracy of the integral profile method

The integral profile method is not an exact technique as the expression developed for the temperature profile in the solid steel is approximate. It is therefore interesting to compare results obtained by the use of this method with exact theoretical results (where available) and with experimental results.

For the case of solid state transformation with

heat removed by convection (where neither boundary temperature nor boundary heat are constant), no exact theoretical solution is available. For this case an original integral profile solution has been obtained and is given in Chapter 3 as an example of the use of the integral profile method. This solution applies to the case of a constant heat transfer coefficient. The accuracy of the integral profile method depends on the order of the polynomial used to represent the temperature profile in the solid steel layer, and on which of the available boundary conditions are used.

2.2 THE FORMATION OF PEARLITE

Hiller⁽⁴⁾ reviewed the literature and gave his contribution to the subject. In the eutectoid decomposition of austenite the two new phases, ferrite and cementite, can arrange themselves in two different ways, giving rise to two different structures, bainite and Pearlite. Consequently, it must be of primary interest to arrive at a picture of the eutectoid transformation of austenite which is capable of explaining the existence of two different structures. Since there is good evidence that bainite is nucleated by ferrite, it may seem quite natural to assume that pearlite is nucleated by cementite although the evidence is not quite as good on this point. Furthermore, it is well known that the formation of nuclei with some special orientation relationship to the parent phase is often favoured in comparison to randomly oriented nuclei. In view of the well established fact that the nuclei for bainite are ferrite crystals of widmanstatten nature, it could thus seem quite safe to assume that pearlite is nucleated by a platelet of cementite in a widmanstatten relationship to the parent austenite. This hypothesis is also very attractive from another point of view. First, it yields an explanation for the lamellar nature of pearlite and, second, it yields some understanding of the accepted fact that all parallel plates which form during sidewise growth by repeated nucleation exhibit the same lattice orientation.

Accepting this view, it must be expected that the orientation relationships between the two new phases and the parent phase will be of much importance during growth.

The active nucleus of a pearlite colony may be defined as the first one, either of ferrite or cementite, to form with the particular lattice orientation which will be found in the pearlite colony. The question of which phase provides the active nucleus is thus intimately related to the question of orientation relationships.

Long before bainite was ever described, pearlite was known to be composed of two phases, ferrite and cementite. In view of this knowledge, Benedicks⁽⁵⁾ made the suggestion that proeutectoid ferrite as well as cementite could act as germs for the formation of troostite (i.e. fine pearlite). Benedicks could support his suggestion by the experimental observation that this kind of pearlite forms preferentially in contact with proeutectoid ferrite or cementite. Later on, when bainite had been described and X-ray methods were available for orientation determinations, Mehl and co-workers⁽⁶⁻⁸⁾ reported that bainitic ferrite has the same orientation relationship to the parent austenite as proeutectoid ferrite, whereas pearlitic ferrite appeared to have quite a different orientation relation with respect to the parent austenite. In the case of cementite, the

X-ray methods did not yield such a definite answer but seemed to indicate that proeutectoid cementite and pearlitic cementite could very well have identical orientation relationships to the parent austenite.

As a consequence doubt started as to the validity of Benedicks' suggestion. Upon microscopic inspection of the junction between proeutectoid ferrite and pearlitic ferrite, Hull and Mehl⁽⁹⁾ found a grain boundary between the two and reported that: "The case is never observed, however, in which proeutectoid ferrite is continuous with ferrite or pearlite".

In view of this, Dube⁽¹⁰⁾ and Aaronson⁽¹¹⁾ suggested that the proeutectoid ferrite should only be considered as an informal nucleus which provides a preferred site for the nucleation of cementite with the correct lattice orientation. This latter crystal being the active nucleus for pearlite, is capable of nucleating ferrite with the lattice orientation characteristic of pearlitic ferrite and thus with a grain boundary toward the proeutectoid grain of ferrite. Furthermore, Hull and Mehl found that on quenching a partially transformed specimen with an insufficient rate of cooling, coarse pearlite will give rise to a rim of very fine pearlite (troostite), whereas proeutectoid ferrite gives rise to bainite. There was thus strong evidence in favour of the idea that bainite is nucleated by ferrite but pearlite is not.

Modin⁽¹²⁾ pointed out that many micrographs published by Hanemann and Schrader in their Atlas Metallographicus⁽¹³⁾ show that there often is no grain boundary between proeutectoid and pearlitic ferrite. After a thorough microscopic investigation Modin came to the same conclusion. Later on Modin⁽¹²⁾ found in a particular case that the grain boundary was missing for about 30% of the pearlite units, a figure which seems too high to be ignored. This result is in serious conflict not only with the metallographic results of Hull and Mehl but also with the conclusions drawn from the X-ray measurements stating that pearlitic ferrite does not have the same lattice orientation as proeutectoid ferrite. As a consequence, Mehl and Hagel⁽¹⁴⁾ found it difficult to accept Modin's result in spite of the high quality of his metallographic work. In this situation it appeared essential to test the validity of the X-ray work which had been carried out on separate specimens, one containing proeutectoid ferrite of widmanstatten character, another containing pearlite. A definite answer would be obtained by an orientation determination of a single colony of pearlite and the adjoining grains of ferrite. This determination could be carried out by means of a microbeam X-ray technique. However, metallographic techniques are also available and have been applied to this problem independently by Hillert⁽¹⁵⁾ and Hultgren and Ohlin⁽¹⁶⁾.

Hiller used the characteristic propensity of etching to attack all ferrite crystals in a polished section except the ones closely perpendicular to the surface.⁽¹⁷⁾ Unetched crystals of ferrite were thus seen in the microstructure of a hypoeutectoid steel. After etching in picral, most of them were found to consist of pearlite as well as adjoining proeutectoid ferrite. Hultgren⁽¹⁸⁾ has refined an etching method which produces etch pits characteristic of the orientation of each grain of ferrite. Different lattice orientation can thus be distinguished microscopically by the application of polarized light. Hultgren and Ohlin applied this etch to partially transformed specimens in which the pearlite colonies were still quite small, the idea being that every pearlite colony found in a microsection should be close to the proeutectoid grain of ferrite which had served as its nucleus, informal or active. This investigation gave a very clear answer to the question concerning the role of proeutectoid ferrite. The ferrite constituent in 60-80% of all the pearlite colonies was found to have the same lattice orientation as some adjoining grain of proeutectoid ferrite, proving that these grains had been active, rather than informal, nuclei.

Although proeutectoid cementite has always been considered able to serve as active nucleus for pearlite in a hypereutectoid steel, this opinion did not seem to be based on any experimental information until Modin⁽¹²⁾

reported that inspection by polarized light revealed that pearlitic and adjoining proeutectoid cementite have the same lattice orientation. This point was again tested by Hultgren and Ohlin⁽¹⁶⁾ who found this to be true for almost 100% of the pearlite colonies in a partially transformed hypereutectoid steel.

In view of this result, it appears necessary to conclude that Benedicks was correct when he suggested that pearlite can be nucleated by either ferrite or cementite. In hypereutectoid steels, cementite will normally form first and will then nucleate pearlite; in hypoeutectoid steels, ferrite will form first and then nucleate pearlite. Nicholson⁽¹⁹⁾ arrived at the same conclusion by analyzing kinetic data for the formation of pearlite. His arguments have been criticized by Cahn⁽²⁰⁾, however, and may not be quite valid although his conclusion now seems to be confirmed.

Accepting the fact that both ferrite and cementite may nucleate pearlite, an explanation of the X-ray results must now be sought out. It seems that an answer can be provided by a hypothesis proposed by Smith⁽²¹⁾. Smith suggested that a crystal of proeutectoid ferrite, formed at the grain boundary between two grains of austenite, would have a definite orientation relationship to one of them, resulting in a partially coherent interface. Ordinarily the lattice orientation of the ferrite crystal cannot at the same time be related

to the other grain of austenite and an incoherent interface will thus form on this side.

At a low degree of undercooling, growth will occur predominantly by the movement of the incoherent interface.

The crystal of ferrite thus grown into the grain of austenite to which it bears no orientation relationship.

At a higher degree of undercooling, the available free energy may be large enough to overcome the high elastic strain energy that opposes the movement of the coherent interface. The crystal of ferrite can then grow into the grain of austenite to which it is related. This growth will result in widmanstatten forms.

Smith further proposed that the ferrite component of a pearlite unit, formed at a grain boundary, should also be related to one of the grains of austenite, whether nucleated before or after the cementite component. By analogy to discontinuous precipitation he suggested that the pearlite unit would only be able to grow by the advance of the incoherent ferrite-austenite interface, i.e. into the grain of austenite to which the lattice orientation of the ferrite is unrelated.

The pearlite ferrite found in a transformed grain of austenite should then bear a specific orientation relationship to a neighbouring grain of austenite, this grain being the true parent grain for the crystal of ferrite which later developed into pearlite. This hypothesis is thus able to explain why an X-ray examination

will yield different orientation relationships for pearlitic and widmanstatten ferrite when referred to the matrix grain of austenite. According to Smith, the lattice orientation of pearlitic ferrite in a particular matrix grain of austenite should be random except for the avoidance of certain orientation, which would give a coherent interface between ferrite and matrix austenite, preventing the formation of pearlite.

The reason for Smith's suggestion concerning the growth of pearlite was two-fold. First, the mobility of an incoherent interface is high whereas a coherent interface sometimes may be rather immobile. Secondly, an appreciable increase of the diffusivity can be expected along an incoherent interface, allowing a rapid lateral diffusion and a high growth rate of a two-phase composite. Smith's hypothesis should thus be generalized to read as follows:

The ferrite and cementite constituents of pearlite can have any orientation relationships to the matrix austenite except for those which the formation of interfaces which are partially coherent with the matrix austenite. The lattice orientations of pearlitic ferrite and cementite are thus random with respect to the matrix austenite except for the avoidance of some orientations.

Hulgren and Ohlin in their study of pearlite⁽¹⁶⁾ independently reached the conclusion that Smith's hypothesis

can be generalized to hold for the cementite constituent of pearlite as well as the ferrite. In order to check the importance of orientation relationships further, they particularly studied the formation of pearlite in a hypereutectoid steel where the individual grains of austenite were first isolated from each other by the formation of a continuous film of proeutectoid cementite. Apparently, in this case the lattice orientation of the ferrite constituent of pearlite cannot be directly related to any of the neighbouring grains of austenite, as had been suggested by Smith⁽²¹⁾. Hulgren and Ohlin found that pearlite could form without any difficulty even under these circumstances, a fact that indicated that orientation relationships of the pearlite phases to austenite are of even less significance than suggested by Smith.

2.3 EFFECT OF COOLING RATE ON PEARLITE TRANSITION

Carpenter and Robertson⁽²²⁾ worked on this problem and they got very important results. In the iron carbon diagram the formation of pearlite is represented as taking place at a point which is the intersection of two lines: 1) that representing the lowering of the allotropic change by addition of carbon, and 2) that representing the decrease in the solubility of carbon in γ -iron with fall in temperature. It is only under certain conditions, however, that pearlite forms at constant temperature from austenite of uniform composition. The conditions are as follows:

- (1) When the rate of cooling between Ar_3 and Ar_1 is sufficiently slow to enable a uniform distribution of carbon in the residual austenite to be maintained.
- (2) When the rate of abstraction of heat during the eutectoid change is sufficiently slow to enable the heat evolved by the change to keep the temperature constant.

The iron carbon diagram shows that the formation of pearlite takes place at a constant temperature, but it does not indicate how long this must be maintained to enable the change to proceed to completion. With the slow rates of cooling usually employed the rate of abstraction of heat exceeds the rate of evolution of heat.

Consequently the change is spread over a range of temperature. But if the temperature is maintained constant at the point where the formation of pearlite begins, or at any lower temperature, the change will proceed to completion.

When the rate of cooling from above the Ar_3 point is more rapid than that required for equilibrium, the following conditions are realised:

- (1) A concentration gradient is produced in the austenite during cooling through the range between Ar_3 and Ar_1 . The austenite in contact with ferrite contains more carbon than that more remote from it, and consequently the eutectoid change begins in non-uniform austenite.
- (2) Even when the austenite is uniform, as in steels in which no separation of ferrite precedes the eutectoid change, this change is lowered by increasing the rate of cooling.
- (3) In hypoeutectoid steels the eutectoid point is moved towards a lower carbon content, and consequently, by increasing the rate of cooling, steels containing considerably less than 0.9 % of carbon may be made to consist entirely of pearlite.
- (4) Whether the austenite in which the eutectoid change begins is uniform or not, the formation of pearlite

is spread over a range of temperature by any rate of cooling faster than the equilibrium rate.

When the rate of cooling of a hypoeutectoid steel is faster than the equilibrium rate the results obtained are affected by all the above factors. The formation of pearlite begins at a lower temperature than that represented by the diagram. The change begins in austenite containing less than 0.9 per cent of carbon, it proceeds as the temperature falls, and austenite containing progressively less carbon is gradually transformed to pearlite.

In some respects the presence of other elements affects the eutectoid change in the same way as an increase in the rate of cooling, but in other respects the effects are different. Some elements lower the temperature of the eutectoid change, while others raise it. All elements decrease the carbon content of pearlite. The presence of other elements does not directly result in a non-uniform distribution of carbon in the residual austenite, but owing to their effect in retarding the diffusion of carbon they tend to facilitate the formation of concentration gradients. When other elements are present the system is not binary, and consequently cannot be accurately represented by the iron-carbon diagram. In a ternary system the eutectoid change takes place over a range of temperature. This may be lowered and widened by increasing

the rate of cooling, but even at the slowest rate the formation of pearlite does not take place at a point. The eutectoid change is accompanied by selective crystallisation, and the ferrite forming part of the eutectoid contains a different concentration of the third element from that in the austenite from which it is derived.

Thus, the eutectoid range resulting from the presence of other elements differs from that produced by increasing the rate of cooling, for in the latter case the formation of pearlite proceeds to completion if the temperature is held constant at any point below that at which the change takes place under equilibrium conditions.

In the experiments on the eutectoid change, no distinction was made between the effect of the rate of cooling and that of the other element present. The specimens were cooled continuously to a certain point and then quenched. It was observed that with slow cooling the eutectoid change took place within a very narrow range of temperature and that this range was widened as the rate of cooling was increased. In the experiments carried out by Whiteley⁽²³⁾ the different effects were distinguished, for, by keeping his specimens at different temperatures for different lengths of time, he observed that the eutectoid change took place over a range of temperature, that at any temperature within that range it proceeded at constant temperature but not to completion, and that it went further

the lower the soaking temperature. Had the specimens contained no element besides carbon and iron, the change would have been completed in time at any of the soaking temperatures below that at which it was observed to begin, and had they been cooled to the soaking temperature at the equilibrium rate, then in the presence of manganese and other elements, no change would have taken place at constant temperature. What was actually observed was the combined effect of a rate of cooling faster than the equilibrium rate and of the presence of other elements.

It is well known that the pearlite lamellae become finer as the rate of cooling is increased, but a rise in the carbon content has the opposite effect, and in a series of slowly-cooled steels the pearlite is finest in the steel of lowest carbon content. It is also well known that increasing the rate of cooling increases the amount of pearlite, so that with suitable cooling, steels with less than 0.5 per cent of carbon can be made to consist entirely of pearlite. In this respect, increases in the rate of cooling and carbon content have a similar effect.

Two other effects of these factors may be discussed, on the way in which pearlite grows, and the relation of this to the structure existing when the eutectoid change begins.

In slowly-cooled steels which contained less than 0.5 per cent of carbon, a considerable amount of ferrite

is formed before the eutectoid change begins. This occurs as irregular masses round the boundaries of the grains, or more rarely as isolated crystals in their interiors. Pearlite begins to form in irregular masses of austenite and extends until these are completely converted.

By increasing the rate of cooling or the carbon content, the amount of proeutectoid ferrite is decreased, and the pearlite begins to form in polyhedral grains of austenite surrounded by envelopes of ferrite. Under these conditions the shapes assumed by the growing particles are not determined so much by the shapes of the areas of austenite in which they form, as by the manner of their growth. It begins at a number of points on the boundaries and extends inwards. The external shape of the pearlite units is determined by their mode of growth. When the transformation is completed each austenite grain is occupied by a number of particles of pearlite which have grown from different points.

With suitable combinations of carbon content and rate of cooling the formation of proeutectoid ferrite may be almost or completely prevented. In this case the formation of pearlite has little relation to the grain structure of the austenite. It may begin at the boundaries of the austenite grains, or at points in their interiors, but the general structure of the steel, at any intermediate stage, or when the change is complete, is largely determined

by the way in which the pearlite grows.

During slow cooling, in any steel of lower carbon content, the transition from austenite to pearlite begins in irregularly shaped particles of austenite. The units of pearlite formed in this way have no definite shape of their own. As the rate of cooling is increased, however, the units exhibit an increasing tendency to grow radially. The pearlite growing from the ferrite boundaries forms nodules round the austenite grains. A further increase in the rate of cooling or carbon content, besides reducing the amount of proeutectoid ferrite, increases the tendency towards radial growth.

In a steel of 0.73 per cent of Carbon, 0.56 per cent of Manganese, 0.23 per cent of Silicon, air cooled, a few narrow boundaries of ferrite were formed, and from them pearlite developed. At some of the ferrite boundaries pearlite grew on one side only, while at others growth took place on both sides. In this same specimen there were many areas in which the formation of pearlite had begun at points remote from existing ferrite. This is the condition necessary for perfect radial growth, for the pearlite may then develop in all directions from the point at which its formation began.

The tendency for pearlite to grow radially when the rate of cooling is increased is the result of the combined operation of two factors. In the first place, it tends to grow so that the edges of the plates will always be

presented to the direction of growth and, in the second place, so that in a given time the maximum amount of austenite will be transformed. Thus, when the rate of cooling is increased, the eutectoid change accommodates itself to the altered conditions, and attains greater rapidity in three ways:

- (1) The individual plates of ferrite and cementite become finer and the distances over which carbon must diffuse are decreased.
- (2) The units of pearlite exhibit an increased tendency to grow radially, and thus produce the maximum amount from the minimum number of centres of growth.
- (3) The formation of pearlite begins at a greater number of points, though this number does not increase to an extent commensurate with the increase in the rate of cooling. Even with the most rapid cooling the number of centres from which pearlite forms is not great, and this factor is of less importance than the others.

As long as the residual austenite is completely converted to pearlite the manner of its growth has little effect on the final structure. It influences the arrangement of the plates of cementite and ferrite within each unit, but at low magnifications the pearlite simply

appears as dark masses filling the spaces occupied by the residual austenite. If, however, the austenite is only partly converted, then the mode of growth of the pearlite determines the shape of the units. In heat treatment the formation of pearlite is not interrupted, except under certain conditions of quenching when large specimens are used, or when the immersion in the water is not sufficiently rapid. When this occurs the pearlite appears in the form of dark nodules, usually located at the boundaries of austenite grains, and more rarely in the interior. It is recognised that these are formed because growth has taken place radially, but this method of formation is regarded as exceptional and different from that of pearlite. It follows, however, from the foregoing description of the effect of the rate of cooling and the pre-existing structure, that these nodules are actually typical of pearlite formed under the imposed conditions. For, as the rate of cooling is increased, pearlite shows an increasing tendency to grow radially, and when no previous separation of ferrite has taken place, its formation begins at a point and spreads radially from it. Thus the dark nodules observed in imperfectly quenched steels are characteristic pearlite structures.

In slowly-cooled low carbon steels the crystals of ferrite assume fairly regular shapes, and with an increase in the rate of cooling or the carbon content they tend to become elongated. The response of pearlite

to these influences is directly opposite to that of ferrite, and under these conditions the units of pearlite tend to become spherical. This difference in the shapes is due to the difference in the conditions under which they are formed. During the formation of ferrite the excess carbon is driven into the austenite, and under conditions of accelerated cooling the ferrite tends to grow in the way that permits the most rapid removal of carbon from the ferrite-austenite interface. During the formation of pearlite, however, there is no diffusion of either constituent into the residual austenite. The units may therefore be of any shape, and during accelerated cooling they tend to become spheres, for this is the shape that permits the most rapid increase in the amount of pearlite forming from a limited number of centres.

2.4 THE INTERLAMELLAR SPACING OF PEARLITE

Pellissier, Hawkes and Mehl⁽²⁴⁾ reviewed the literature about this important subject and gave their contribution to it. Attention was called to the importance of the interlamellar spacing in pearlite by Belaiew in 1922⁽²⁵⁾; Belaiew's work followed the earlier studies of Oknof^{(26), (27)}, and Forsman⁽²⁸⁾ on the stereometry of pearlite. In 1929 Greene attempted to correlate the mechanical properties of pearlite with its interlamellar spacing⁽²⁹⁾. The usefulness of pearlite spacing measurements in studying the mechanical properties of anneal steels, and also in studying the rate of formation of pearlite, has become more generally recognized. Systematic investigations of the correlation of the mechanical properties with spacing of pearlite have been conducted by Gensamer and his collaborators^{(30), (31)}.

Belaiew has proposed the use of spacing data to describe the fineness of pearlite, in place of the qualitative terms coarse, medium, and fine frequently used, in order to avoid confusion or ambiguity in nomenclature, and has suggested that such data might be used to decide whether there is any real justification for the belief that the range of pearlite structures is discontinuous⁽³²⁾.

Mehl in a study of the mechanism and rate of the decomposition of austenite, has shown that pearlite spacing data must be considered in any effort to analyze the rate of growth of pearlite nodules and, therefore, also the rate of formation of pearlite⁽³³⁾. Moreover, spacing

measurements have been used to predict a change in the mechanism of austenite decomposition (i.e. from the pearlite to the bainite reaction) as the temperature of transformation is decreased below about 550 degrees centigrade⁽³³⁾.

The need of a treatment of the interlamellar⁽³⁴⁾ spacing of pearlite more comprehensive than that provided by Belaiew became evident in studies on the physics of hardenability of steel⁽³⁵⁾, and also in the studies by Eensamer and his co-workers on the correlation of the mechanical properties and spacing of pearlite. The basic assumption in Belaiew's work that the interlamellar spacing of pearlite is constant when the pearlite is formed under controlled conditions was the result of casual observation and heretofore has not been subjected to experimental test. In fact, reasonable doubt has existed that the spacing is strictly constant even in pearlite formed isothermally, for a statistical variation seemed more likely. There is need also for a more accurate method of determining pearlite spacing. Furthermore, information should be available on the possible effects of such variables as prior austenite grain size, carbon content of the austenite, and the presence of various alloying elements upon the interlamellar spacing of pearlite.

Constancy of Interlamellar spacing

Belaiew drew attention to the rather obvious fact that the wide variation in interlamellar spacing observed

on a plane of polish is not real but apparent⁽²⁵⁾. The true spacing (Δ_o) of pearlite formed under controlled conditions was believed to be constant, and the variation in spacing on a plane of polish was attributed to the intersection with this plane of randomly oriented groups of parallel ferrite and cementite lamellae (pearlite colonies) at a range of angle from 0 to 90 degrees. The apparent spacing (Δ_W) on the sectioning plane was related to the true spacing by means of the angle (W) between the normal to the lamellae and the plane.

This secant relationship, $W = \sec^{-1} \frac{\Delta_W}{\Delta_o}$, provided a simple means of determining Δ_o in pearlite completely resolved by the microscope.

The smallest apparent spacing encountered on scanning a sufficiently large area of the specimen presumably was equal to the true spacing. This method of determining Δ_o apparently involves two assumptions:
a) that the true spacing is strictly constant, and
b) that the orientation of pearlite colonies with respect to the plane of polish is random. Obviously, values of Δ_o for fine pearlites, incompletely resolvable under the microscope, could not be obtained by this method. A more indirect method of measurement was devised for this case.

Belaiew had noted that at a few locations on the plane of polish where the apparent spacing was very large, the edges of the cementite plates exhibited a characteristic

frayed or broken appearance. Using a completely resolvable pearlite specimen, Δo was determined by the method just described, and it was shown that this peculiar aspect of the cementite lamellae corresponded to values of W greater than about 83 degrees. Evidently this critical value of W was of real significance, for the secant relationship predicted a greatly accelerated increase in the apparent spacing (ΔW) as the value of W approached and exceeded 83 degrees. This phenomenon was assumed to apply generally to pearlite of any Δo and it was used to determine Δo values of incompletely resolved pearlite. The apparent spacing of cementite plates which exhibited this frayed appearance was measured, the angle was assumed to be 83 degrees, and the Δo was calculated from the secant relationship.

The basic assumption in this treatment, that the interlamellar spacing is characteristic of the heat treatment (Belaiew used no iso-thermal treatment) and is a constant (Δo) throughout the entire specimen when cooling conditions are uniform, has been questioned.

Rosenhain⁽³⁴⁾ and Benedicks⁽³⁵⁾ both doubted the validity of this claim and suggested methods for its experimental verification. The supposition of the constancy of Δo was, however, not without some foundation, qualitative though it was. Belaiew observed that the proportion of specimen area occupied by lamellae oriented at very oblique angles to the plane of polish is relatively

2, 10

much less than that occupied by lamellae oriented nearly normal to the surface, as the geometry of the case predicts. Certainly, this conception of the constancy of spacing requires some modification in the light of research by Bain, Davenport and co-workers⁽³⁶⁾. At least qualitatively, Δ_0 appears more precisely to be a function of the temperature of isothermal decomposition of austenite to pearlite, rather than a function of the cooling rate⁽³⁷⁾. It is true that slow cooling results in complete transformation to pearlite (at a high temperature) within a narrow temperature interval, but at faster rates of cooling, this is not true within wide limits. In fact, it is believed that the recalescence in a large specimen, isothermally transformed to pearlite at temperatures near the knee of the S-curve, may result in an appreciable range of spacing⁽³¹⁾. Furthermore, it was suspected that pearlite formed isothermally under the most carefully controlled temperature conditions does not possess a strictly constant interlamellar spacing, but rather a statistical distribution of true spacings about a mean.

Experimental methods

The problem of investigating the constancy of the interlamellar spacing (S_0)⁽²⁶⁾ and that of determining S_0 are related but not necessarily identical. The constancy of S_0 may be tested either by determining S_0 at several random locations in a specimen or by other less direct means. Speculation reveals at least three possible

procedures, as hinted by Rosenhain⁽³⁴⁾ and Benedicks⁽³⁵⁾:

(1) A specimen of pearlite is polished repeatedly on one surface and a selected pearlite colony is photographed at the successively lower levels to determine whether the apparent spacing⁽³³⁾ remains constant. If these successive sections are maintained exactly parallel, it can be assumed that any variation in S reflects a variation in S_0 .

The true spacing cannot be determined by this method nor can the extent of any variation in S_0 be ascertained owing to extreme manipulative difficulties in determining the lateral displacement of a given lamella on successive polishing. The method can be refined so as to permit the construction at considerable magnification of a spatial model of a pearlite colony⁽²⁸⁾, though the difficulties in registry affect its accuracy.

(2) A second method involves polishing a specimen of coarse pearlite on two surfaces intersecting in an edge at a known angle; selecting a pearlite colony which exhibits traces of the same lamellae on both surfaces; and measuring (a) the plane angles between the lamellae traces and the edge, (b) the apparent spacing of the lamellae on each surface. S_0 may be computed from this data by the methods of descriptive geometry or more simply by the use of the stereographic projection⁽³⁸⁾. The constancy

of S_0 can be tested by applying this method at several locations along the edge. Calculations show that an uncertainty of as much as 10 degrees, in determining the dihedral angle between surfaces, results in a minor error in the calculated S_0 (< 10 per cent). This method may be shortened considerably, for it may be shown that if the traces of the lamellae on one surface make an angle of from 60 degrees to 120 degrees with the edge, then the apparent spacing of the lamellae on an adjoining perpendicular surface may be taken as the true spacing with less than 14 per cent error. The major difficulty and at the moment apparently an insuperable one, lies in the feat of polishing two surfaces so as to maintain an edge between them sufficiently sharp to provide the requisite accuracy for a single pearlite colony. This difficulty might be minimized by electropolishing.

- (3) A method which involves less experimental difficulty consists in measuring the relative amount of surface area occupied by various small ranges of apparent spacing and comparing these data with values calculated on the assumption of a constant S_0 by probability mathematics. Such a statistical method is tedious, but it has been used with success.

Methods of Determining Interlamellar Spacing

It is convenient to classify the methods of determining

interlamellar spacing into two groups:

1. Methods applicable to coarse pearlite which are completely resolvable under the microscope.
2. Methods applicable to fine pearlites which are only partially resolvable under the microscope.

In Group 1 at least three methods are available.

One method, which was devised by Belaiew⁽²⁵⁾, consists in adopting the smallest observed spacing as the true interlamellar spacing. A second method was developed by Scheil⁽³⁹⁾. This method yields accurate and complete information about the spacing, but it is rather lengthy.

A third method is an abbreviated form of the latter method developed by Miss E. B. Pearsall, and is more useful⁽³¹⁾. The absolute accuracy of this method is not known; certainly it is dependent to a large degree on the validity of the assumption that the limit of resolution practically achieved is equivalent to the theoretical resolving power of the objective. An evaluation of this assumption is difficult because of the many variables which influence the limit of resolution.

In Group 2 there are two methods. One system developed by Belaiew⁽²⁵⁾. Some experience with this method has indicated that it is not capable of providing consistent results. Evidently the source of greatest inaccuracy is the uncertainty in assigning a definite value of the orientation angle to lamellae which exhibit this irregular

appearance; an error of as little as 5 degrees in estimating this angle results in an inaccuracy of about 100 per cent in the calculated S_0 . Furthermore, it is believed that polishing technique, as well as the true spacing (S_0), may affect the empirical correlation of this characteristic appearance with the orientation angle.

The other method available for determining the interlamellar spacing of incompletely resolvable pearlite is the method developed by Miss Pearsall⁽³¹⁾. This method may be applied equally well to completely resolvable pearlite and to partially resolvable pearlite; it has been used almost exclusively to study effects of variables on the interlamellar spacing.

Other methods were developed to determine interlamellar spacing by Brown and Ridley⁽⁴⁰⁾, and Asundi and West⁽⁴¹⁾. They pointed out that the mean spacing value is known to vary with time, temperature and composition.

EFFECT OF TEMPERATURE VARIATION AND OF HEAT
TRANSFER PROCESSES

The very important work of Davenport and Bain⁽³⁶⁾ about transformation of austenite at constant subcritical temperature in which they presented the results of a study of the time required for the transformation of austenite to ferrite and carbide at a variety of temperatures and also of the time required for the reaction austenite — martensite at the temperatures at which this reaction occurs instead of the one first mentioned, is considered now a pioneer work on structural prediction. In the discussion of the results the authors concluded that the C-shaped curves for all steels resulting from plotting temperature of transformation (between eutectoid temperature and that of maximum time) against time required may be predicted from purely physical-chemical considerations. Following this work, Austin and Rickett⁽⁵⁰⁾ in their paper Kinetics of the decomposition of austenite at constant temperature, studied existing data with a view to finding some function of the direct observations that will reduce the data to a straight line, a device for treating observations that often offers advantages and has been widely used.

The first data taken for study were the original dilatometric measurements made by Davenport and Bain⁽³⁶⁾. Their investigations, which included six steels of different composition and covered the temperature range from 370°C to room temperature, are particularly suitable because the observations were carefully made, were almost completely

objective and furnished a practically continuous record of the transformation. Measurements of the rate of decomposition of austenite at constant temperature can be made to plot on a straight line, if time is plotted on a logarithmic scale and the percentage transformed is plotted on the integrated-probability scale.

The straight line plot permits easy and rapid interpolation and also extrapolation to 1 per cent and 99 per cent transformation, which are convenient points to take as the beginning and end of the transformation. It has a further use as an aid in judging the consistency of a set of measurements from the scatter of the points.

The isothermal rate curves for a given steel plotted in this manner have the same slope over the temperature range in which austenite transforms to bainite. Moreover, within this same range the time required for completion of a given fraction of the transformation varies inversely with the absolute temperature.

Below about 250°C the isothermal rate curves show two steps instead of one. The rate at which the second reaction goes on is also represented by a straight line on log-probability paper. The logarithm of the time required for completion of a given fraction of the transformation varies inversely with the absolute temperature. Johnson and Mehl⁽⁵¹⁾ in their paper reaction kinetics in processes of nucleation and growth, derived an analytical expression for the rate of reaction in a reaction proceeding by nucleation and growth when nucleation occurs without

regard for matrix structure and the nuclei tend to grow into spherical nodules. The effects upon the reaction curve of variations in the rate of nucleation and in the rate of growth, have been derived from the analytical expression. Distribution curves are derived for the sizes of nodules and for the corresponding areas of the surface of polish. The application of the analysis to the process of freezing and recrystallization is discussed. The calculation of the rate of nucleation and the rate of growth from easily obtained experimental data is described.

It was soon realized that a method of predicting the anisothermal transformation was required. Scheil's rule⁽⁵²⁾ has been used extensively up to now to compute the beginning of transformation from the incubation periods during isothermal transformation. Manning and Lorig⁽⁵³⁾ suggested the existence of two independent domains of validity of the rule of additivity resulting from the work of Scheil. After that a few models were outlined which extended the prediction to the growth period of the transformation:

- (a) Grange and Kiefer⁽⁵⁴⁾ developed an empirical method for estimating the cooling transformation from isothermal data. The isothermal diagram shows the fundamental transformation behaviour of austenite at constant temperature; most actual heat treatments involve transformation as it occurs during cooling through a range of temperatures. The isothermal diagram is not, therefore, directly

applicable to cooling transformation but can be used provided the relationship between the two types of transformation can be evaluated.

The results of a systematic study of cooling transformation in S.A.E. 4340 steel indicate that the transformation occurs over a temperature range in which transformation at any instant during the cooling corresponds to isothermal transformation at the same temperature. Cooling transformation is therefore related to isothermal transformation; the relationship can be predicted with sufficient accuracy for most practical purposes from the isothermal diagram by a method developed empirically from experimental observations.

A cooling transformation diagram analogous to the isothermal diagram can be derived from isothermal data or determined experimentally; it lies below and to the right of the corresponding isothermal diagram. The amount of the displacement in general increases with more rapid cooling up to the rate which just produces on cooling to room temperature a fully martensitic structure.

The derived relationship between transformation on cooling and isothermal transformation may be employed to advantage in actual heat treatments provided the cooling history is known; it may also be used for determining the rate of cooling necessary to achieve a desired final product and combination of mechanical properties.

- (b) Liedholm⁽⁵⁵⁾ presented a method whereby a series of Jominy end quench bars is used to predict the structure and hardness in normal quenches.
- (c) Pumphrey and Jones⁽⁵⁶⁾ proposed a model based on the discretization of the cooling law and on adding the increments of transformation calculated for each time step.

The method adopted by the authors for the calculation of continuous cooling data from the isothermal transformation diagram, has enabled the hardness along a Jominy bar to be calculated. For the three steels considered the hardenability curves calculated in this way were found to be in reasonable agreement with those determined experimentally. Although calculations and experiments have not been carried out with all possible steel compositions, the investigation indicates the validity of the method for steels of the types considered and suggests that the hardenability of a steel may be related quantitatively with its S curve. A further point of great practical importance is the question of the range of temperatures over which transformation occurs in a steel during continuous cooling, since the mechanical properties are considerably affected by the temperature at which a steel transforms. The method used by the authors enable the transformation range during continuous cooling to be obtained from the S curve. For the types of steel used the range calculated in this way shows fair agreement with that obtained by the method of the interrupted Jominy

quench.. Cahn⁽⁵⁷⁾ had shown that a transformation which nucleates heterogeneously will quite often obey a rule of additivity and transform non isothermally according to simple rate laws which can be calculated from isothermal data.

The problem of transformation kinetics under non isothermal conditions is of tremendous practical importance. It has not been extensively studied, using fundamental kinetics quantities. Part of the difficulty is that both the nucleation rate and growth rate of the transformation product are time-dependent if the temperature is time-dependent. However, it has been found that some transformation obey an additivity rule⁽⁵²⁾. Avrami⁽⁵⁸⁾ has shown that for the case where the nucleation rate is proportional to the growth rate over a range of temperatures, the reaction is additive. This is a very special condition, and it would not expect to encounter such a system. Especially for the case of the pearlite reaction where, even isothermally, the nucleation rate is a function of time, this condition would not hold. Many systems in which nucleation is heterogeneous exhibit the property that all nucleation occurred early in the reaction. This may be due to the fact that only a limited number of sites for nucleation exist, such as impurity particles or grain corners, or in case of grain surface or edge nucleation that these sites can be consumed very early in the reaction. This is a general property of heterogeneous nucleation, and will be called site saturation.

Many reactions where the nucleation is apparently homogeneous also are describable by the assumption that all nucleation occurred early in the reaction.

The above mentioned literature concerns the transformations with nucleation and growth.

As a consequence of the greater possibilities offered by computers since the 1960s, much work has been done in writing programs based on models of increasing complexity; Markowitz and Richman's work⁽⁵⁹⁾ using the Kiefer and Grange method⁽⁵⁴⁾ wrote a basic program for the computation of the continuous transformation diagrams from isothermal-transformation data. All that is needed as input data are the co-ordinates of several points on the isothermal curve above the nose temperature, several cooling rates, and the temperature at which the cooling curve is to start. The isothermal curves are approximated by straight-line segments and the data points must be chosen so that they are closer together near the nose than at longer times.

The computed continuous transformation curves representing the start of pearlite and bainite formation agree quite well with the experimental curves taken from the work of Grange and Kiefer; and the pearlite finish curve does not exhibit a very large discrepancy. Much of the errors are introduced as uncertainties in the isothermal-transformation data at long transformation times. Lindholm⁽⁶⁰⁾ presented a composed model for the

temperature distribution within a steel body during cooling where phase transformation occurs. The calculations have been executed in a computer.

Calculated and measured structures and temperatures conformed well for the steel rollers dealt with as an example.

The proposed model seems to be valid under the conditions tested. Consequently, all material constants used, such as thermal conductivities, specific heats and phase transformation diagrams, are sufficiently correct in these particular cases. In addition, the measured coefficient of heat transfer and its temperature dependence have proved to be valid for the case. All these constants are critical since it is obvious that the model cannot be more accurate than its constants. Because of this all input data have to be thoroughly examined and carefully simulated to the real tests undertaken. However, it is evident that the hardening process may be treated in a theoretical way by numerical solution.

Hildenwall and Ericsson⁽⁶¹⁾ presented a computer calculation model for the response to the hardening of carburized steel. The model avoids many of the previously used simplifying assumptions and approximations. The temperature calculation and calculation of phase transformations has been tested in several ways and they give good starting conditions for the stress calculations. The calculated stresses are in good agreement with experimental experiences.

Agarwal and Brimacombe⁽⁶²⁾ developed a mathematical model incorporating both heat transfer and the transformation of austenite to pearlite in eutectoid carbon steel rods. A computer program based on the implicit finite-difference technique has been written which permits the temperature distribution and fraction of austenite transformed to be predicted as a function of cooling conditions, rod diameter and the transformation characteristics of the steel. The program takes into account the temperature-dependent heat transfer and thermophysical properties; and stresses the importance of the enthalpy of transformation. The model has been checked for internal consistency with theoretical equations, and model predictions have been compared to published industrial data for rod cooling in water at 100°C. The effect on the temperature distribution and fraction of austenite transformed of several variables, rod diameter, starting temperature, heat transfer conditions, transformation characteristics and quenchant temperature, has been predicted using the model. The range of variables studied is typical of those found in industrial processes such as patenting and controlled cooling.

Umemoto, Komatsubara and Tamura⁽⁶³⁾ presented a mathematical formulae describing anisothermal structural evolution for linear cooling laws. They considered the relationship between the size of material, fraction of martensite and austenite grain size for a certain eutectoid steel under a certain cooling condition. It is assumed that the isothermal pearlite transformation is

additive over the whole transformation range. The cooling rate is determined as a function of section size. Umemoto, Horuchi and Tamura⁽⁶⁴⁾ studied the isothermal and continuous cooling transformation kinetics of bainite using an automatic quench dilatometer. It was found that the overall isothermal bainite transformation kinetics were well expressed by Johnson-Mehl type equation and that the transformation rate decreased with increase in the austenite grain size. The analysis of transformation kinetics and the optical microscope observations suggested that the nucleation site of bainite was both on the grain boundaries and inside the austenite grain. This effect of austenite grain size on the rate of isothermal transformation to bainite was found to be smaller than that to pearlite. Comparisons of the observed cooling transformation kinetics with that predicted from the isothermal kinetic data showed that the transformed fractions were additive in bainite transformation. This result might be understood if it were assumed that the bainite transformation proceeds with repeated nucleation and growth of basic subunits, each attaining the limit size rapidly.

Fernandes, Deins and Simon⁽⁶⁵⁾ developed a model for the prediction of a cooling law and of the kinetics of phase transformation in steels. The input data required to run the computations are the kinetics of isothermal transformations, the coefficient of heat transfer, and the thermophysical properties of the metal, including the enthalpy of transformation; all these parameters are

expressed as functions of the temperature and the percentage of phase formed.

It was shown that a good prediction of the cooling law as well as that of the kinetics of pearlitic transformation can be obtained without taking into account the effect of stress on the transformation for slow cooling rates or small specimens. For faster cooling rates and larger specimens it is necessary to introduce a mechanical parameter, namely, the effect of the internal stresses developed during cooling on the kinetics of transformation. On introducing this parameter into the computation, the calculated values showed to agree very well with those from experiments.

In the main, the work that has been carried out previously relates to transformations occurring in relatively small components under intense heat transfer conditions. The slowest cooling rate considered in the work of Agarwal and Brimacombe⁽⁶²⁾ for example, was some $7^{\circ}\text{C}.\text{s}^{-1}$. At this, and higher cooling rates, there is a significant interactive coupling between the heat transfer process and the kinetics of transformation. The coupling becomes less and less significant as the cooling rate is decreased.

3.1 HEAT TRANSFER DURING SOLID STATE TRANSFORMATIONS

THEORETICAL TREATMENT

The theoretical treatment of heat transfer during solid state transformations presented here follows the integral-profile method developed by Hills⁽⁶⁶⁾ for the prediction of solidification rates. The metal billet undergoing transformation is considered to be cooled from its outer surface and the heat transfer is considered to be one-dimensional i.e. in the direction normal to the cooled surface. A remote insulated plane is identified which is either the central plane of a billet cooled from both sides or the uncooled surface of a billet cooled from one side only. The co-ordinate system within the billet has its origin in the cooled surface and the remote insulated surface is positioned at a distance 'L' from this surface.

Cooling Modes

The metal billet undergoing transformation is considered in three sections: uncooled metal, cooled metal and transformed metal. The billet is initially at a uniform temperature above the transformation temperature and is of finite extent so that four different cooling modes can be recognised. These modes are described below and illustrated in Figure 1. The figure shows the temperature distribution set up in each mode together with a schematic picture which will be used subsequently to represent that mode.

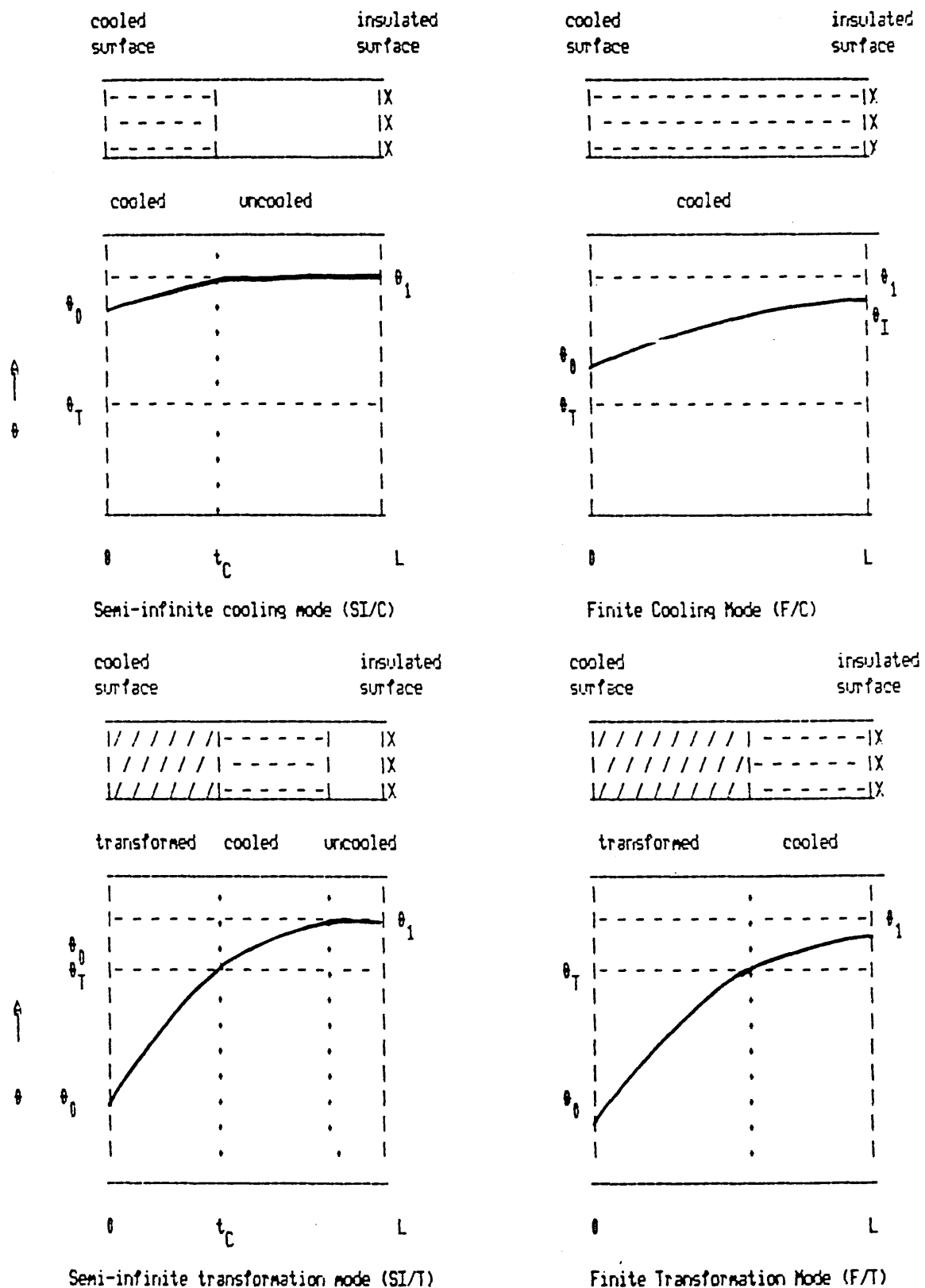


Figure 1 The four different cooling modes that operate during the transformation of a large metal component.

1. Semi-infinite cooling mode (SI/C)

During this mode, the entire billet is above the transformation temperature but its surface is being cooled down towards the transformation temperature. At the same time the extent of the region of cooled metal is extending inwards from the cooled surface so that the layer of cooled metal can be regarded as growing into uncooled metal. There are thus two variables changing during this mode, the temperature of the cooled surface θ_0 and the thickness of the cooled layer, t_C .

2. Finite cooling mode (F/C)

During this mode, the entire billet is still above the transformation temperature but the extent of the cooled layer has grown to encompass the entire billet. Thus both the temperature of the cooled surface, θ_0 , and the temperature of the insulated surface, θ_I , are falling, these being the two variables characterising this mode.

3. Semi-infinite transformation mode (SI/T)

The temperature of the cooled surface is below the transformation temperature during this mode so that the outer layers of the billet have already transformed. The transformation front has moved into the billet, a layer of transformed metal existing on the outside of the billet. The layer of cooled metal exists inside the transformed layer but does not extend as far as the insulated surface. There are three variables that describe the progression

of this mode, the thicknesses of the transformed and cooled layers and the temperature of the cooled surface.

4. Finite transformation mode

In this mode, the layer in which the metal has been cooled but not transformed has grown to encompass all the untransformed metal. Thus the temperature of the remote surface of the billet has started to cool below the original billet temperature. The three variables that describe this cooling process are the thickness of the transformed layer, the temperature of the cooled surface and the temperature of the remote surface.

Cooling/Transformation Path

The actual cooling/transformation process in any given billet can follow one of two paths through the different modes depending upon the initial temperature of the billet, the billet size and the severity with which the billet is cooled. In all cases the initial mode will be the semi-infinite cooling mode. However, if the layer of cooled metal extends to the remote insulated surface before the temperature of the cooled surface falls to the transformation temperature ($t_C = L: \theta_0 > \theta_T$), the next mode will be the finite cooling mode, the entire billet cooling but remaining above the transformation temperature. If these conditions are not met, the second mode will be the semi-infinite transformation mode. Both these modes terminate in the finite transformation mode.

The two possible paths are illustrated in the cooling/transformation algorithm shown in Figure 2. As will be seen later, the computational scheme must follow the same algorithm. Separate equations will be used in the computation for the thickness of the transformed layer, for the temperature of the cooled surface once it has transformed, and for whichever is the current appropriate parameter necessary to describe the state of the cooled layer. The equations are first order ordinary differential equations each expressing the differential of one of the variables as a non-linear function of all three. The equations thus form a set of simultaneous differential equations.

The equations are derived in the following sections, the first dealing with the transformed layer and the second with the cooled layer. The subsequent sections describe their solution using a Runge-Kutta routine.

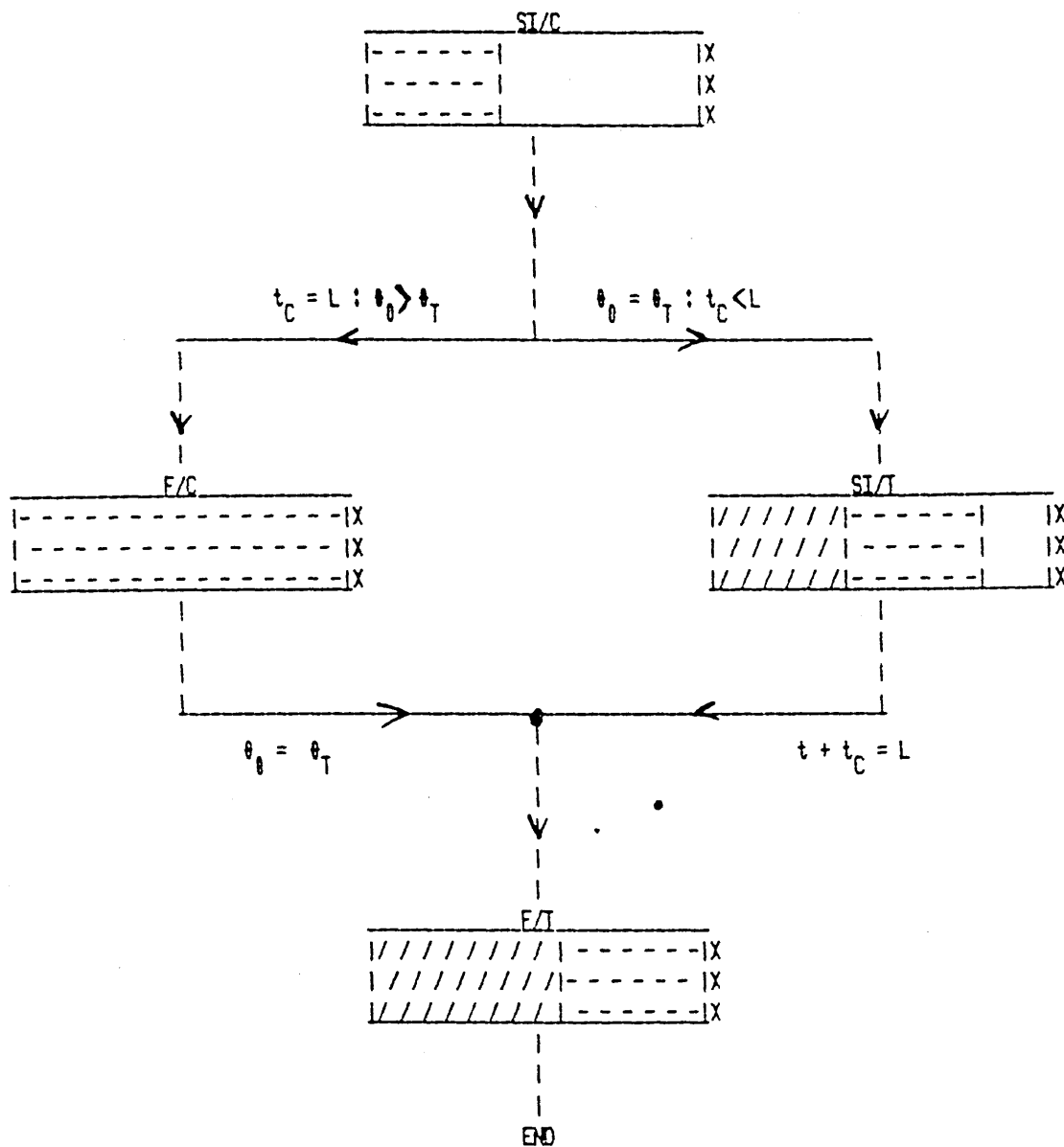


Figure 2 The cooling/transformation algorithm showing the two routes possible for the heat transfer process during transformation cooling.

3.2 EQUATIONS FOR THE TRANSFORMED LAYER

There are two variables that describe the state of the transformed layer at any one time, the thickness of the layer and the temperature of the cooled surface. These two variables are analogous to the thickness of the solidified layer and the temperature of the cooled surface used to describe the thickness of solidified metal in a solidification process such as continuous casting.

The derivation of the equations for the temperature of the cooled surface and the thickness of the transformed layer thus follow fairly closely the method used by Hills to describe solidification processes.

Temperatures within the transformed layer must satisfy the heat conduction equation:

$$k \frac{\partial^2 \theta}{\partial x^2} = \rho c \frac{\partial \theta}{\partial \tau} \quad (1)$$

This equation cannot be solved formally under the conditions that apply during transformation. Instead, it will be solved 'on average' by satisfying its integral form across the transformed layer:

$$\int_0^t k \frac{\partial^2 \theta}{\partial x^2} dx = \int_0^t \rho c \frac{\partial \theta}{\partial \tau} dx \quad (2)$$

The right hand side of this equation can be evaluated by applying the Leibnitz integral formula⁽⁶⁷⁾ so that the equation becomes:

$$k \left[\frac{\partial \theta}{\partial x} \right]_{x=t} - k \left[\frac{\partial \theta}{\partial x} \right]_{x=0} = \frac{d}{d\tau} \left(\int_0^t \rho c \theta dx \right) - \rho c \frac{dt}{d\tau} [\theta]_t \quad (3)$$

The left hand side can be derived by applying the conservation of heat at the two boundaries of the transformed layer:

$$- k \left[\frac{\partial \theta}{\partial x} \right]_{x=0} = \dot{q}''_0 = - h(\theta_0 - \theta_a) \quad (4)$$

and:

$$- k \left[\frac{\partial \theta}{\partial x} \right]_{x=t} = \dot{q}''_t - \rho_H \frac{dt}{d\tau} \quad (5)$$

where h is the heat transfer coefficient at the cooled surface, θ_a the temperature of the cooling air, \dot{q}''_t the heat received at the transformation front from the cooled layer of metal and H the latent heat of transformation.

Experimental determinations of the heat transfer coefficient show that it varies slightly with surface temperature.

In the treatment presented here, however, we will assume that the heat transfer coefficient is constant throughout the cooling and transformation process.

Thus, equation (3) becomes:

$$\rho_H \frac{dt}{d\tau} - \dot{q}''_t - h(\theta_0 - \theta_a) = \frac{d}{d\tau} \int_0^t \rho c \theta dx - \rho c \theta_T \frac{dt}{d\tau} \quad (6)$$

Since equation (6) is linear in temperature, we can arbitrarily allot the zero of temperature measurement as the temperature of the cooling air. Thus θ_a is zero, and all temperature values used subsequently in theoretical equations will be measured from the air temperature.

Equation (6) cannot be solved formally so that we provide an average or integral solution to it by representing temperature profile across the transformed metal in the form of a quadratic:

$$\theta = \theta_0 + a_1 x + a_2 x^2 \quad (7)$$

The constants in this equation can be evaluated from the following three boundary conditions:

$$x = 0 : \theta = \theta_0 \text{ and } \frac{\partial \theta}{\partial x} = (h/k)\theta_0 : x = t : \theta = \theta_T$$

whence the quadratic temperature function becomes:

$$\theta = \theta_0 - \left(\frac{ht}{k} \theta_0 \right) \frac{x}{t} + \left(\theta_T - \theta_0 + \frac{ht}{k} \theta_0 \right) \frac{x^2}{t} \quad (8)$$

so that the integral across the transformed layer is:

$$\int_x^t \theta dx = \left(\frac{1}{3} \theta_T + \frac{2}{3} \theta_0 - \frac{1}{6} \frac{ht}{k} \theta_0 \right) t \quad (9)$$

If this integral is substituted into equation (6), we get:

$$\rho H \frac{dt}{d\tau} - \dot{q}'' t - h\theta_0 = \frac{d}{d\tau} \left\{ \frac{1}{3} \theta_T + \frac{2}{3} \theta_0 - \frac{1}{6} \frac{ht}{k} \theta_0 \right\} t - \int_{\infty}^{\theta_T} C_o T \frac{dt}{d\tau} \dots \dots \dots \quad (10)$$

Evaluating the differential and rearranging gives:

$$\left\{ \begin{aligned} & \rho_H + \frac{1}{3} \rho_C \left(2(\theta_T - \theta_0) + \frac{ht}{k} \theta_0 \right) \frac{dt}{d\zeta} - \frac{2}{3} t \rho_C \frac{d\theta_0}{d\zeta} \\ & + \frac{1}{6} \frac{t^2 h \rho C}{k} \frac{d\theta_0}{d\zeta} = h\theta_0 + \dot{q}'' t \end{aligned} \right. \quad (11)$$

Following Hills, we now define a set of dimensionless variables:

dimensionless thickness: $t^* = ht/k$;

dimensionless temperature of cooled surface: $\theta^* = \theta_0/\theta_T$;

dimensionless time: $-\zeta = h^2 \zeta / (\rho C k)$;

dimensionless latent heat of transformation: $H^* = H/(C\theta_T)$;

dimensionless heat flux from cooled metal: $q^* = \dot{q}'' t / (-h\theta_T)$

whence equation (11) becomes:

$$H^* + \frac{2}{3} (1 - \theta^*) - \frac{1}{3} t^* \theta^* \frac{dt^*}{d\zeta} - \frac{t^*}{6} (4 + t^*) \frac{d\theta^*}{d\zeta} = \theta^* - q^*$$

..... (12)

This equation contains three unknown quantities, the thickness of the transformed layer, the surface temperature of the cooled surface and the heat flux from the layer of untransformed metal. Before the progress of the transformation process can be determined, equations must be available for these other two variables. This will allow the transformation process to be represented as the solution of three simultaneous ordinary differential equations.

An equation for the surface temperature can be derived by assuming that the $\partial\theta/\partial\zeta$ varies linearly within the

transformed layer. Thus we can write:

$$\left[\frac{\partial \theta}{\partial \tau} \right]_{x=t} = \left[\frac{\partial \theta}{\partial \tau} \right]_{x=0} + b \frac{x}{t} \quad (13)$$

The coefficient 'b' is the gradient of $\partial \theta / \partial \tau$ across the transformed layer which, since we assume a linear relation, can be expressed as:

$$b = \frac{\partial}{\partial x} \left[\frac{\partial \theta}{\partial \tau} \right]_{x=0} \quad (14)$$

The order of differentiation can be reversed so that equation (14) becomes:

$$b = \frac{\partial}{\partial \tau} \left[\frac{\partial \theta}{\partial x} \right]_{x=0} \quad (15)$$

Applying the heat transfer boundary condition, equation (4) gives:

$$\left[\frac{\partial \theta}{\partial x} \right]_{x=0} = \frac{h}{k} \theta_0 \quad (16)$$

since we are taking the air temperature as the effective temperature zero. h and k are constant so that the substitution of equation (15) into (16) gives:

$$b = \frac{h}{k} \frac{\partial \theta}{\partial \tau} \quad (17)$$

At the cooled surface, $x = 0$, we can write:

$$\left[\frac{\partial \theta}{\partial \tau} \right]_{x=0} = \frac{d\theta_0}{d\tau} \quad (18)$$

As far as the heat transfer process is concerned, the transformation temperature can be assumed to be constant. Thus we can write the following condition at the transformation front:

$$\frac{d}{d\zeta} \left[\theta(t, \zeta) \right] = \left[\frac{\partial \theta}{\partial x} \right]_{t, \zeta} + \left[\frac{\partial \theta}{\partial \zeta} \right]_t = 0 \quad (19)$$

The value of $\left[\frac{\partial \theta}{\partial x} \right]_t$ is given by the boundary condition, equation (5). Substitution of this equation into (19) and rearranging gives:

$$\left[\frac{\partial \theta}{\partial \zeta} \right]_t = - \frac{dt}{d\zeta} \left(\frac{\rho_H}{k} \frac{dt}{d\zeta} - \frac{\dot{q}_t''}{k} \right) \quad (20)$$

Substituting equations (17), (18) and (20) into equation (13) gives the following ordinary differential equation for the temperature of the cooled surface:

$$\frac{d\theta}{d\zeta} \left(1 + \frac{ht}{k} \right) = - \frac{\rho_H}{k} \left(\frac{dt}{d\zeta} \right)^2 + \frac{\dot{q}_t''}{k} \frac{dt}{d\zeta} \quad (21)$$

In terms of the dimensionless variables defined above, this becomes:

$$\frac{d\theta^*}{d\zeta} (1 + t^*) = - H^* \left(\frac{dt^*}{d\zeta} \right)^2 - q_t^* \frac{dt^*}{d\zeta} \quad (22)$$

Using equation (22) to eliminate $d\theta^*/d\xi$ from equation (12) and rearranging gives the following quadratic ordinary differential equation for t^* :

$$\Omega \frac{dt^*}{d\xi}^2 + \Gamma \frac{dt^*}{d\xi} - \Delta = 0 \quad (23)$$

where $\Omega = H^*t^*(4 + t^*)$ (24)

$$\Gamma = [6H^* + 4(1 - \theta^*) - 2t^*\theta^*] (1 + t^*) + q_t^*t^*(4 + t^*) \quad (25)$$

$$\Delta = 6(\theta^* - q_t^*) (1 + t^*) \quad (26)$$

Using the theory of quadratic equations gives:

$$\frac{dt^*}{d\xi} = \frac{-\Gamma \pm \sqrt{\Gamma^2 + 4\Delta\Omega}}{2\Omega} \quad (27)$$

As long as q_t^* is less than θ^* , $dt^*/d\xi$ will be positive.

Thus it is the positive root of equation (27) that is relevant. The value of Ω is zero at the start of the transformation process so that equation (27) gives an indeterminate value for this root under these conditions.

This indeterminacy is avoided, however, if it is remembered that the constant term in a quadratic equation is equal to the product of the two roots. The positive root can thus be expressed as:

$$\frac{dt^*}{d\xi} = 2\Lambda / \left\{ \Gamma + \sqrt{\Gamma^2 + 4\Delta\Omega} \right\} \quad (28)$$

in which form it does not suffer from any indeterminacy.

Equation (28), together with equations (24) to (26) and

equation (22), conveniently rearranged in the form:

$$\frac{d\theta^*}{d\zeta} = \frac{-H^* \left(\frac{dt^*}{d\zeta} \right)^2 - q_t^* \frac{dt^*}{d\zeta}}{1 + t^*} \quad (29)$$

constitute two out of three simultaneous differential equations. The third equation will show how q_t^* varies with dimensionless time and is to be derived for the layer of cooled metal.

The actual state of the thermal layer at any time during the cooling and transformation process depends on the cooling mode currently operating. Figure 3 illustrated the layer in a generalised way. It extends from $x = t$ to $x = t + t_C$ where t_C is its thickness. Initially, the entire billet is above the transformation temperature so that $t = 0$, the near boundary of the cooled layer is stationary, but the temperature there is falling. Once transformation has started, however, this boundary is moving into the billet but its temperature is constant. If the cooled layer has not extended, by that time, as far as the insulated surface, the other boundary will also be moving into the billet, but at a faster rate, and its temperature will also be constant - equal to the initial temperature of the billet.

In the final stages, the cooled layer will have extended to reach the insulated boundary so that this will form the remote boundary of the cooled layer, no longer moving but with its temperature falling.

The conditions at the boundaries of the cooled layer can thus be expressed as:

$$x = t : \theta = \theta_t \quad (30)$$

$$x = t : k(\partial\theta/\partial x) = - \dot{q}_t'' \quad (31)$$

$$x = t + t_C : \theta = \theta_{(t + t_C)} \quad (32)$$

$$x = t + t_C : k(\frac{\partial \theta}{\partial x}) = 0 \quad (33)$$

Equation (33) arises because the remote surface of the cooled layer is either extending into uncooled metal or is stationary at the insulated surface of the billet. In both cases, no heat can cross the surface by conduction.

As with the transformed layer, the heat conduction equation applies:

$$k \frac{\partial^2 \theta}{\partial x^2} = \rho c \frac{\partial \theta}{\partial \tau} \quad (34)$$

and is to be integrated across the entire layer from $x = t$ to $x = t + t_C$:

$$\int_t^{t+t_C} k \frac{\partial^2 \theta}{\partial x^2} dx = \int_t^{t+t_C} \rho c \frac{\partial \theta}{\partial \tau} dx \quad (35)$$

which gives:

$$k \left| \frac{\partial \theta}{\partial x} \right|_{t+t_C} - k \left| \frac{\partial \theta}{\partial x} \right|_t = \rho c \frac{d}{dt} \left\{ \int_t^{t+t_C} \theta dx \right\} - \left(\frac{dt}{d\tau} + \frac{dt_C}{d\tau} \right) \theta_{(t+t_C)} + \frac{dt}{d\tau} \theta_t \quad (36)$$

Equation (34) is comparable to equation (3) for the transformed layer and has been derived in the same way. The extra term on the right hand side arises from application

of the Leibnitz integral formula because, in the case of the cooled layer, both of the boundaries for the integration can be moving.

As in the case of the transformed layer, we represent the temperature distribution in the cooled layer in the form of a quadratic equation:

$$\theta = a_0 + a_1 \left(\frac{x-t}{t_c} \right) + a_2 \left(\frac{x-t}{t_c} \right)^2 \quad (37)$$

Choosing values of the coefficients in this equation to satisfy boundary conditions (30), (32) and (33) gives the temperature distribution in the cooled layer as:

$$\theta = \theta_{(t+t_c)} + \left[\theta_{(t+t_c)} - \theta_t \right] \left(1 - \frac{x-t}{t_c} \right)^2 \quad (38)$$

Thus the integral of the temperature distribution across the cooled layer is:

$$\int_t^{(t+t_c)} \theta dx = \left\{ \frac{2}{3} \theta_{(t+t_c)} + \frac{1}{3} \theta_t \right\} t_c \quad (39)$$

Substituting this integral into equation (36) together with boundary condition (31) and (33) and rearranging gives:

$$\dot{q}_t'' = \rho C \frac{d}{dt} \left\{ \frac{2}{3} \theta_{(t+t_c)} + \frac{1}{3} \theta_t \right\} t_c - \left(\frac{dt}{d\zeta} + \frac{dt_c}{d\zeta} \right) \theta_{(t+t_c)} + \frac{dt}{d\zeta} \theta_t \quad (40)$$

Evaluating the differentials in equation (40) and rearranging gives:

$$\dot{q}_t'' = \rho_C \frac{1}{3} t_C \left\{ 2 \frac{d\theta_{(t+t_C)}}{d\xi} + \frac{d\theta_t}{d\xi} \right\} - (\theta_{(t+t_C)} - \theta_t) \left\{ \frac{1}{3} \frac{dt_C}{d\xi} + \frac{dt}{d\xi} \right\} \dots \quad (41)$$

In terms of dimensionless numbers, equation (41) becomes:

$$q_t^* = \frac{t^* C}{3} \left\{ 2 \frac{d\theta_{(t+t_C)}}{d\xi} + \frac{d\theta_t^*}{d\xi} \right\} - (\theta_{(t+t_C)}^* - \theta_t^*) \left\{ \frac{1}{3} \frac{dt^* C}{d\xi} + \frac{dt^*}{d\xi} \right\} \dots \quad (42)$$

The heat flux from the cooled layer cannot be determined other than from the temperature distribution within the cooled layer. Thus equation (38) must be substituted into equation (31) to give:

$$\dot{q}_t'' = -k \frac{2(\theta_{(t+t_C)} - \theta_t)}{t_C} \quad (43)$$

In terms of dimensionless numbers, this becomes:

$$q_t^* = \frac{2(\theta_{(t+t_C)}^* - \theta_t^*)}{t^* C} \quad (44)$$

The elimination of q_t^* between equations (41) and (44) gives

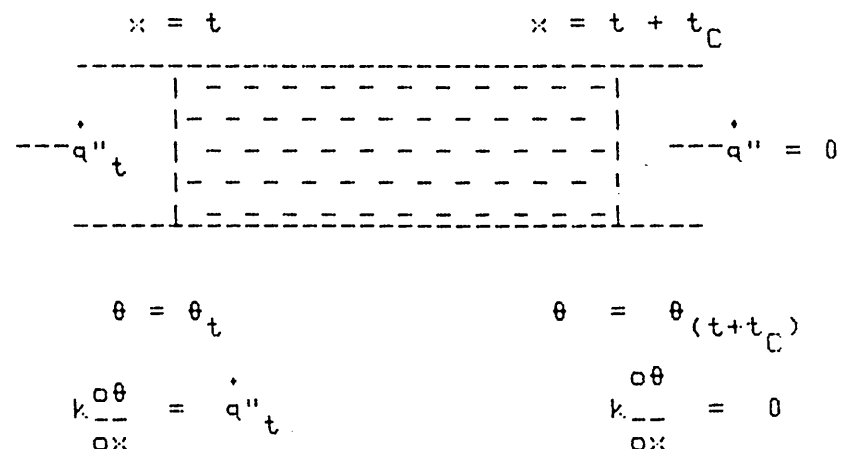


Figure 3 Generalised schematic diagram of the cooled layer

the required differential equation for the cooled layer. The actual form that this equation takes during any given stage of the cooling and transformation process depends upon the particular mode in operation. The derivation of individual equations that operate in the different modes is discussed in the different sections below. In the case of the modes in which the transformed layer is also growing, equation (44) is available to generate the values of q^*_t that are required for the evaluation of equations (28) and (29) for thickness and surface temperature of the cooled layer.

The equations for the different cooling/transformation modes are derived in the subsequent sections.

There is no transformed layer during this mode so that the cooled layer extends into the billet from the cooled surface. We can therefore write:

$$t^* = 0; \quad \theta^*(t+t_C) = \theta^*_1 = \theta_1/\theta_T; \quad \theta^*_t = \theta^*_0 \quad (45)$$

Since θ_1 is the initial temperature of the uncooled billet, it is constant so that equation (42) becomes:

$$q^*_t = -\frac{1}{3} t_C \frac{d\theta^*_0}{d\xi} - \frac{1}{3} (\theta^*_1 - \theta^*_0) \frac{dt^*_C}{d\xi} \quad (46)$$

This equation contains the differentials of the two variables that are changing - the temperature of the cooled surface and the thickness of the cooled layer. The heat flux condition at the cooled surface allows these two variables to be related. The heat flux condition at the cooled surface during this mode is obtained by equating equation (4) to equation (43) since \dot{q}''_t is equal to \dot{q}''_0 . Thus we have:

$$\dot{q}''_0 = -k \frac{2(\theta_1 - \theta_0)}{t_C} = h \theta_0 \quad (47)$$

In terms of the dimensionless numbers, this becomes:

$$\theta^*_0 = 2(\theta^*_1 - \theta^*_0)/t^*_C \quad (48)$$

and this equation can be used to eliminate one of the two variables from equation (46). It is most convenient if the thickness of the cooled layer, t^*_C is the variable that is

eliminated. Re-arranging equation (48) gives:

$$t^* C = 2(\theta^*_{-1}/\theta^*_{-0} - 1) \quad (49)$$

which, on differentiating, is:

$$\frac{dt^* C}{d\xi} = - \frac{2\theta^*_{-1}}{\theta^*_{-0}^2} \frac{d\theta^*_{-0}}{d\xi} \quad (50)$$

Substituting equations (49) and (50) into equation (46) and rearranging gives:

$$\frac{d\theta^*_{-0}}{d\xi} = \frac{-(3/2)\theta^*_{-0}^3}{\theta^*_{-1}^2 - \theta^*_{-0}^2} \quad (51)$$

This equation is to be solved from the initial starting conditions which we assume to be the entire billet uniformly heated to a temperature, θ_1 , above the transformation temperature, θ_T . Thus we can write the initial time boundary condition as:

$$\xi = 0 : \theta^*_{-0} = \theta^*_{-1} \quad (52)$$

Equation (51) can be integrated formally to determine how the surface temperature varies during this mode. The surface temperature is given by the equation:

$$\xi = \int_{\theta^*_{-1}}^{\theta^*_{-0}} \frac{2(\theta^*_{-1}^2 - \theta^*_{-0}^2)d\theta^*_{-0}}{3\theta^*_{-0}^3} \quad (53)$$

Evaluating the integral gives:

$$\xi = \frac{1}{3} \left\{ \left(\frac{\theta^*_1}{\theta^*_0} \right)^2 - 1 - 2 \ln \left(\frac{\theta^*_1}{\theta^*_0} \right) \right\} \quad (54)$$

Duration of the Semi-infinite Cooling Mode

The transformation process will always start in the semi-infinite cooling mode. The duration of this mode depends upon whether it is followed by the semi-infinite transformation mode or by the finite cooling mode.

If the surface of the billet cools to the transformation temperature before the cooled layer has expanded to occupy the entire billet, it is the semi-infinite transformation mode that follows the semi-infinite cooling mode. In this case, the duration of the semi-infinite cooling mode is given in dimensionless terms by putting θ^*_0 equal to unity in equation (54):

$$\xi_1 = 1/3 \left[\theta^*_1^2 - 1 - 2 \ln(\theta^*_1) \right] \quad (55)$$

On the other hand, if the temperature of the cooled surface is still above the transformation temperature by the time the cooled layer has expanded to occupy the entire billet, the second mode will be the finite cooling mode. If L^* is the dimensionless thickness of the billet, its surface temperature at the time the cooled layer has expanded to occupy the entire billet will be given by substituting L^* for t^*_C in equation (49). After rearrangement, there results:

$$\theta^*_0 = 2 \theta^*_1 / (2 + L^*) \quad (56)$$

Substituting this value into equation (54) and rearranging gives:

$$\xi_2 = 1/3 \left[(1 + L^*/2)^2 - 1 - 2 \ln(1 + L^*/2) \right] \quad (57)$$

Which of the two modes it is that follows the semi-infinite cooling mode will depend upon the initial temperature and upon the cooling conditions used. If the value of θ^*_0 given by equation (56) is greater than unity, then the surface will still be above the transformation temperature when the cooled layer has expanded to occupy the entire billet. Thus the critical value of θ^*_1 is given by putting θ^*_0 equal to unity in equation (56) and re-arranging:

$$\theta^*_{1,Crit.} = 1 + L^*/2 \quad (58)$$

If θ^*_1 is above this critical value, the finite cooling mode will follow the semi-infinite cooling mode. If it is not, it is the semi-infinite transformation mode that will follow.

During the finite cooling mode, the entire billet is cooling but it is above the transformation temperature at all points. Thus we can write:

$$\theta^*_{t+0} = \theta^*_0; \quad \theta^*_{(t+0)} = \theta^*_1; \quad t^* = 0; \quad t^*_{C} = L^* \quad (59)$$

so that equations (42) and (44) become:

$$-\theta^*_{00} = \frac{L^*}{3} \left\{ 2 \frac{d\theta^*_{11}}{d\xi} + \frac{d\theta^*_{00}}{d\xi} \right\} \quad (60)$$

and

$$\theta^*_{00} = \frac{2(\theta^*_{11} - \theta^*_{00})}{L^*} \quad (61)$$

Re-arranging equation (61) gives:

$$\theta^*_{11} = (L^*/2 + 1)\theta^*_{00} \quad (62)$$

Differentiating this equation and substituting into equation (60) gives:

$$-\theta^*_{00} = L^*(L^*/3 + 1) \frac{d\theta^*_{00}}{d\xi} \quad (63)$$

This mode starts to operate when the surface temperature is given by equation (56). Surface temperatures during this mode are thus given by the equation:

$$\int_{\theta^*_0}^{\theta^*_0} \frac{d\theta^*_0}{\theta^*_0} = - \frac{\xi}{L^*(L^*/\beta + 1)} \\ 2\theta^*_{-1}/(2+L^*) \quad (64)$$

The mode ends when the surface temperature has dropped to the transformation temperature ($\theta^*_{-1} = 1$). Thus the duration of the solidification mode is given by:

$$\xi_3 = L^*(L^*/\beta + 1) \ln \left[\theta^*_{-1} / (1 + L^*/2) \right] \quad (65)$$

Depending on the conditions, one or both of the above cooling modes must be completed before the metal can start to transform. Thus a transformation delay will exist.

$$\text{If: } \theta^*_0 < (1 + L^*/2)$$

then the transformation delay is given by equation (55):

$$\sum_{\text{Delay}} = \sum_1 = 1/3 \left[\theta^*_1^2 - 1 - 2 \ln(\theta^*_{1/}) \right] \quad (66)$$

$$\text{If: } \theta^*_0 > (1 + L^*/2)$$

then the transformation delay is the sum of \sum_2 and \sum_3 given by equations (57) and (65):

$$\begin{aligned} \sum_{\text{Delay}} &= \sum_2 + \sum_3 \\ &= 1/3 \left[(1+L^*/2)^2 - 1 - 2 \ln(1+L^*/2) \right] + k \left(L^*/3 + 1 \right) \ln \left[\theta^*_{1/} / (1+L^*/2) \right] \\ &\dots \dots \dots \quad (67) \end{aligned}$$

Equation (66) or equation (67), whichever is appropriate, is used in the computer programme to determine the value of the transformation delay.

In this mode, the cooled layer is still growing into uncooled metal ahead of the growing transformed layer. The development of the transformed layer is now to be described by equations (28) and (29). The value of q^*_t required for these equations is derived from the appropriate form of equation (44), the development of the cooled layer being determined from equation (42).

The conditions in the cooled layer are:

$$\theta^*_t = 1; \quad \theta^*_{(t+t_c)} = \theta^*_1; \quad t^* = t^*; \quad t^*_{C} = t^*_{C} \quad (59)$$

Equation (42) thus becomes:

$$q^*_t = (\theta^*_1 - 1) \frac{1}{3} \frac{dt^*_{C}}{d\zeta} + \frac{dt^*}{d\zeta} \quad (60)$$

This equation can be re-arranged to give:

$$\frac{dt^*_{C}}{d\zeta} = 3 \left\{ \frac{3q^*_t}{\theta^*_1 - 1} - \frac{dt^*}{d\zeta} \right\} \quad (61)$$

with q^*_t determined from the relevant form of equation (44):

$$q^*_t = \frac{2(\theta^*_1 - 1)}{t^*_{C}} \quad (62)$$

These equations are incorporated into the Runge-Kutta method used in the computer programme to solve equations (28), (29), (61); with equation (62) providing the linking value of q^*_t .

In this mode, the cooled liquid layer has expanded to occupy all the untransformed metal in the billet. The remote boundary of the cooled layer is thus stationary in the insulated surface but the temperature there is falling.

Thus we have:

$$\theta^*_{t_c} = 1; \quad \theta^*(t+t_c) = \theta^*_{T_c}; \quad t^* = t^*; \quad t^*_{C_c} = L^* - t^* \quad (63)$$

In this case, equation (42) becomes:

$$q^*_{t_c} = \frac{2}{3} \left\{ (L^* - t^*) \frac{d\theta^*_{T_c}}{d\xi} - (\theta^*_{T_c} - 1) \frac{dt^*}{d\xi} \right\} \quad (64)$$

which can be re-arranged to give:

$$\frac{d\theta^*_{T_c}}{d\xi} = \frac{\frac{3}{2} q^*_{t_c} + (\theta^*_{T_c} - 1) dt^*/d\xi}{L^* - t^*} \quad (65)$$

and equation (44) gives:

$$q^*_{t_c} = \frac{2(\theta^*_{T_c} - 1)}{L^* - t^*} \quad (66)$$

These equations are incorporated into the Runge-Kutta method used in the computer programme to solve equations (28), (29), and (65); with equation (66) providing the linking value of $q^*_{t_c}$.

C This Program predicts the rate of transformation in a steel billet
C under one dimensional heat transfer conditions.
C
C The Program uses a two Runge-Kutta subroutines named **RUKUT4** and
C **STEP4** to solve the three relevant differential equations for
C whichever cooling/transformation mode is in operation:-
C

Mode	Transformed layer		Cooled layer	
	Variable	Equation	Variable	Equation
Semi-infinite	t^*	(@.28)	t^*_C	(@.61)
"	θ^*_0	(@.29)	q^*_t	(@.62)
Finite	t^*	(@.28)	θ^*_I	(@.65)
"	θ^*_0	(@.29)	q^*_t	(@.66)

C The evaluation of the differential expressions that are the subject of
C these equations is carried out by a differentiation subroutine called
C **DIFREL** which is called by **STEP4**.
C

C The main program first calls a subroutine called **VALUES** which asks
C the operator to provide the relevant property values and process
C conditions for which predictions are to be made, the values being set
C into the un-named COMMON block used by all the subroutines.
C

C The main program then calculates the value of $(1 + L^*/2 - \theta^*_0)$ so
C that the initial transformation mode may be determined and the mode
C indicator MODE set to the appropriate value:-
C

$(1 + L^*/2 - \theta^*_0)$	Initial Transformation Mode	MODE
Positive	semi-infinte	1
Zero or Negative	finite	2

C The value of MODE is also set into common
C

C The transformation delay is then calculated together with the value
C of the dimensionless thickness of the cooled layer or of the
C dimensionless temperature of the insulated surface depending on the
C mode in which the transformation starts.
C

C Runge-Kutta integration is then commenced, the cooling layer variable
C and its corresponding equation being determined by the value of MODE.
C

C The integration is managed by the subroutine **RUKUT4** which calls
C **STEP4**. After each integration step has been completed, it is
C repeated twice with half the step length, the pairs of values for
C each variable being compared. Integration only proceeds if the values
C agree to an acceptable level of error; if not the initial step length
C is halved and the integration step re-traversed. Five such reductions
C in step-length are allowed. If integration cannot be commenced,
C **RUKUT** returns control to this main programme with the values of
C INT = 1, and JST greater than 1. These values are contained in the
C COMMON block CTRL.

C
C If the value of MODE is 1 (the current mode is the semi-infinite mode),
C the value of ($L^* - t^* - t^*_C$) is evaluated so that the change to the
C finite mode can be signalled by changing the value of MODE to 2.

C
C In order for the time of the change to be accurately determined, the
C final integration step in the semi-infinite mode is adjusted by trial
C and error before integration is restarted in the finite mode.

C
C The different sections of the main Program and indicated below with
C clear headings in common.

C
C The dimensioned dimensionless variables are defined as set out below:-

C Variable | Definition

C Variable	Definition
C KSI()	Dimensionless time
C TD()	Transformed thickness
C TCD()	Thickness of cooled layer
C TMPOD()	Temperature of the cooled surface
C TMPIND()	Temperature of the insulated surface

C
REAL LR, LD, LATENT, LTNTD, KSI(5)
DIMENSION TD(5), TCD(5), TMPOD(5), TMPIND(5)
COMMON LR, LD, COND, DNSTY, SPCFHT, H, LATENT, LTNTD, THTRNS,
1 THTAIR, THT1, THT1D, THKCNV, TIMCNV, MODE, NEXP

C
C The definitions and relevant units of the variable names in common
C are as set out below:-

C Variable | Definition

C Variable	Definition	Units
C LR	Real length of slab	m
C LD	Dimensionless length of slab	-
C COND	Thermal conductivity of metal	$\text{W} \cdot \text{m}^{-1} \text{K}^{-1}$
C DNSTY	Density of metal	$\text{kg} \cdot \text{m}^{-3}$
C SPCFHT	Specific heat of metal	$\text{J} \cdot \text{kg}^{-1} \text{K}^{-1}$
C H	Surface heat transfer coefficient	$\text{W} \cdot \text{m}^{-2} \text{K}^{-1}$
C LATENT	Heat of transformation	$\text{J} \cdot \text{kg}^{-1}$
C LTNTD	Dimensionless heat of transformation	-
C THTRNS	Transformation temperature	K
C THTAIR	Temperature of cooling air	K
C THT1	Initial temperature of billet	K
C THT1D	Dimensionless initial temperature	-
C THKCNV	Thickness conversion factor	mm
C TIMCNV	Time Conversion Factor	min
C MODE	Mode change logic switch	-

C
COMMON /CTRL/JST, INTL
CALL VALUES

C
C Determine in which mode the transformation starts

C
C the insulated surface temperature when transformation starts:-
C

IF (1 + LD/2.0 - THT1D) 2,2,1

```

1 MODE = 1
TMDDLA = (THTLD**2 - 1.0 - 2.0*ALOG(THTLD))/3
TCD(1) = 2.0*(THTLD - 1.0)
TMPIND(1) = THTLD
GO TO 3
2 MODE = 2
0TMDDLA = ((1+LD/2.0)**2 - 1.0 - 2.0*ALOG(1+LD/2.0))/3.0 +
1 LD*(LD/3.0 + 1.0)*ALOG(THTLD/(1+LD/2.0))
TCD(1) = LD
TMPIND(1) = THTLD/(1.0 + LD/2.0)

C
C Convert the dimensionless value of the delay time into the real
C delay time in minutes:-
C
3 TMDDLA = TIMCNV*TMDDLA
C
C Set and print out the initial values:-
C
TIMIN = 0
TRNSD = 0
COOLED = LR
TEMPSF = THT1
TEMPIN = THT1
KSI(2) = 0.0
TD(2) = 0.0
TCD(2) = 0.0
TMPOD(2) = THTLD
TMPIND(2) = THTLD
WRITE(2,513) NEXP, LR, LD, COND, DNSTY, SPCFHT, LATENT, THTRNS,
1THTAIR, LTNTD, THT1, THTLD, H, TIMCNV, THKONV
513 0FORMAT(1X,'THEORETICAL CALCULATIONS FOR EXPERIMENTAL RUN NUMBER ',
1I2,/1X,'DATA USED IN THE CALCULATIONS:-'/1X,'LR/m' LD
2COND/W.m-1K-1 DNSTY/kg.m-3 SPCFHT/J.kg-1K-1'/1X,F4.2,4X,
3E10.3, 8X, F4.1, 10X, E10.3, 9X, F5.1 //1X,'LATENT/J.KG-1' THTRNS/
4C THTAIR/C LTNTD THT1/C THTLD H/W.m-1K-1'/3X, E10.3, 4X,
5F5.1, 6X, F4.1, 3X, E10.3, 2X, F5.1, 2X, F5.3, 4X, F5.1//'
61X,'CONVERSION FACTORS:- TIMCNV = ', E10.3,', THKONV = ',
7E10.3//)
WRITE(2,500)
500 0FORMAT(1X,'TIME/MIN THCKNSSES/MM TEMPERATURES/C DIMENSNLSS VARI
1ABLIS(*100)'/1X,' TRNSD COOLD SURFCE INSLTD KSI T*
2 TC* TH0* TH10*' )
WRITE(2,501) TIMIN, TRNSD, COOLED, TEMPSF, TEMPIN, KSI(2), TD(2),
1 TCD(2), TMPOD(2), TMPIND(2)
501 0FORMAT(3X, F4.1, 3X, F4.0, 3X, F4.0, 4X, F4.0, 4X, F4.0, 3X,
1 5(1X, 2PF4.0))

```

```

C
C Set and print out the values at the end of the transformation delay
C
TIMIN = TMDLA
KSI(2) = TMDDLA
TCD(2) = TCD(1)
COOLED = TCD(2)*THKCNV
TMPOD(2) = 1.0
TEMPSF = THTRNS
TMPIND(2) = TMPIND(1)
TEMPIN = (THTRNS - THTAIR)*IMPIND(2) + THTAIR
WRITE(2,501) TIMIN, TRNSD, COOLED, TEMPSF, TEMPIN, KSI(2), TD(2),
1           TCD(2), TMPOD(2), TMPIND(2)

```

```

C
C Now we will calculate from the end of the transformation delay up to
C the end of the first five minute period. First of all, we calculate
C the dimensionless time interval:-
C

```

```

HINT = (5.0 - TMDLA)/TIMCNV
RELERR = 0.001
TIMREF = 0.0

```

```

C
C
C Then we set the initial values for the integration:-
C

```

```

504 KSI(1) = KSI(2)
TD(1) = TD(2)
TMPOD(1) = TMPOD(2)
GO TO (5041, 5042), MODE
5041 TCD(1) = TCD(2)
GO TO 5043
5042 TMPIND(1) = TMPIND(2)
5043 CONTINUE

```

```

C
C
C This is the sequence for calling RUKUT4:-
C

```

```

506 GO TO (5061, 5062), MODE
5061 CALL RUKUT4(KSI, TD, TMPOD, TCD, 1, HINT, HCH, RELERR)
IF (INTL .EQ. 1) GO TO 5064
IF((TD(2)+TCD(2)) .GT. LD) GO TO 507
GO TO 5063
5062 CALL RUKUT4(KSI, TD, TMPOD, TMPIND, 1, HINT, HCH, RELERR)
IF (INTL .EQ. 1) GO TO 5064
5063 HINT = 5.0/TIMCNV
GO TO 5065
5064 HINT = HINT/2.0
GO TO 506
5065 CONTINUE

```

C This is now the print out sequence:-

C

```
505 TIMIN = KSI(2)*TIMCNV
TRNSD = TD(2)*THKCNV
TEMPSF = (THTRNS - THTAIR)*TMPOD(2) + THTAIR
TEMPIN = (THTRNS - THTAIR)*TMPIND(2) + THTAIR
GO TO (5051, 5052), MODE
5051 COOLED = TCD(2)*THKCNV
GO TO 5053
5052 COOLED = (LD - TD(2))*THKCNV
5053 WRITE(2,501) TIMIN, TRNSD, COOLED, TEMPSF, TEMPIN, KSI(2), TD(2),
1           TCD(2), TMPOD(2), TMPIND(2)
IF (TRNSD .GT. 1000.0*LR) STOP
GO TO 504
```

C

C

C Now we have got to the mode change and end of transformation sequence:

C

```
507 HINT = 0.5*HINT
CALL RUKUT4(KSI, TD, TMPOD, TCD, 1, HINT, HCH, REVERR)
IF (TD(2) + TCD(2) - LD) 5071, 5071, 507
5071 TIMREF = TIMREF + HINT
KSI(1) = KSI(2)
TD(1) = TD(2)
TMPOD(1) = TMPOD(2)
TCD(1) = TCD(2)
IF (ABS(TD(2) + TCD(2) - LD) .GT. 0.001) GO TO 507
HINT = 5.0/TIMCNV - TIMREF
MODE = 2
GO TO 505
END
```

C

```

C
C SUBROUTINE RUKUT4(Y, Z, U, V, NWRITE, H1, H2, ERR)
C
C This subroutine controls the Runge-Kutta integration of four equations
C using STEP4. The differential expressions are calculated by a further
C subroutine - DIFREL - that is called by STEP4.
C
C The calling statement for this subroutine applied to the transformation
C of a steel billet is:-
C
C call rukut4(ksi, td, tmpos, tcd, hprt, hint, relerr)
C
C Comparison between the two shows the relationship between the
C variables in the calling programme and the subroutine.
C
C The steplength 'hprt' is the printing length overwhich the calling
C programme requires RUKUT to operate, 'hint' being the initial
C integration steplength that the calling programme recommends.
C
C
DIMENSION X1(5), Y1(5), Z1(5), U1(5), V1(5), Y(3), Z(3), U(3),
1 V(3)
COMMON /CTRL/JST, INTL
CT      WRITE(1,2000)
CT 2000 FORMAT(1X,'AT LEAST RUKUT4 HAS BEEN CALLED')
      Y1(1) = Y(NWRITE)
      Z1(1) = Z(NWRITE)
      U1(1) = U(NWRITE)
      V1(1) = V(NWRITE)
CT      WRITE(1,2001) Y1(NWRITE), Z1(NWRITE), U1(NWRITE), V1(NWRITE)
CT 2001 FORMAT(1X,'WITH THE FOLLOWING VALUES RECEIVED:- ')
      11X,'Y(1) = ',F6.4,'Z(1) = ',F6.4,'U(1) = ',F6.4,'V(1) = ',F6.4)
C
C The subroutine will reduce the steplength if this is necessary
C to start the integration to the accuracy set by the calling programme
C in the argument ERR. RUKUT4 counts the number of such reductions in
C the counter JST which must first be set equal to its initial value:-
C
      JST = 0
C
C
C The steplength is only reduced at the beginning of the printing
C interval, the rest of the interval being traversed at the reduced
C steplength. It is necessary to count the number of successful
C integrations so as to insure that the entire interval of 'hprt' has
C been covered. This counting is done in a counter called JINT which
C is first set to its initial value:-
C
      JINT = 1
C
C If the integration steplength that is initially successful,
C subsequently causes integration errors outside the the specified
C error band integration is aborted. The 'integration-commenced' toggle
C INTL shows whether or not this is the case. It must first be cleared:-
C
      INTL = 0
C
C The COMMON block CTRL is used to send values of INTL and JST back to

```

```

C the calling programme.
C
C STEP4 is called for the first (and any subsequent) integration(s):-
C
 40 CALL STEP4(Y1,Z1,U1,V1,H1,1)
C
C (The final integer argument in this calling statement denotes the
C position in the arrays at which integration is to start. Each time
C STEP4 is called, it returns the new values to an array position
C advanced by one.)
C
C After the first integration, integration is then repeated twice with
C half the steplength:-
C
  Y1(3) = Y1(1)
  Z1(3) = Z1(1)
  U1(3) = U1(1)
  V1(3) = V1(1)
  DO 50 JTEST = 3,4
  50 CALL STEP4(Y1,Z1,U1,V1,0.5*H1,JTEST)
C
C Followed by an instability test involving defining
C
  ER1 = ABS(Y1(2)-Y1(5))
  ER2 = ABS(Z1(2)-Z1(5))
  ER3 = ABS(U1(2)-U1(5))
  ER4 = ABS(V1(2)-V1(5))
C
C and testing:-
C
  IF (ER1.GT.ERR .OR. ER2.GT.ERR .OR. ER3.GT.ERR .OR. ER4.GT.ERR)
C
C THEN
C
  1           GO TO 65
C
C (in order to reduce the step length in search for stability)
C
C OR
C
C signal successful completion of an integration step -
C
  JINT = JINT - 1
C
C and test for successful traverse of the overall interval.-.
C
  IF (JINT) 99, 99, 39
C
C Statement 39 sets the variables for a further integration and sets
C the 'integration-commenced' toggle:-
C
C
  39  Y1(1) = Y1(5)
      Z1(1) = Z1(5)
      U1(1) = U1(5)
      V1(1) = V1(5)
      INTL = 1
      GO TO 40

```

```

C Statement 99 sets the variables for the return to the calling
C programme:-
C
CT 99 WRITE(1,4000)
CT 4000 FORMAT(1X,'(99) INTEGRATION COMPLETED - RETURN TO TRNIST')
99 Y(NWRITE + 1) = Y1(5)
Z(NWRITE + 1) = Z1(5)
U(NWRITE + 1) = U1(5)
V(NWRITE + 1) = V1(5)
INTL = 0
JST = 0
C
C and returns to the calling programme:-
C
GO TO 100
C
C
C 65 IF (INTL .EQ. 1)
C
C then the significant integration errors have occurred somewhere into the
C overall interval, and RUKUT4 returns control to the calling programme:-
C
1 GO TO 100
C
C otherwise, if integration has not started, the steplength can be reduced
C in order to obtain stable integration conditions:-
C
H1 = 0.5*H1
JST = JST + 1
JINT = 2**JST
C
C and the terminal informed -
C
WRITE(1,64) H1
64 FORMAT(' INTEGRATION STEP HAS BEEN REDUCED TO ',E10.3)
C
C No more than 5 such reductions are allowed
C so that only
C
IF (JST.LE.6)
C
C is it possible to continue the integration
C by instructing control to
C
1 GO TO 40
C
C
C Otherwise, the integration is aborted, this fact being reported to the
C terminal:-
C
WRITE(2,66) H1
66 FORMAT(' INTEGRATION HAS BEEN ABORTED WITH THE STEPLENGTH REDUCED
I TO ',E10.3)
C
C and control transferred back to the calling programme:-
C

```

C SUBROUTINE VALUES

C This programme allows data to be read into the programme

C
REAL LR, LD, LATENT, LTNTD
0 COMMON LR, LD, COND, DNSTY, SPCFHT, H, LATENT, LTNTD, THTRNS,
1 THTAIR, THT1, THT1D, THKCNV, TIMCNV, MODE, NEXP

C
C The definitions and relevant units of these variable names are as set
C out below:-

C Variable	Definition	Units
C LR	Real length of slab	m
C LD	Dimensionless length of slab	-
C COND	Thermal conductivity of metal	W.m ⁻¹ K ⁻¹
C DNSTY	Density of metal	kg.m ⁻³
C SPCFHT	Specific heat of metal	J.kg ⁻¹ K ⁻¹
C H	Surface heat transfer coefficient	W.m ⁻² K ⁻¹
C LATENT	Heat of transformation	J.kg ⁻¹
C LTNTD	Dimensionless heat of transformation	-
C THTRNS	Transformation temperature	K
C THTAIR	Temperature of cooling air	K
C THT1	Initial temperature of billet	K
C THT1D	Dimensionless initial temperature	-
C THKCNV	Thickness Conversion Factor	mm
C TIMCNV	Time Conversion Factor	min
C MODE	Mode change logic switch	-

C The default values of the variables are now set -

LR = 0.15
COND = 30.0
DNSTY = 7.6E3
SPCFHT = 546
LATENT = 81000.0
THTRNS = 710.0
THTAIR = 40.0
THT1 = 840.0
H = 236.0
NEXP = 99

C
C Checking the value of the billet length:-

101 WRITE (1,111)
1110 FORMAT (1X,'IS THE CALCULATION TO SIMULATE AN EXPERIMENTAL RUN?')
1/1X, 'ENTER 1 FOR YES OR PRESS RETURN ')
READ (1,22) NEW
22 FORMAT (I1)
IF (NEW.EQ.0) GO TO 201
WRITE (1,131)
131 FORMAT (1X,'OK - THEN ENTER THE EXPERIMENTAL RUN NUMBER IN I2 ')
READ (1,121) NEXP
121 FORMAT (I2)
201 WRITE (1,211) LR
2110 FORMAT (1X,'THE CURRENT VALUE OF THE BILLET LENGTH IS ',

1F5.3,' M')

WRITE (1,21)

READ (1,22) NEW

210FORMAT (1X, 'DO YOU WISH TO CHANGE THIS VALUE - 1 FOR YES OR 0 FOR
1 NO ')

IF (NEW.EQ.0) GO TO 202

WRITE (1,231)

231 FORMAT (1X,'OK - THEN ENTER THE NEW VALUE IN F5.3')

READ (1,221) LR

221 FORMAT (F5.3)

C
C Checking the value of the conductivity:-
C

202 WRITE (1,212) COND

2120FORMAT (1X,'THE CURRENT VALUE OF THE CONDUCTIVITY IS ',F5.1,
1' W./M.K')

WRITE (1,21)

READ (1,22) NEW

IF (NEW.EQ.0) GO TO 203

WRITE (1,232)

232 FORMAT(1X,'OK - THEN ENTER THE NEW VALUE IN F5.1')

READ (1,222) COND

222 FORMAT (F5.1)

C
C Checking the value of the density:-
C

203 WRITE (1,213) DNSTY

2130FORMAT (1X,'THE CURRENT VALUE OF THE DENSITY IS ',F5.0,' KG/M3')

WRITE (1,21)

READ (1,22) NEW

IF (NEW.EQ.0) GO TO 204

WRITE (1,233)

233 FORMAT(1X,'OK - THEN ENTER THE NEW VALUE IN F5.0 ')

READ (1,223) DNSTY

223 FORMAT (F5.0)

C
C Checking the value of the latent heat:-
C

204 WRITE (1,214) LATENT

2140FORMAT (1X,'THE CURRENT VALUE OF THE LATENT HEAT IS ',F7.0,

1' J/KG.K')

WRITE (1,21)

READ (1,22) NEW

IF (NEW.EQ.0) GO TO 205

WRITE (1,234)

234 FORMAT(1X,'OK - THEN ENTER THE NEW VALUE IN F7.0 ')

READ (1,224) LATENT

224 FORMAT (F5.0)

C
C Checking the value of the transformation temperature:-
C

```

205 WRITE (1,215) THTRNS
2150FORMAT (1X,'THE CURRENT VALUE OF THE TRANSFORMATION TEMPERATURE
    1IS ',F5.0,' C')
    WRITE (1,21)
    READ (1,22) NEW
    IF (NEW.EQ.0) GO TO 206
    WRITE (1,235)
235 FORMAT(1X,'OK - THEN ENTER THE NEW VALUE IN F5.0 ')
    READ(1,225) THTRNS
    225 FORMAT (F5.0)

```

C
C Checking the value of the air temperature:-
C

```

206 WRITE (1,216) THTAIR
2160FORMAT (1X,'THE CURRENT VALUE OF THE COOLING AIR TEMPERATURE IS '
    1,F5.0,' C')
    WRITE (1,21)
    READ (1,22) NEW
    IF (NEW.EQ.0) GO TO 207
    WRITE (1,236)
236 FORMAT(1X,'OK - THEN ENTER THE NEW VALUE IN F5.0 ')
    READ (1,226) THTAIR
    226 FORMAT (F5.0)

```

C
C Checking the value of the initial temperature:-
C

```

207 WRITE (1,217) THT1
2170FORMAT (1X,'THE CURRENT VALUE OF THE INITIAL TEMPERATURE IS ',
    1F5.0,' C')
    WRITE (1,21)
    READ (1,22) NEW
    IF (NEW.EQ.0) GO TO 208
    WRITE (1,237)
237 FORMAT(1X,'OK - THEN ENTER THE NEW VALUE IN F5.0 ')
    READ (1,227) THT1
    227 FORMAT (F5.0)

```

C
C Checking the value of the heat transfer coefficient:-
C

```

208 WRITE (1,218) H
2180FORMAT (1X,'THE CURRENT VALUE OF THE HEAT TRANSFER COEFFICIENT IS
    1',F5.0,' W/(M.K)')
    WRITE (1,21)
    READ (1,22) NEW
    IF (NEW.EQ.0) GO TO 209
    WRITE (1,238)
238 FORMAT(1X,'OK - THEN ENTER THE NEW VALUE IN F5.0 ')
    READ (1,228) H
    228 FORMAT (F5.0)

```

C
C Checking the value of the specific heat:-
C

```
209 WRITE (1,219) SPCFHT
2190FORMAT (1X,'THE CURRENT VALUE OF THE SPECIFIC HEAT IS ',F5.1,
1' J/(KG.K)')
WRITE (1,21)
READ (1,22) NEW
IF (NEW.EQ.0) GO TO 230
WRITE (1,239)
239 FORMAT(1X,'OK - THEN ENTER THE NEW VALUE IN F5.1 ')
READ (1,229) SPCFHT
229 FORMAT (F5.1)
```

C
C Finished checking the values
C

```
230 LTNTD = LATENT/(SPCFHT*(THTRNS-THTAIR))
THT1D = (THT1-THTAIR)/(THTRNS-THTAIR)
THKCNV = 1000.0*COND/H
TIMCNV = DNSTY*SPCFHT*COND/(H**2*60.0)
LD = 1000.0*LR/THKCNV
WRITE (1,4000) LTNTD, THT1D, THKCNV, TIMCNV
4000 FORMAT (1X, 'LTNTD = ', F8.2, 2X, 'THT1D = ', F5.2, 2X, 'THKCNV =
1', E10.3,/1X, 'TIMCNV = ', E10.3/)
RETURN
END
```

C

C

SUBROUTINE STEP4(Y,Z U,V,H,N)

C

C Runge-Kutta subprogram that integrates 4 simultaneous differential
C equations over an integration STEP H, set by the calling program
C the dummy variable N is the position in one dimensional arrays from
C which the subprogram reads the initial values, returning the final
C values to positions N+1. Should the differential expressions
C involve X, one variable must be X.

C

C NB STEP4 requires the further subroutine DIFREL to calculate
C the differentials. If the expressions for the differentials involve
C X, its differential must be included and put equal to 1.

C

DIMENSION Y(3), Z(3), U(3), V(3), YINC(5), ZINC(5), UINC(5),

1 VINC(5)

YA = Y(N)

ZA = Z(N)

UA = U(N)

VA = V(N)

DO 100 J = 1,4

CALL DIFREL(YA, ZA, UA, VA, ADY, ADZ, ADU, ADV)

YINC(J) = H*ADY

ZINC(J) = H*ADZ

UINC(J) = H*ADU

VINC(J) = H*ADV

IF (J-3) 101,102,100

101

YA = Y(N) + 0.5*YINC(J)

ZA = Z(N) + 0.5*ZINC(J)

UA = U(N) + 0.5*UINC(J)

VA = V(N) + 0.5*VINC(J)

GO TO 100

102

YA = Y(N) + YINC(J)

ZA = Z(N) + ZINC(J)

UA = U(N) + UINC(J)

VA = V(N) + VINC(J)

100

CONTINUE

Y(N+1) = Y(N) + (YINC(1)+2.0*YINC(2)+2.0*YINC(3)+YINC(4))/6

Z(N+1) = Z(N) + (ZINC(1)+2.0*ZINC(2)+2.0*ZINC(3)+ZINC(4))/6

U(N+1) = U(N) + (UINC(1)+2.0*UINC(2)+2.0*UINC(3)+UINC(4))/6

V(N+1) = V(N) + (VINC(1)+2.0*VINC(2)+2.0*VINC(3)+VINC(4))/6

RETURN

END

C

C

```
SUBROUTINE DIFREL(Y,Z,U,V,DY,DZ,DU,DV)
REAL LR, LD, LATENT, LTNTD
0 COMMON LR, LD, COND, DNSTY, SPCFHT, H, LATENT, LTNTD, THTRNS,
1           THTAIR, THT1, THT1D, THKCNV, TIMCNV, MODE, NEXP
```

C

C

C The actual equations involved in DIFREL depend on the mode that is in
 C operation. In both modes, $y = \text{ksi}$, $z = \text{td}$, and $u = \text{tmpod}$. The
 C equations for the last two variables are (6.28) and (6.29) respectively
 C and these equations involve q^*_t . It is the form of the equation
 C for this variable that depends upon the mode.

C

C In the semi-infinite mode, when MODE = 1, the equation for q^*_t is
 C equation (62) which involves the cooled layer thickness, tcd ($v = \text{tcd}$
 C in this mode), so that DV is the differential of this cooled layer
 C thickness - given by equation (6.61).

C

C In the finite mode, MODE = 2, the equation for q^*_t is equation
 C (66) which involves the temperature of the insulated surface, tmpind
 C ($v = \text{tmpind}$ in this mode) so that DV is the differential of this
 C temperature - given by equation (6.65).

C

```
DY = 1.0
GO TO (401, 402), MODE
401 Q = 2.0*(THT1D - 1.0)/V
      GO TO 403
402 Q = 2.0*(V - 1.0)/(LD - Z)
403 OMEGA = LTNTD*Z*(4.0 + Z)
      ADLAM = (6.0*LTNTD + 4.0*(1.0-U) - 2.0*Z*U)*(1.0+Z) + Q*Z*(4.0+Z)
      GAMMA = 6.0*(U-Q)*(1.0+Z)
      ARGMNT = ADLAM**2 + 4.0*GAMMA*OMEGA
```

C

C During the initial attempts to establish stability in the Runge-Kutta
 C regime, ARGMNT might be incorrectly negative. In order to allow
 C computation to continue for stability to be established, a positive
 C value of ARGMNT must be presented to the SQRT function:

C

```
IF (ARGMNT .LT. 0.0) ARGMNT = - ARGMNT
DZ = 2.0*GAMMA/(ADLAM + SQRT(ARGMNT))
DU = -(LTNTD*DZ**2 + Q*DZ)/(1.0+Z)
      GO TO (404, 405), MODE
404 DV = 3.0*(Q/(THT1D - 1.0) - DZ)
      GO TO 406
405 DV = - (1.5*Q + (V - 1.0)*DZ)/(LD - Z)
406 RETURN
      END
```

C

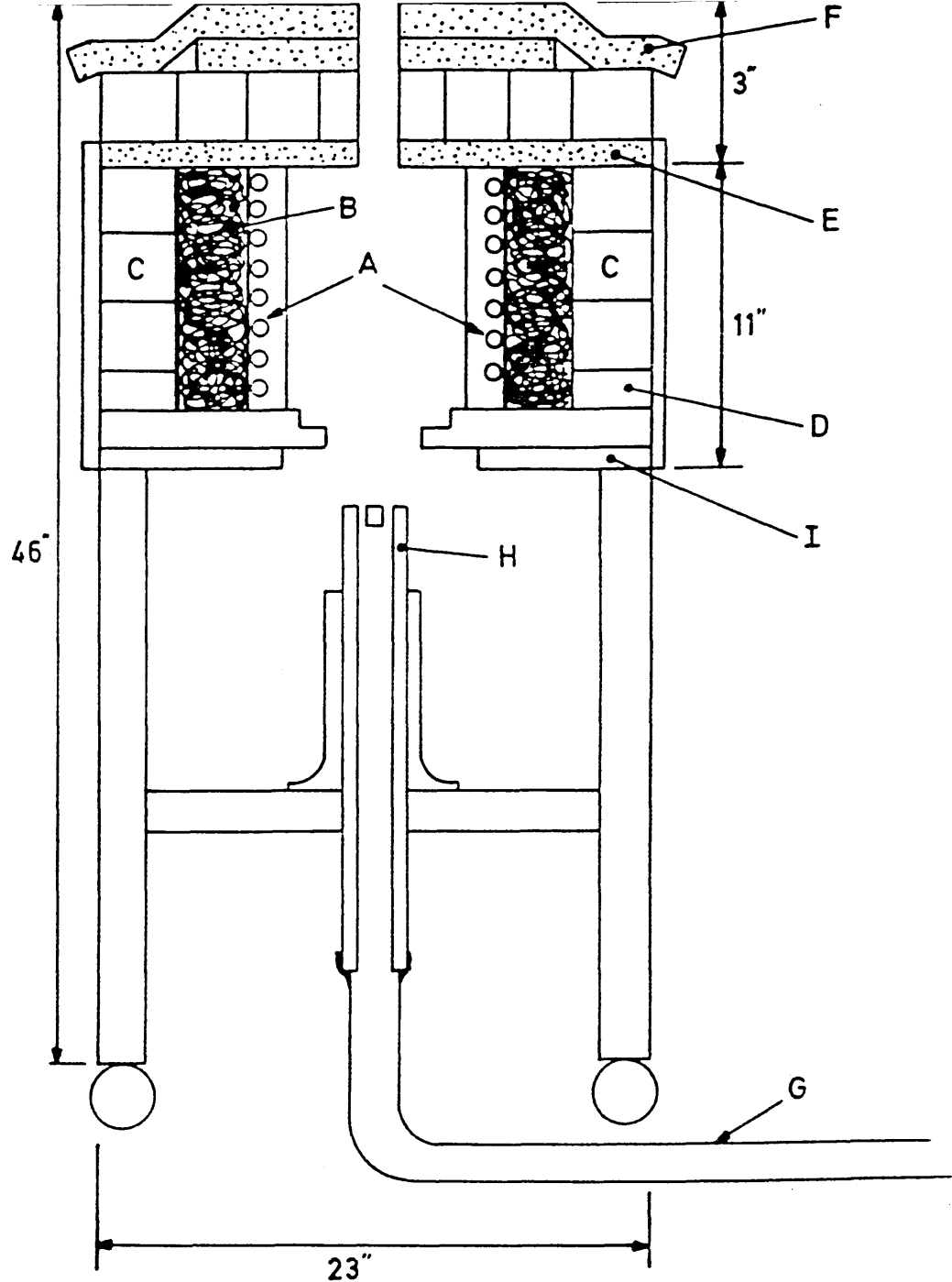
4.1 DESIGN OF THE APPARATUS

An apparatus was designed to study heat transfer and transformation kinetics in steels. This consists of a metal case, which is lined with H.G.I. insulating bricks. The base is made of a 23cm x 23cm x 2.5cm thick syndanyo plate with an 15.2cm diameter recessed hole. At the centre of the base is placed an 20.3cm ID x 25.4cm OD x 20.3cm high electrical heater with 3 Kw of power and 240 volts. The space between this and the side insulating bricks is packed with Kaowool bulk fibre (Triton). The top is made of H.G.I. insulating bricks unit, a layer of Kaowool board (Triton) above and below, and covered with a Kaowool blanket (Triton). More details in Figure 4.

Also used are 1.5 mm x 1 m Chromel-Alumel pyrote max thermocouples, 50 BM Variac transformer, an ammeter and a Leeds and Northrup Speedimax Multi-Point chart recorder.

In order to obtain one dimensional heat flow, the apparatus was designed with thermally insulating sides and with heat removal from the base only.

Heat removal by convection is obtained by directing a cold air blast onto the base. (Details of the cooling system are given in Section 4.2).



- A = HEATER 20.3cm ID X 25.4cm OD X 26.4cm HIGH 3 KW 240 V
 B = KAOWOOL BULK FIBRE (TRITON)
 C = H.G.I. INSULATION BRICKS
 D = METAL CASE
 E = KAOWOOL BOARD (TRITON)
 F = KAOWOOL BLANKET (TRITON)
 G = FLEXIBLE TUBE FROM BLOWER
 H = ADJUSTABLE BLOWER NOZZLE
 I = 23cm X 23cm X 2.5cm THICK SYNDANYO WITH 15.2cm DIA
 RECESSED HOLE

Figure 4 Diagram of Apparatus.

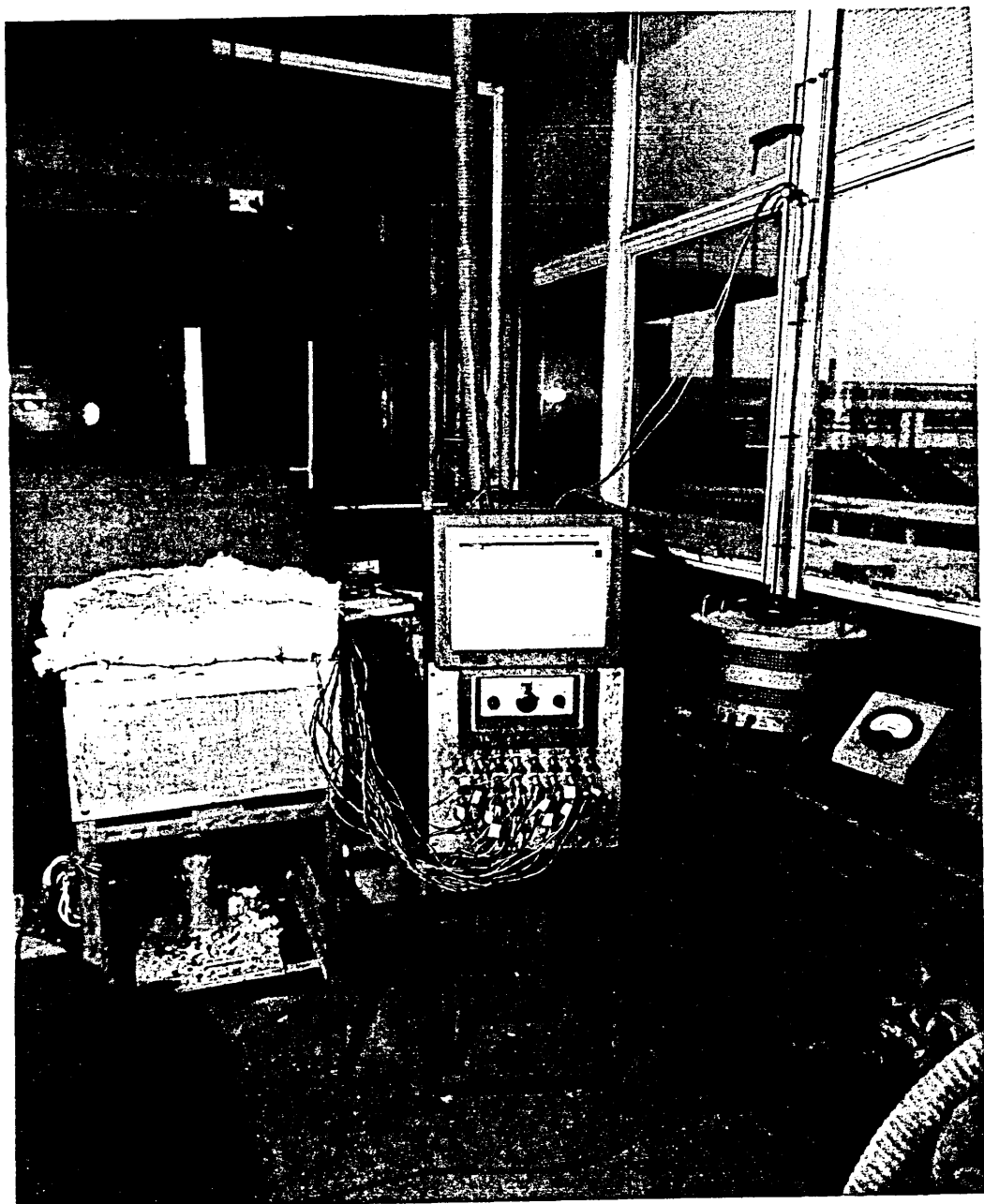


Figure 4A Apparatus used to study heat transfer and transformation.

4.2 COOLING SYSTEM

A five horse power centrifugal blower is available to provide the cold air blast. This blower gives a maximum air flow rate of 37.4 litres/s through the cooling system (pipework, orifice plate and multiple nozzle), which gives a heat transfer coefficient from the solid metal to the cooling air in the range of 130 to 220 W/m²-C. (The measurement of the heat transfer coefficient is described in Sections 4.3 and 4.4). The air blast is blown through a seven centimeters diameter pipe work with a seven centimeters diameter flexible pipe where required. The air flow is controlled by a gate valve and measured by an orifice plate with a 2.6 centimeters diameter orifice and pressure tappings at distances of one pipe diameter (upstream) and half a pipe diameter (downstream).

The pressure drop across the orifice plate is measured by a water manometer.

The multiple nozzle was designed with three factors in mind. The air blast has to be directed from a seven centimeters diameter pipe onto the fifteen centimeters diameter steel sample base. A high mean value of the heat transfer coefficient is required but a uniform distribution of the local heat transfer coefficient over the steel sample base must be maintained. Heat transfer from surfaces to impinging air jets from multiple nozzle is a complex situation for which no

theoretical solution is available. Little experimental work has been done on the subject but some useful work has been reported by Huang⁽⁴²⁾ who studied heat transfer coefficients for air flow through round, holed multiple nozzle impinging normally onto a heat transfer surface. Huang studied the effects of changes in D' , N/D' , Y/D' and A_f on the distribution of the local heat transfer coefficient over the heat transfer surface and on the value of the mean heat transfer coefficient for the surface. In this work D' represents the diameter of the nozzle hole, N is the spacing between the nozzle and the heat transfer surface, Y is the spacing between the nozzle holes and A_f is the ratio of the total area of nozzle holes to the area of the heat transfer surface expressed as a percentage. Huang worked with hole sizes from 0.317 cms diameter to 0.635 cms diameter and Reynolds Numbers (based on the hole diameter as the characteristic length) from 10^3 to 10^4 .

Huang found that in order to obtain a uniform distribution of the local heat transfer coefficient N/D' should be of the order of twelve or greater. In this range of N/D' values the Y/D' and A_f values have very little effects.

In order to obtain a high value for the mean heat transfer coefficient A_f should be approximately five per cent.

The nozzle used in this work is based on Huang's

results. The value of D' is 0.476 cms and the Reynolds Number is in the region 10^3 to 10^4 . The value of N is 6 cms, 8.5 cms and 9.6 cms and these give N/D' greater than thirteen in order to approach a uniform distribution of the local heat transfer coefficient. A_f is approximately five per cent in order to obtain a high value for the mean heat transfer coefficient. The nozzle used is shown in Figure 5. The arrangement of the holes was selected to give a regular distribution of the holes. The inclination of the holes was chosen to expand the jet centre line positions from the seven centimeters diameter nozzle plate to the comparable positions on the fifteen centimeters diameter steel sample base over the spacing distance (N) of 6 cms, 8.5 cms and 9.6 cms. The measurement of the mean heat transfer coefficient for this nozzle is discussed in Sections 4.3 and 4.4.

In order to evaluate the volumetric flow rate of air from the manometric reading across the orifice plate, the formulae shown⁽⁴³⁾ below were used:

$$\begin{aligned}\bar{V}_o &= K_f \sqrt{\frac{2}{\rho} (P_1 - P_2)} \\ K_f &= 0.65 \\ \rho &= 1.29 \text{ Kg/m}^3 \\ P_1 - P_2 &= \Delta p \\ \dot{V} &= \bar{V}_o \times A_o \\ A_o &= 5.31 \text{ cm}^2\end{aligned}$$

For the evaluation of the pressure drop the formulae overleaf was used⁽⁴⁴⁾:

$$\Delta p = H_0 \rho g$$

$$H_0 = 0 \text{ cm}, 5 \text{ cm}, \dots, 100 \text{ cm}$$

$$\rho = 1 \text{ gr/cm}^3$$

$$g = 981 \text{ cm/s}^2$$

An independent check was made against a rotameter,
and the results are presented in Tables No. 1 and No. 2.

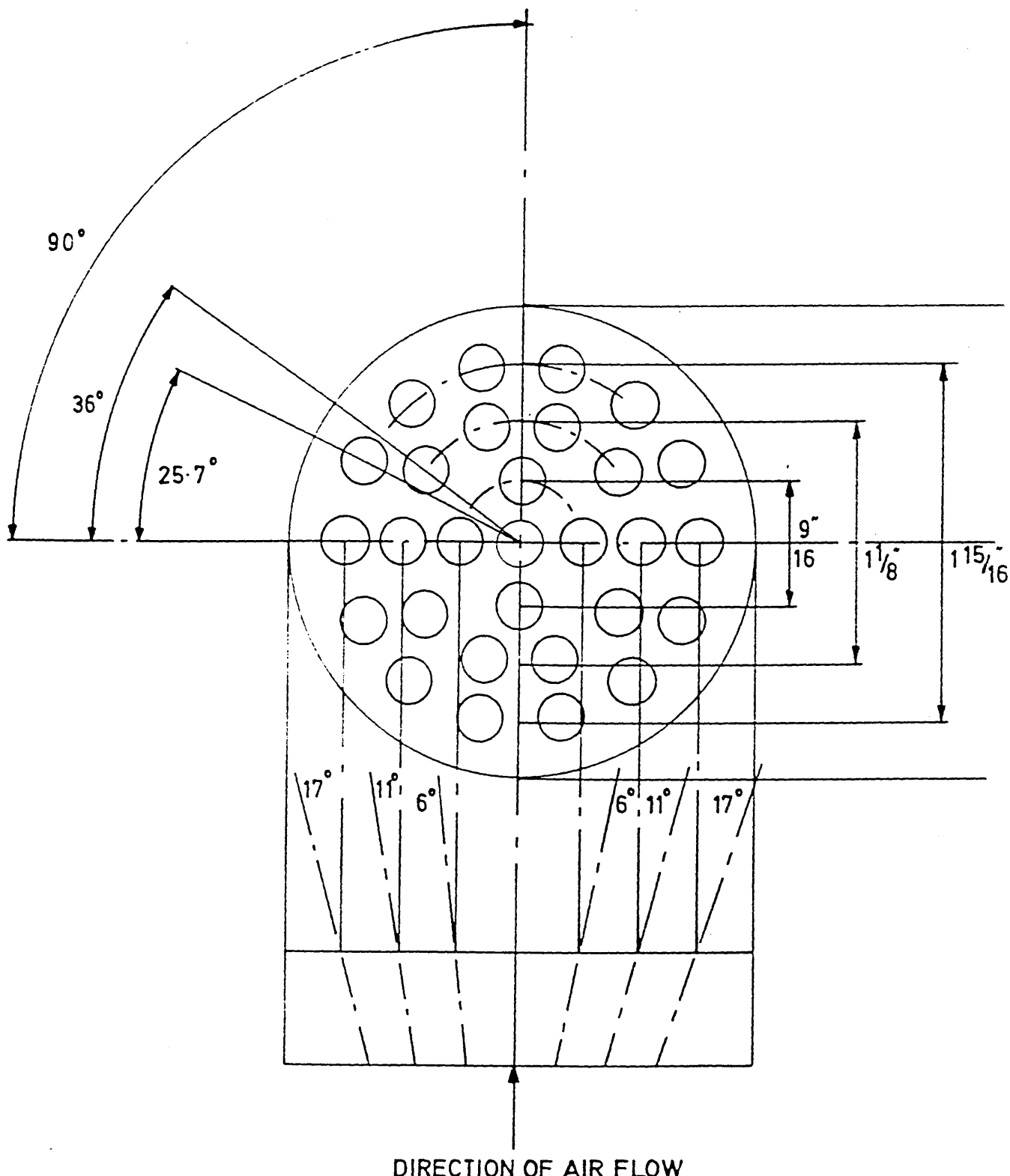


Figure 5 Multiple nozzle.

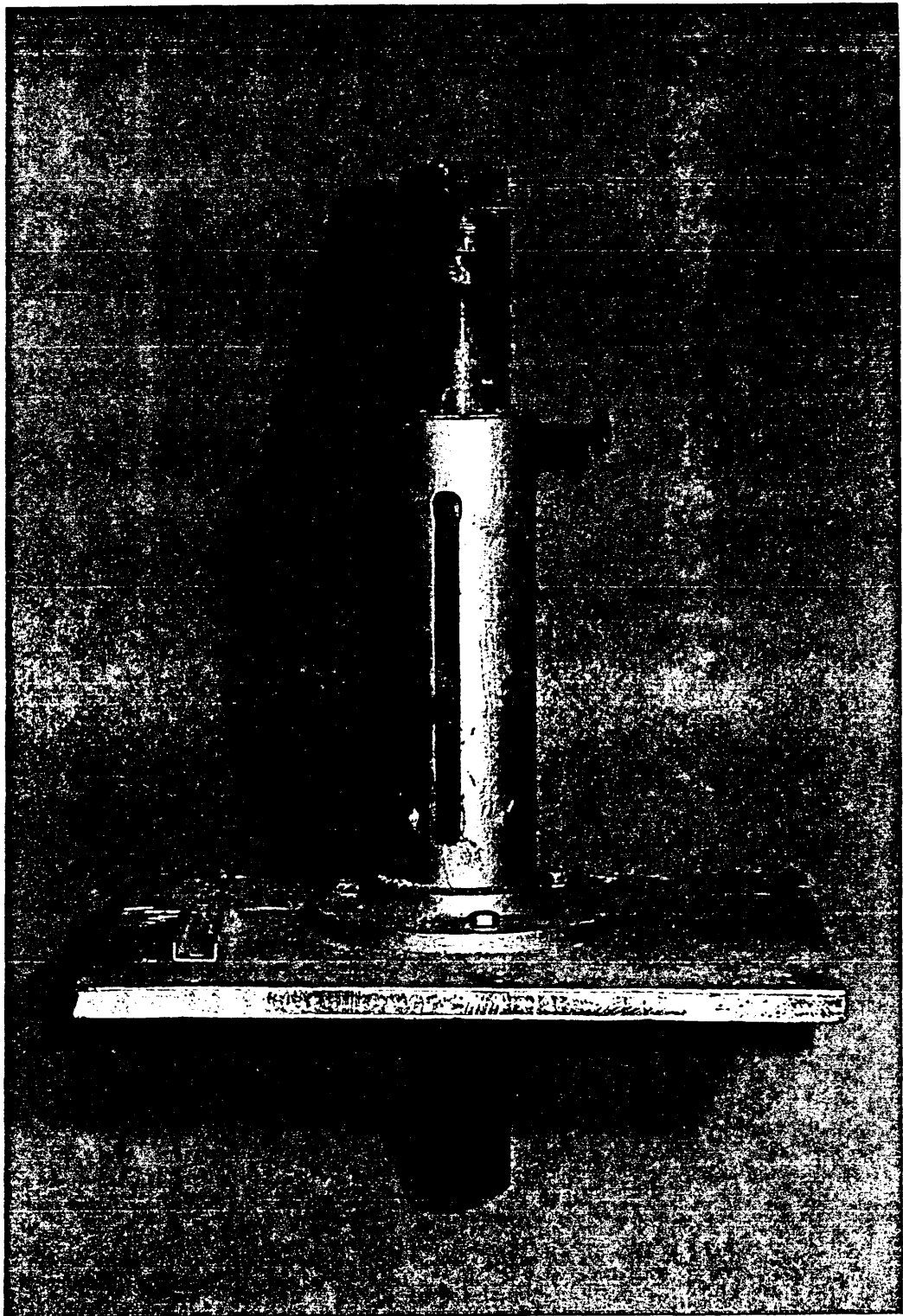


Figure 5A Multiple nozzle.

H (cms)	\sqrt{H} (cms)	Δp (N/m ²)	\bar{v}_o (m/s)	\dot{V} (litres/s)
0	0	0	0	0
5	2.24	791	17.9	9.5
10	3.16	981	25.4	13.5
15	3.87	1470	31.1	16.5
20	4.47	1960	35.9	19.0
25	5.00	1750	30.1	21.3
30	5.78	1940	43.9	23.3
35	5.92	3420	47.4	25.2
40	6.32	3920	50.7	26.9
45	6.71	4410	53.8	28.5
50	7.07	4910	56.7	30.1
55	7.42	5400	59.5	31.6
60	7.75	5890	62.1	33.0
65	8.06	6380	64.6	34.3
70	8.37	6870	67.1	35.6
75	8.66	7360	69.4	36.9
80	8.94	7850	71.7	38.1
85	9.22	8340	73.9	39.2
90	9.49	8830	76.1	40.4
95	9.75	9320	78.1	41.5
100	10.00	9810	80.2	42.6

TABLE No. 1

Calculated flow rates against manometric height

MANOMETER HEIGHT (cms)	5	10	15	20
ROTAMET. MEASURED (cms)	8.5	13.2	16.4	19.2
AIR FLOW RATE (litres/s)	9.4	13.2	13.8	18.0

TABLE No. 2

Measured rotameter flow against orifice manometer reading

4.3 MEASUREMENT OF THE HEAT TRANSFER COEFFICIENT

BY A MASS TRANSFER ANALOGY

In order to get a reliable value for the heat transfer coefficient from the surface of the steel sample base to the cooling air, two independent methods were used to evaluate it. One of these methods depended on steady state heat transfer and is described in Section 4.4; the other method was a mass transfer analogy.

This depends on the fact that convective mass transfer and convective heat transfer can be described by analogous mathematical expressions. Thus, if the mass transfer coefficient can be determined for a given geometry the heat transfer coefficient can be calculated from it.

The mass transfer method used was developed by Dauckwerts and Anolick⁽⁴⁵⁾ who used it to measure mass transfer from grid packing to an air stream. They deposited a uniform thin film of naphthalene on the grid packing and studied its evaporation by the air stream. The mean mass transfer coefficient was measured by weighing after different periods of time. In the present work, a naphthalene replica was made of the steel sample surface by casting into a cavity in a perspex plate. The plate is illustrated in Figure 7. This replica was then placed over the multiple nozzle described in Section 4.2, at different distances from the nozzle surface.

Three different methods were used to obtain a compact uniform surface of solid naphthalene of small

crystal size:

- (a) The naphthalene was melted slightly above the fusion point and poured into the cavity in the perspex plate to solidify it. It was impossible to get a uniform surface of solid naphthalene.
- (b) The naphthalene was melted in the same way and poured into the cavity in the perspex plate which was exposed to vibration. A uniform surface of solid naphthalene could not be obtained in this way either.
- (c) This method was different from the others because the naphthalene was poured into the perspex plate through an aluminium plate with a circular tube at the centre of it. An uniform surface of solid naphthalene was obtained because the surface was formed by rapid solidification against the aluminium plate.

The c method was chosen for the experiment (see Figures 6 and 7). The air blower was run until an equilibrium input air temperature was obtained. This was measured by a thermometer placed periodically just above the nozzle. The naphthalene surface was then exposed to the air blast in the steel sample geometry. The rate of weight loss of the naphthalene was measured and from this the mass transfer coefficient was obtained. The variation of mass transfer coefficient (and by analogy

4/12

heat transfer coefficient) with air flow rate was investigated. Visual qualitative examination of the naphthalene surface after it had been exposed to the air blast for long periods (up to four and a half hours) showed no obvious non-uniformity of the surface. This supported the existence of a uniform distribution of the local mass transfer coefficient. Details of the results and the method of calculation are given in Section 5.1.

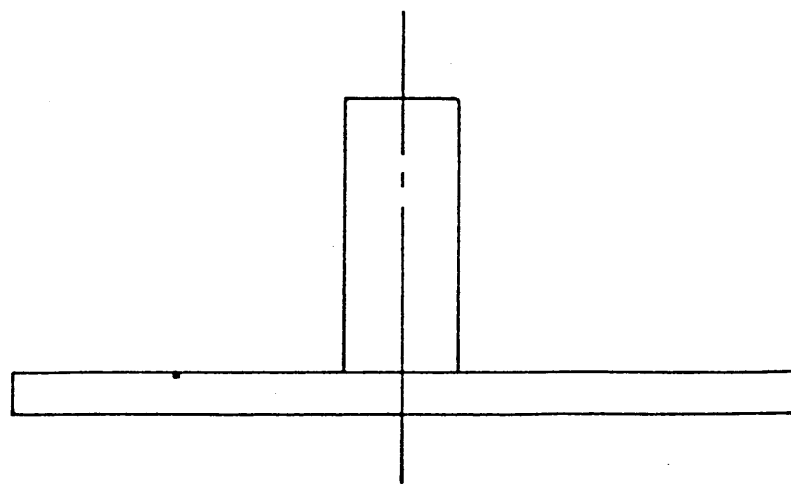
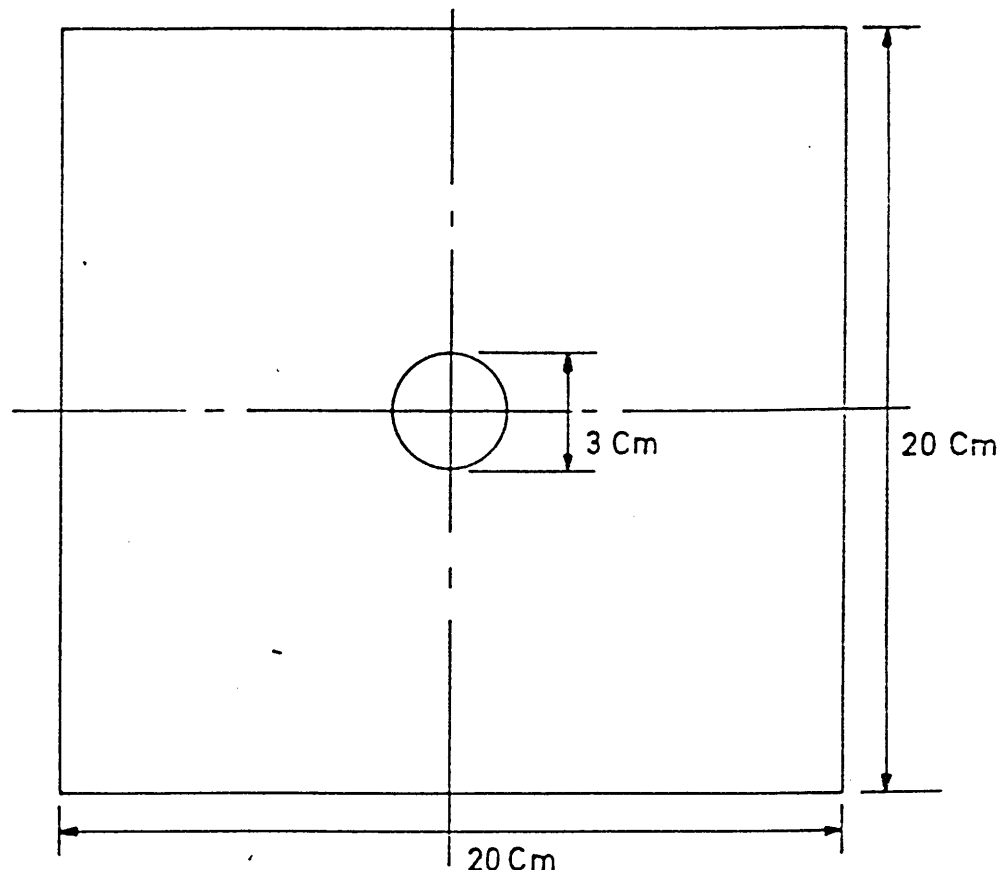


Figure 6 Aluminium plate.

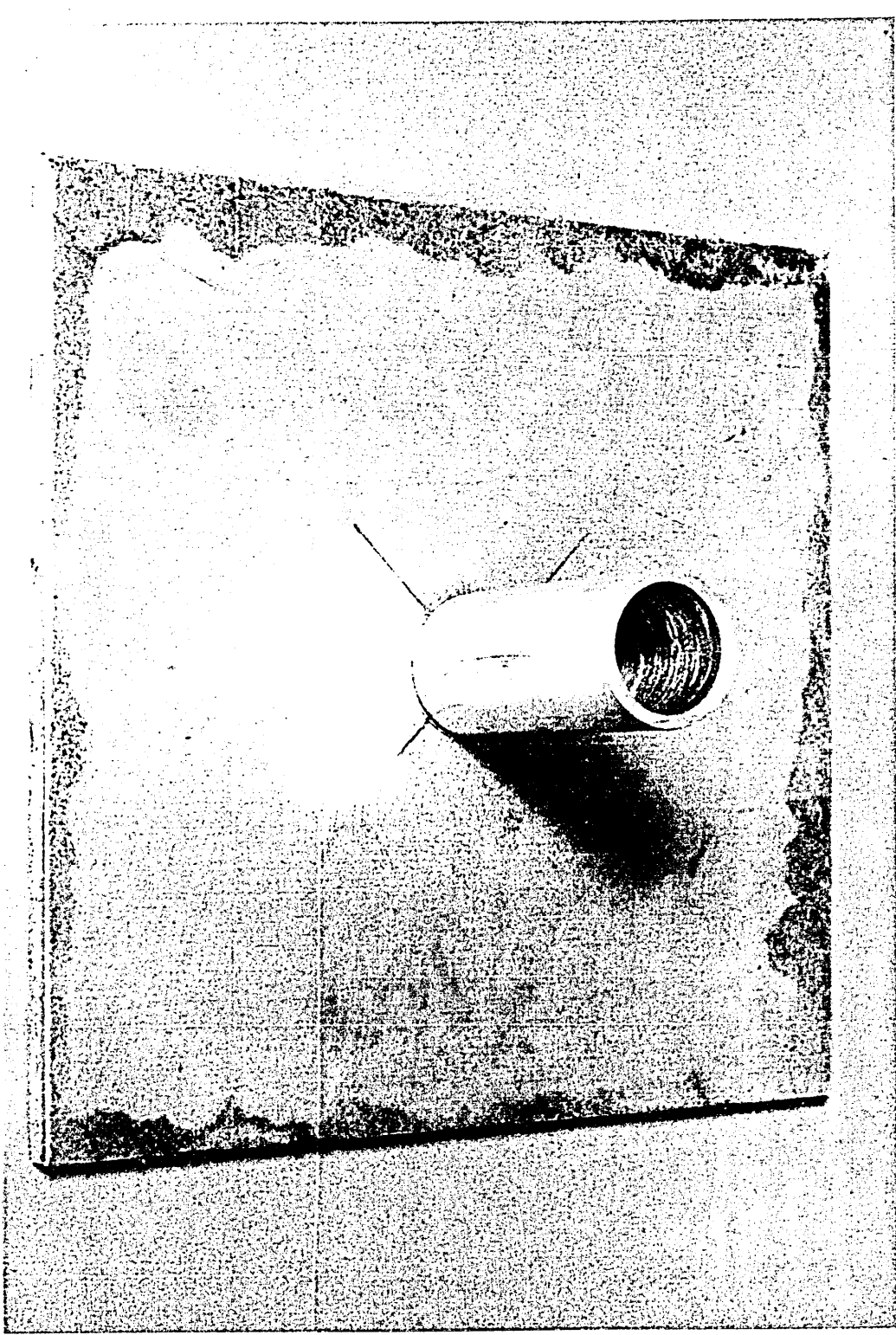


Figure 6A Aluminium plate.

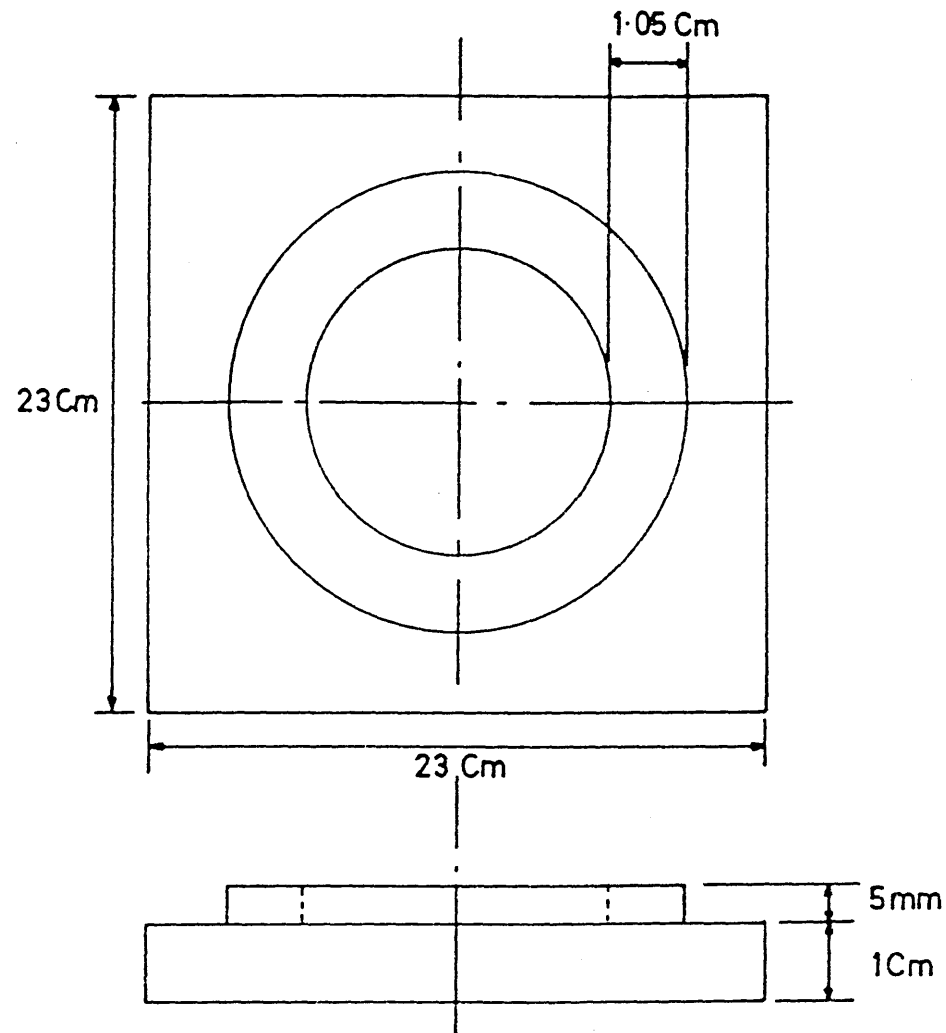


Figure 7 Perspex replica.

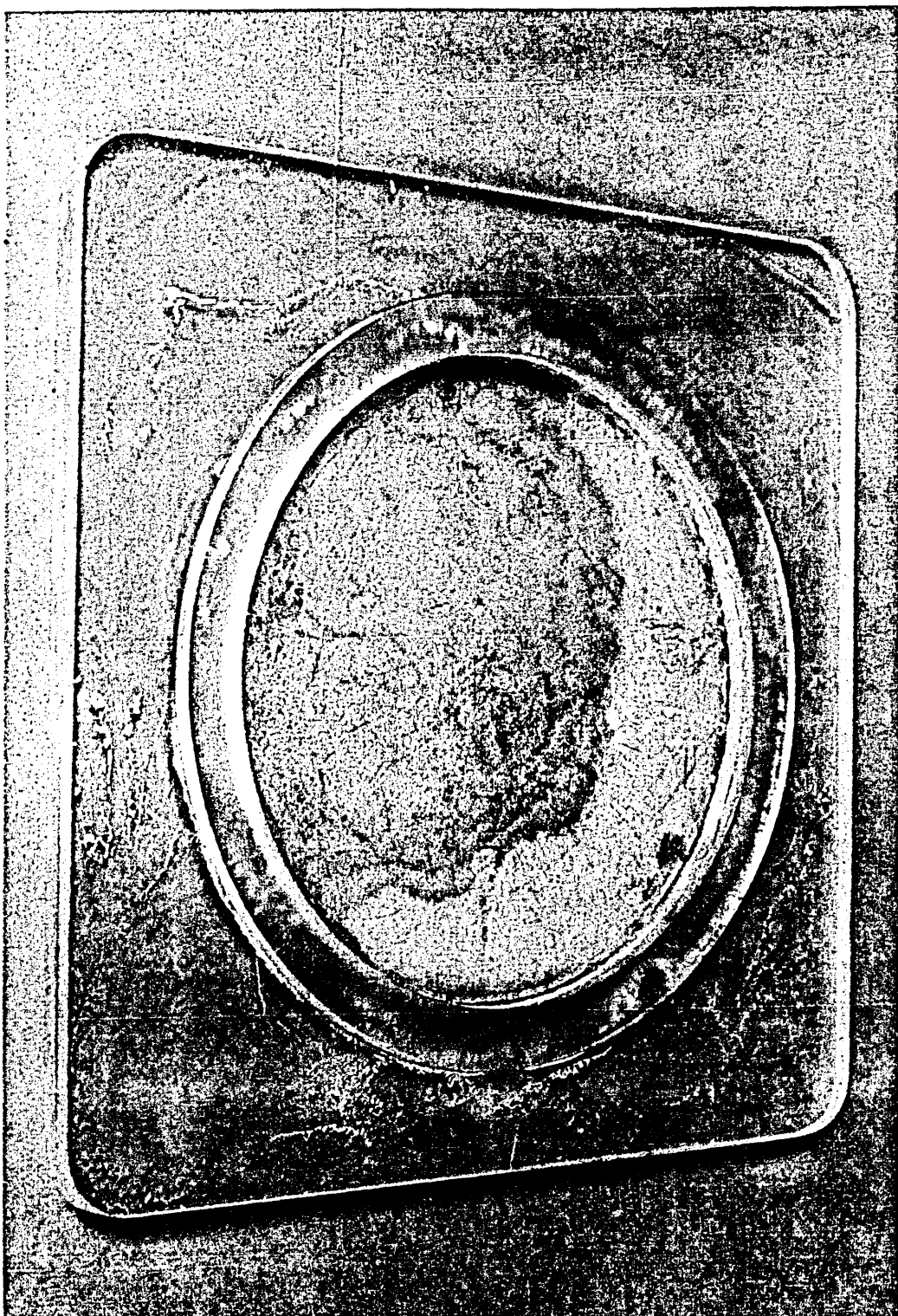


Figure 7A Perspex replica.

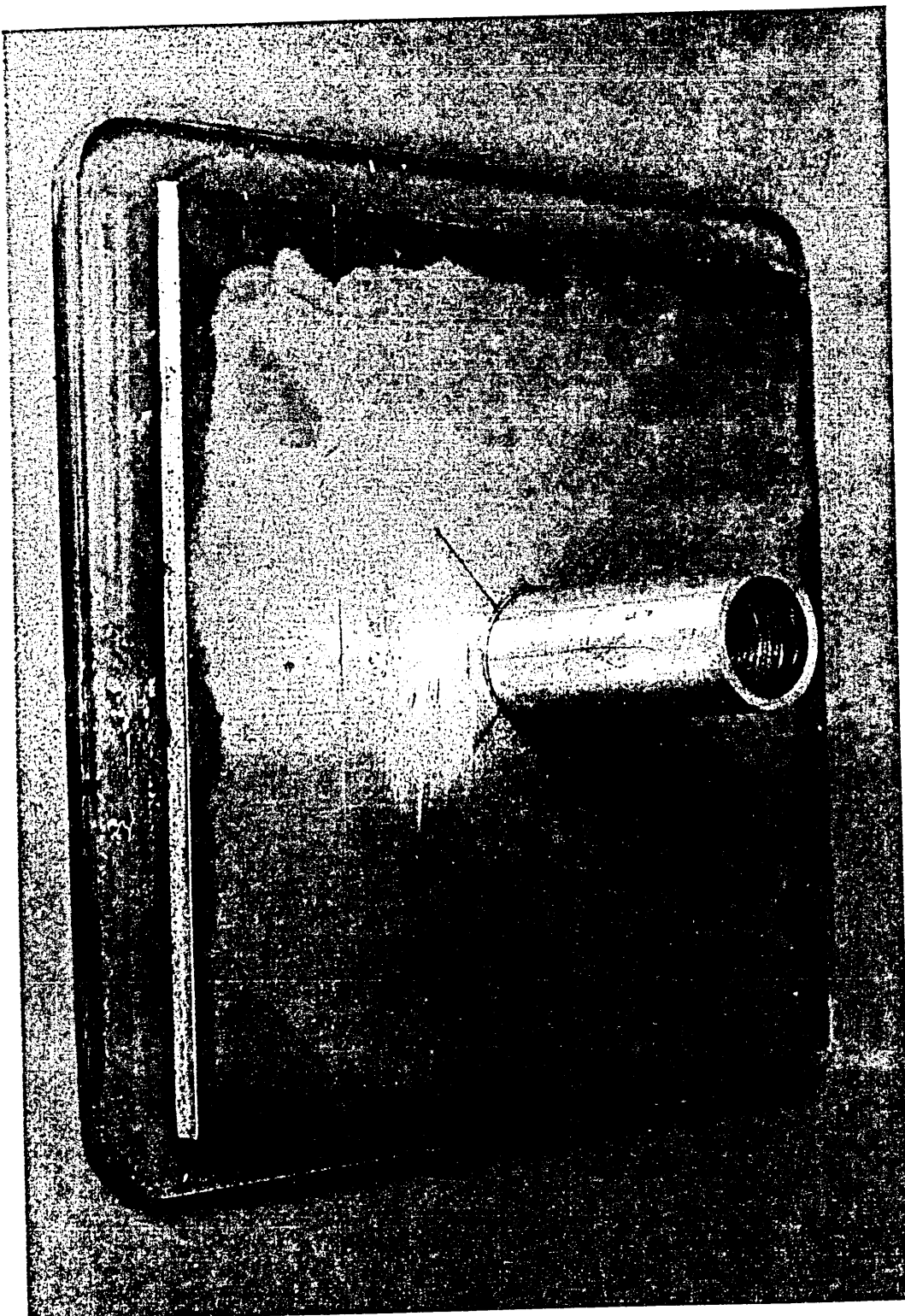


Figure 7B Perspex replica with the Aluminium plate.

4.4 MEASUREMENT OF THE HEAT TRANSFER COEFFICIENT

BY STEADY STATE HEAT TRANSFER

The apparatus shown in Figure 4 was used for these experiments. Also used are a copper disc of sixteen centimeters diameter and one centimeter thick, four Inconel thermocouples (Chromel-Alumel), an electric cooker element of two Kwatts of power, 50 BM Variac transformer, a recorder of temperature, an Ammeter and a Voltmeter. The thermocouples were arranged in the copper disc to measure the average temperature; details in Figure No. 8. The electric cooker element was used for heating the copper disc. These experiments were performed under conditions of steady state heat transfer. When the whole unit was at thermal equilibrium, the cold air blast and the power to the electric cooker element were turned on simultaneously. Under these steady state conditions the heat produced by the electric cooker element is conducted through the copper disc and removed by the cold air blast. Several experiments were performed at different temperatures of the copper disc. The heat flow needed for the calculation of the heat transfer coefficient can be obtained measuring the Voltage and the Amperage of the circuit used. Details of the results and the method of calculation are given in Section 5.2.

4.5 PROFILE OF TEMPERATURE IN THE SAMPLE OF
STEEL AT 500°C, 600°C 700°C AND 800°C
WITHOUT AIR COOLING

The sample used was a cylinder of carbon steel 15 centimeters in diameter and 15 centimeters in height.

Thirteen Chromel-Alumel thermocouples were distributed in the steel sample in order to get the profile of temperature in it, positioned as follows:

One central thermocouple at 40 mm, 60 mm, 100 mm and 120 mm from the bottom of the steel sample.

Four radially placed thermocouples at 20 mm, and 80 mm from the bottom of the steel sample.

One central thermocouple in a surface slot (see Figure No. 10).

After that the steel sample was allocated into the apparatus described in Section 4.1 and the power was turned on, until the temperature had reached 500°C approximately. The temperature for each thermocouple was recorded. The same method was used for the experiments at 600°C, 700°C and 800°C. Details of the results are given in Section 5.3.

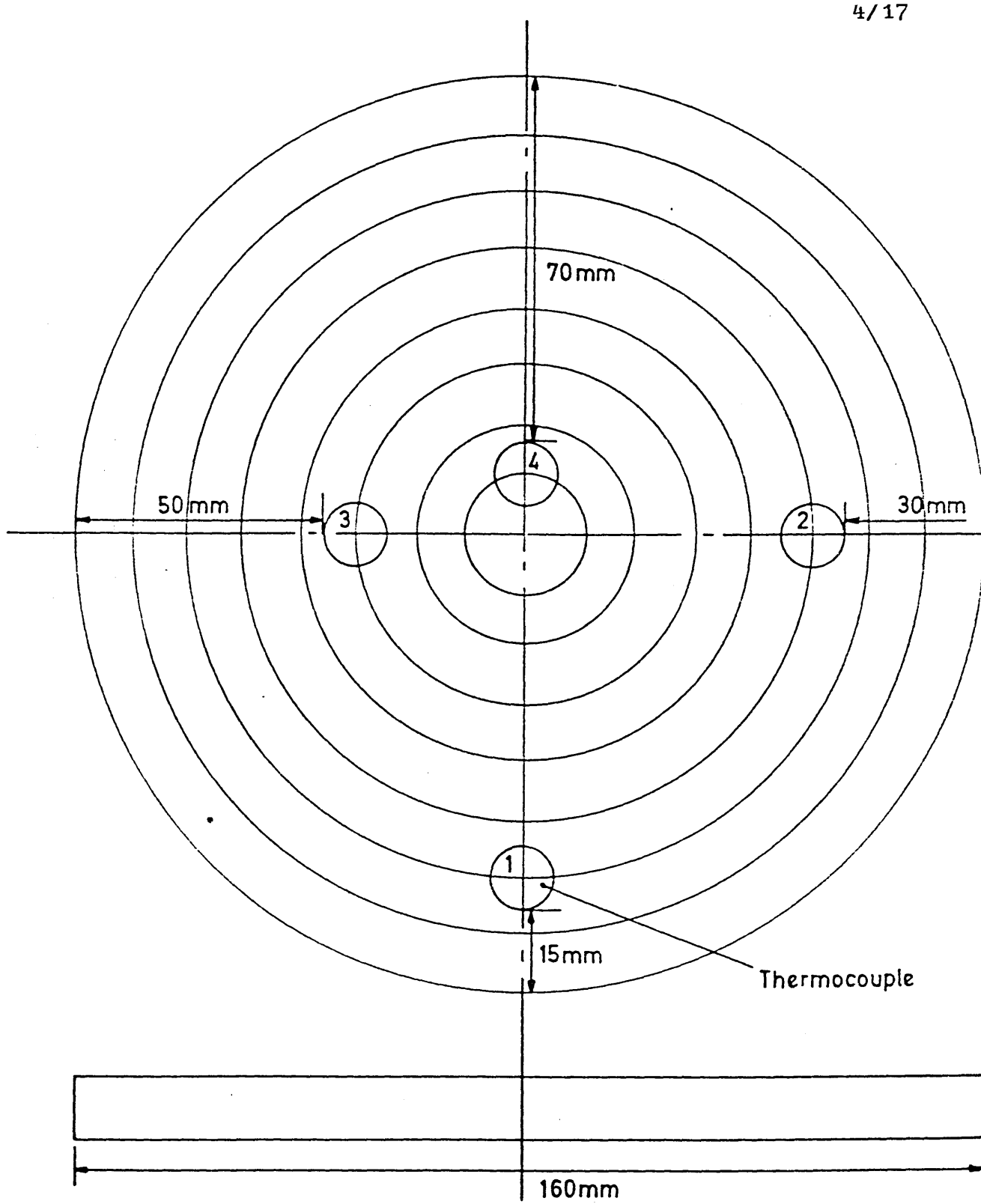


Figure 8 Copper disc and thermocouples position.



Figure 8A Copper disc and thermocouples position.

4.6 PROFILE OF TEMPERATURE IN THE SAMPLE OF STEEL

AT 850°C WITH AIR COOLING

The cylinder sample of 15 centimeters diameter and 15 centimeters height of carbon steel was used for these experiments (see Figure 9). The sample with the thermocouples positioned in it, was allocated into the apparatus described in Section 4.1 and the power was turned on, until the temperature had reached 850°C approximately, then the power was turned off and, simultaneously, the air blast turned on. Experiments were carried out with different heat transfer coefficients. The temperatures of the axial thermocouples were recorded for one and a half hours of each experiment.

These experiments were not very good because the gradient of temperature in the sample at the start of cooling was very large. After that, the experiments were improved to decrease the initial gradient of temperature. The sample was completely insulated with refractories during the time it was being heated up to temperature by the insertion of a porous alumina refractory disc between the bottom of the sample and the cooling nozzle. This disc was then removed immediately prior to the cooling process. Several experiments were carried out with this improvement. Details of the results are given in Section 5.4.

4.7 CHEMICAL COMPOSITION OF THE STEEL USED

The steel used had the following chemical composition:

C	Mn	Si	S	P	Ni	Cr	Mo
0.72	0.71	0.17	0.017	0.028	0.02	0.03	<0.01

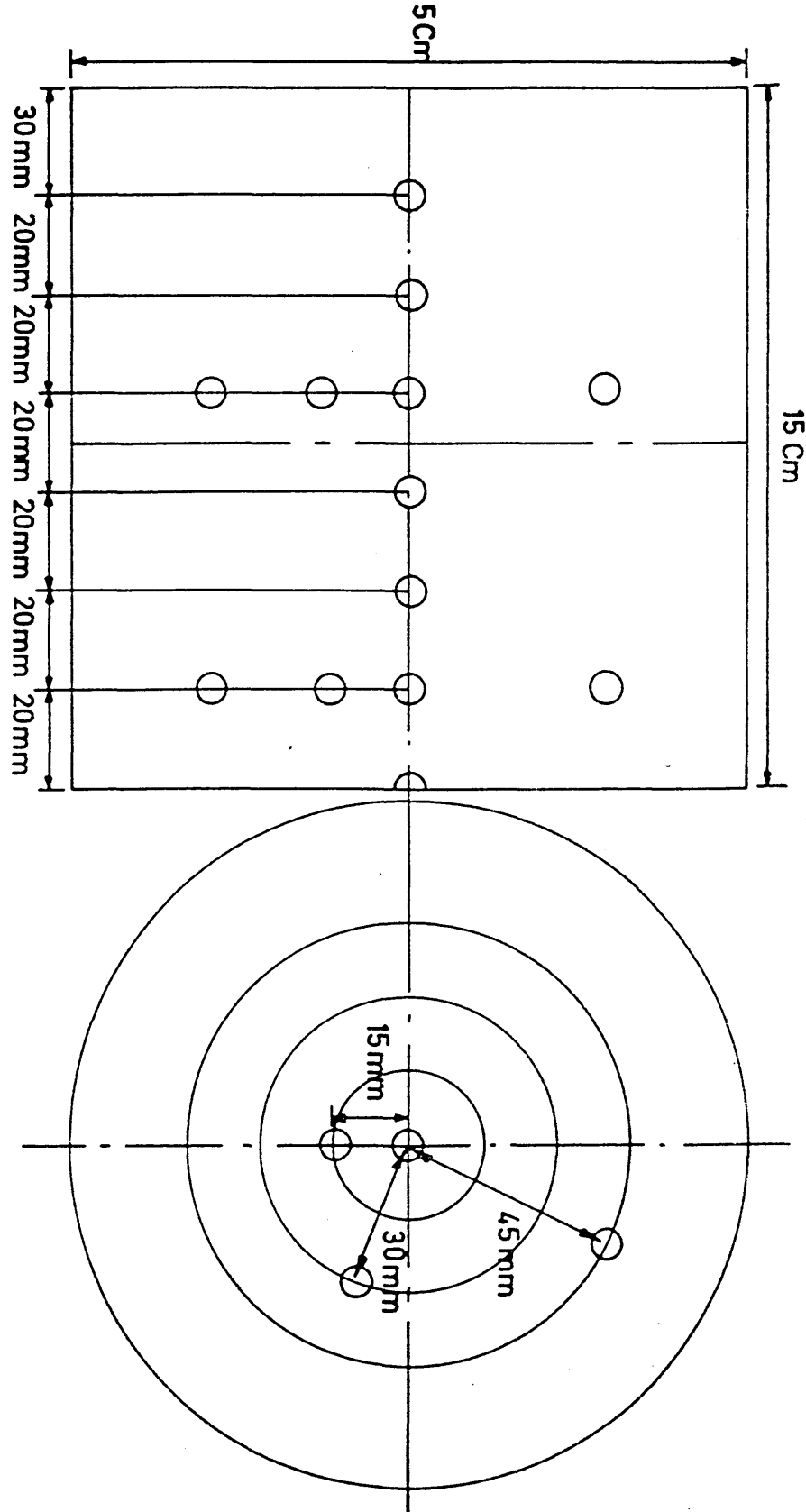


Figure 9 Thermocouples position in the steel sample.

571

5.1 HEAT TRANSFER COEFFICIENT MEASURED BY THE
 MASS TRANSFER ANALOGY

Fifty four experiments were made of exposition of the perspex replica with naphthalene to the air blast by periods of time of one and a half hours each, at 6 cm, 8.5 cm and 9.6 cm from the air blast in order to measure the heat transfer coefficient by the mass transfer analogy. The results are shown in Tables 3, 4, 5, 6, 7, 8.

AIR FLOW RATE (litres/s)	37. <i>4</i>	37. <i>4</i>	37. <i>4</i>
NAPHTHALENE REMOVED DURING 1½ HOURS (grs)	15. <i>4</i> 15. <i>8</i> 16. <i>6</i>	15. <i>9</i> 16. <i>8</i> 17. <i>2</i>	15. <i>7</i> 16. <i>7</i> 16. <i>2</i>
MEAN VALUE (\bar{x})		16. <i>25</i>	
STANDARD DEVIATION (s)		0. <i>32</i>	
TEMPERATURE AIR BLAST DURING 1½ HOUR PERIOD ($^{\circ}\text{C}$)	42 43 44	42 42 43	42 43 43

TABLE No. 3

Naphthalene removed by the air blast during one and a half hours at the distance of
six centimeters and maximum air flow.

AIR FLOW RATE (litres/s)	32.3	32.3	32.3
NAPHTHALENE REMOVED DURING $1\frac{1}{2}$ HOURS (grs)	13.1 13.5 14.1	12.5 13.1 14.3	12.8 13.2 14.0
MEAN VALUE (\bar{x})		13.4	
STANDARD DEVIATION (s)		0.64	
TEMPERATURE AIR BLAST DURING $1\frac{1}{2}$ HOUR PERIOD ($^{\circ}\text{C}$)	42 43 43	42 42 43	42 43 43

TABLE NO. 4

Naphthalene removed by the air blast during one and a half hours at the distance of six centimeters and three quarters of the air flow.

AIR FLOW RATE (litres/s)	26.4	26.4	26.4
NAPHTHALENE REMOVED DURING $1\frac{1}{2}$ HOURS (grs)	11.9	12.4	11.6
MEAN VALUE (\bar{x})			11.99
STANDARD DEVIATION (s)			0.45
TEMPERATURE AIR BLAST DURING $1\frac{1}{2}$ HOUR PERIOD ($^{\circ}\text{C}$)	41	42	43
	41	42	43
	41	42	43
	41	42	43

TABLE No. 5

Naphthalene removed by the air blast during one and a half hours at the distance of six centimeters and half of the air flow.

AIR FLOW RATE (litres/s)	18.7	18.7	18.7
NAPHTHALENE REMOVED DURING $1\frac{1}{2}$ HOURS (grs)	6.5	6.5	6.9
MEAN VALUE (\bar{x})			6.73
STANDARD DEVIATION (s)			0.42
TEMPERATURE AIR BLAST DURING $1\frac{1}{2}$ HOUR PERIOD ($^{\circ}\text{C}$)	40	41	39
		41	42
		39	41
		42	42

TABLE NO. 6

Naphthalene removed by the air blast during one and a half hours at the distance
of six centimeters and a quarter of the air flow.

AIR FLOW RATE (litres/s)	37.4	37.4	37.4	37.4	37.4
NAPHTHALENE REMOVED DURING 1½ HOURS (grs)	14.7 14.5 16.4	13.6 15.0 15.7	15.2 15.6 15.8	14.9 14.6 15.4	15.1 14.8 15.4
MEAN VALUE (\bar{x})			15.16		
STANDARD DEVIATION (s)			0.68		
TEMPERATURE AIR BLAST DURING 1½ HOURS (T) (°C)	42 44 45	42 43 44	42 44 45	42 43 45	42 44 45

TABLE No. 7

Naphthalene removed by the air blast during one and a half hours at the distance of
8.5 centimeters and maximum air flow.

AIR FLOW RATE (litres/s)	37.4	37.4	37.4
NAPHTHALENE REMOVED DURING $1\frac{1}{2}$ HOURS (grs)	11.5	12.5	13.2
MEAN VALUE (\bar{x})	12.7		
STANDARD DEVIATION (s)		0.68	
TEMPERATURE AIR BLAST DURING $1\frac{1}{2}$ HOURS PERIOD ($^{\circ}\text{C}$)	41	42	43

TABLE No. 8

Naphthalene removed by the air blast during one and a half hours at the distance of 9.6 centimeters and maximum air flow.

The mass transfer coefficient was calculated from the naphthalene weight loss by the following method:

The mass transfer rate is given by:

$$\dot{n}''_N = \left[h_M \right]_N \frac{\left[P_{eq} \right]_N}{R\theta}$$

which gives:

$$\left[h_M \right]_N = \frac{R\theta \dot{n}''_N}{\left[P_{eq} \right]_N}$$

where \dot{n}''_N is the number of moles of naphthalene lost in unit time from unit area of the subliminating surface, R is the gas constant, $\left[h_M \right]_N$ is the mass transfer coefficient, θ is the temperature of the surface, and $\left[P_{eq} \right]_N$ is the equilibrium evaporation pressure of naphthalene.

This equilibrium pressure was taken from Perry's Chemical Engineering Handbook⁽⁴⁶⁾ using the best fit curve:

$$P/(mm Hg) = 7.632 \times 10^8 \exp (-6.601 K \times \left(\frac{1}{\theta} \right) \times 10^3)$$

Values of the mass transfer coefficient were calculated from the mass loss data presented in Tables 3 to 8, using the above equations, and taking the relative molecular mass of naphthalene as 128 g.mol^{-1} . The values are plotted against air flow rate in Figure 10 together

with values obtained by Moore⁽⁴⁷⁾ for a similar system.

Analogous heat transfer coefficients were obtained from these mass transfer results using the similarity between the dimensionless correlations for heat and mass transfer.⁽⁴⁸⁾

$$Nu = \propto (Re)^m Pr^{1/3}$$

and

$$Sh = \propto (Re)^m Sc^{1/3}$$

Dividing one of these equations by the other:

$$\frac{h}{[h_M]_N} = \left(\frac{K}{D_N} \right)^{2/3} (\rho_c)^{1/3}$$

The property values to be used in this equation are:

$$K = 0.0274 \text{ W.m}^{-1}\text{K}^{-1} \quad (46)$$

$$C = 1.01 \text{ KJ Kg}^{-1} \text{ K}^{-1} \quad (46)$$

$$\rho = 1.17 \text{ Kg.m}^{-3}$$

$$[D_N]_{40^\circ\text{C}} = 0.0730 \text{ cm}^2.\text{s}^{-1} \quad (49)$$

Substituting these values into the above equation gives:

$$\frac{h}{[h_M]_N} = 2.55 \times 10^3 \text{ J.m}^{-3} \text{ K}^{-1}$$

which, rearranged, gives:

$$h = 25.5 \cdot \text{Wm}^{-2} \text{ K}^{-1} \times \frac{[h_M]_N}{\text{cm}^2.\text{s}^{-1}}$$

Values of the mass and heat transfer coefficients

determined in this way are set out in Table 9.

The heat transfer coefficients obtained are

plotted against air flow rate in Section 6.

AIR FLOW RATE (litres/s)	37.4	32.3	26.4	18.7
CALCULATED VALUES OF MASS TRANSFER COEFFICIENT (cm/s)	7.89	7.34	6.24	4.39
CALCULATED VALUES OF HEAT TRANSFER COEFFICIENT (w/m ² °C)	201	187	159	112

TABLE No. 9

Heat transfer coefficient values obtained using the mass transfer analogy.

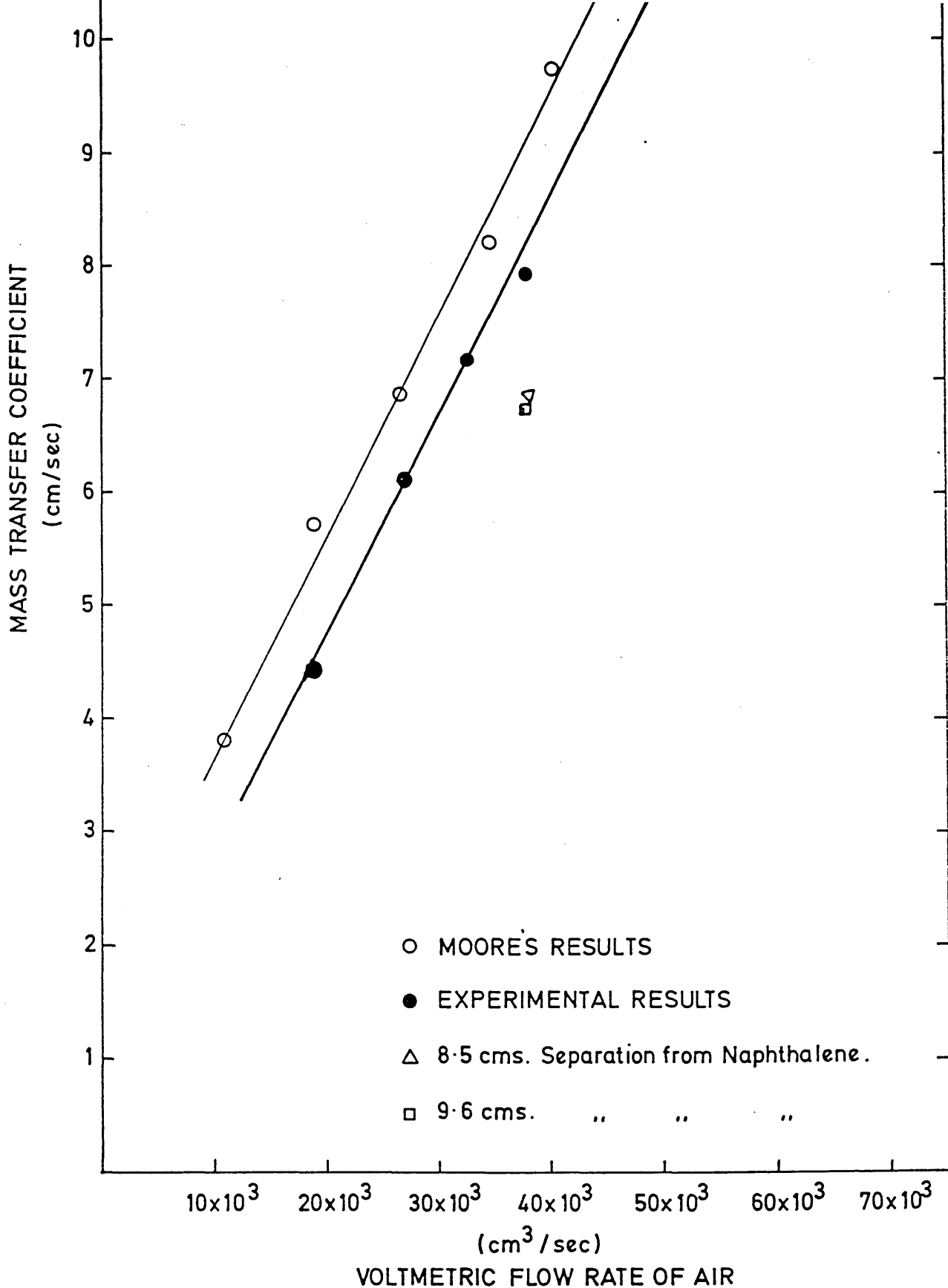


Figure 10 Mass transfer coefficients against air flow rate (together with Moore's results).

5.2 HEAT TRANSFER COEFFICIENT MEASURED BY STEADY
 STATE HEAT TRANSFER

Sixteen experiments were made with the copper disc at different temperatures and with different air flow rates in order to measure the heat transfer coefficient by steady state heat transfer. The results are shown in Table 10.

Air flow (litre/s)	Surface Temp (°C)	Voltage (V)	Amperage (A)	Air blast Temp (°C)
37.4	283	190	5.85	40
32.3	"	183	5.58	40
26.4	"	170	5.2	40
18.7	"	155	4.75	40
37.4	143	120	3.70	40
32.3	"	115	3.63	40
26.4	"	108	3.32	40
18.7	"	98	3.02	40
37.4	136	115	3.55	40
32.3	"	110	3.40	40
26.4	"	103	3.18	40
18.7	"	93	2.88	40

TABLE NO. 10

Voltages and amperages obtained during the steady state heat transfer experiments

The heat transfer coefficient was calculated by the following formulae:

$$\dot{q} = hA(\theta_s - \theta_a)$$

$$\dot{q} = v \cdot a$$

$$h = \frac{v \cdot a}{A(\theta_s - \theta_a)}$$

In this work:

v = See table 10.

a = See table 10.

θ_s = See table 10.

θ_a = 40°C.

A = 0.02 m².

The results obtained for the heat transfer coefficient are shown in Table 11. They will be discussed in Section 6.

Air flow (litre/s)	Surface Temp (°C)	Heat transfer Coe.(W/m²°C)
37.4	283	222
32.3	"	209
26.4	"	181
18.7	"	151
37.4	143	214
32.3	"	197
26.4	"	172
18.7	"	142
37.4	136	213
32.3	"	195
26.4	"	170
18.7	"	139

TABLE NO. 11

Heat transfer coefficients obtained during
the steady state heat transfer experiments

5.3 PROFILE OF TEMPERATURE IN THE SAMPLE OF
 STEEL AT 500°C, 600°C, 700°C AND 800°C
 WITHOUT AIR COOLING

The results of the profile of temperature obtained at different distances from the bottom of the sample of steel are given in Table No. 12 and Figure No. 11, and the results at different radius and different distances from the bottom of the sample of steel, in Tables No. 13, 14 and Figure No. 12.

TEMPERATURE (°C)				DISTANCE FROM BOTTOM OF SAMPLE (mm)
800	700	600	500	
795	680	580	475	0
780	685	590	495	20
810	695	595	490	40
815	700	610	500	60
810	705	610	505	80
810	705	615	505	100
825	710	615	510	120

TABLE No. 12

Temperature at different distances from the bottom of
the sample

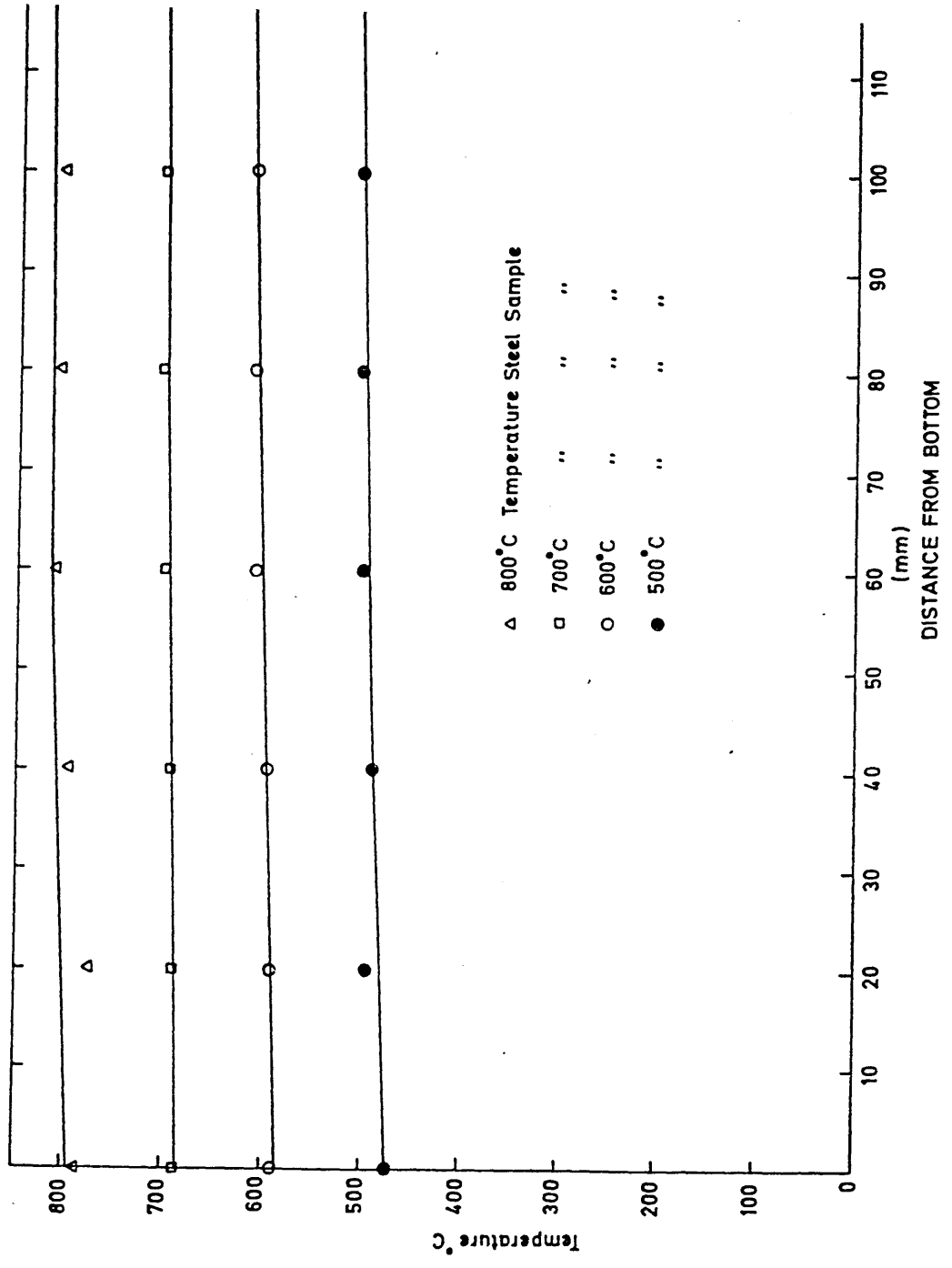


Figure 11 Temperature distribution in the uncooled billet.

TEMPERATURE (°C)				RADIUS (cms)
800	700	600	500	
780	685	590	495	0
790	690	595	500	1.5
795	700	595	599	3.0
800	695	600	505	4.5

TABLE No. 13

Temperature at different radius and two centimeters
from the bottom

TEMPERATURE (°C)				RADIUS (cms)
800	700	600	500	
810	705	610	505	0
805	710	605	510	1.5
810	715	610	510	3.0
815	710	615	515	4.5

TABLE No. 14

Temperature at different radius and eight
centimeters from the bottom

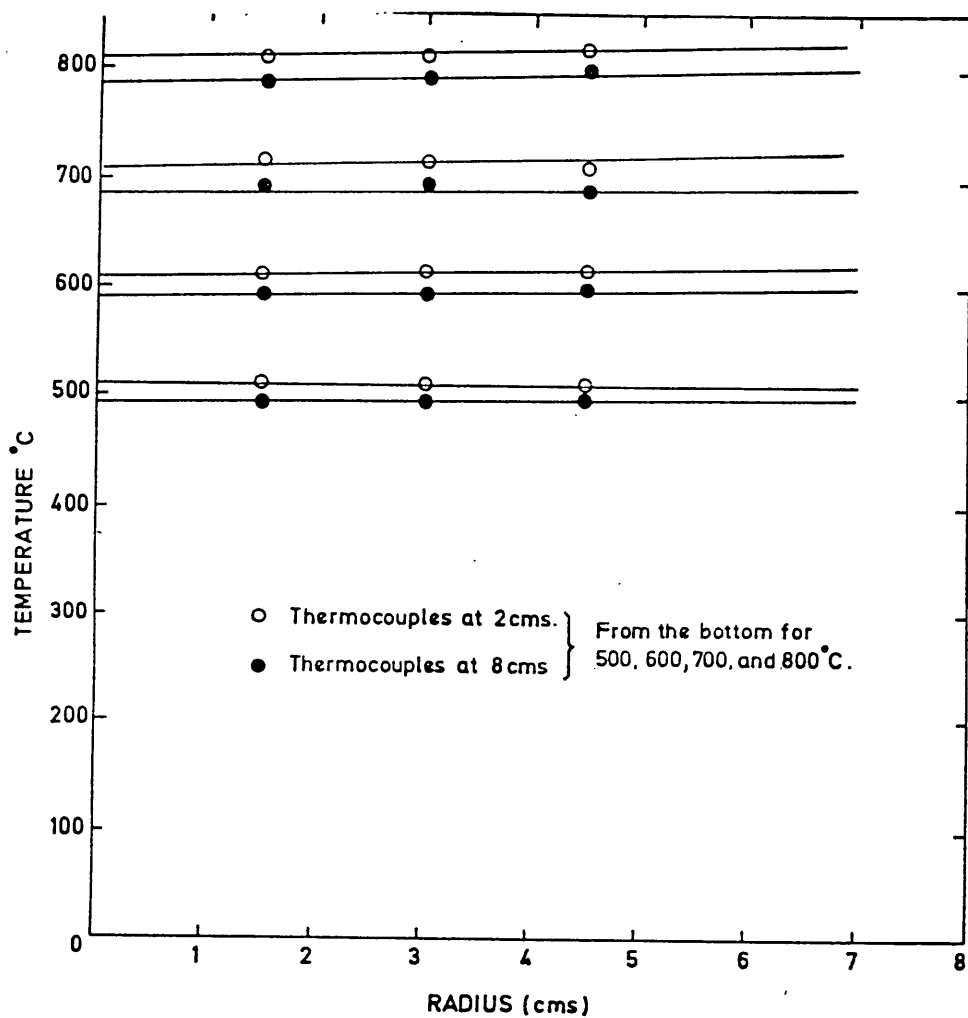


Figure 12 Temperature variation with radii at 2 and 8 cms from the base of the steel sample.

5.4 PROFILE OF TEMPERATURE IN THE SAMPLE OF STEEL

AT 850°C WITH AIR COOLING

This section contains temperatures measured during the cooling of the billet sample from temperatures above the transformation temperature. Tables 15 to 18 and Figures 13 to 16 present results for the first series of experiments in which the slab was not completely insulated during the preheating period. Considerable temperature variation therefore existed axially within the sample before cooling started.

Tables 19 to 23 and Figures 17 to 21 present the results for those experiments for which the billet sample was completely insulated during the preheat period, a refractory block having been inserted between the base of the billet and the air cooling jet.

TIME (min)	DISTANCE FROM COOLED BASE (mm)							
	0	20	40	60	80	100	120	
00	731	780	830	870	875	880	886	
05	538	656	733	775	806	830	853	
10	503	614	691	745	779	806	830	
15	485	585	662	715	745	769	794	
20	462	561	626	679	721	739	748	
25	444	532	597	644	686	709	727	
30	427	509	570	613	652	688	709	
35	409	485	549	591	626	664	709	
40	397	474	526	568	603	625	675	
45	385	450	503	544	568	591	635	

TABLE 15 Temperatures of axial thermocouples at different times during transformation

Cooling Air Flow = 37.4 litres/s

Preheat Insulation: Incomplete

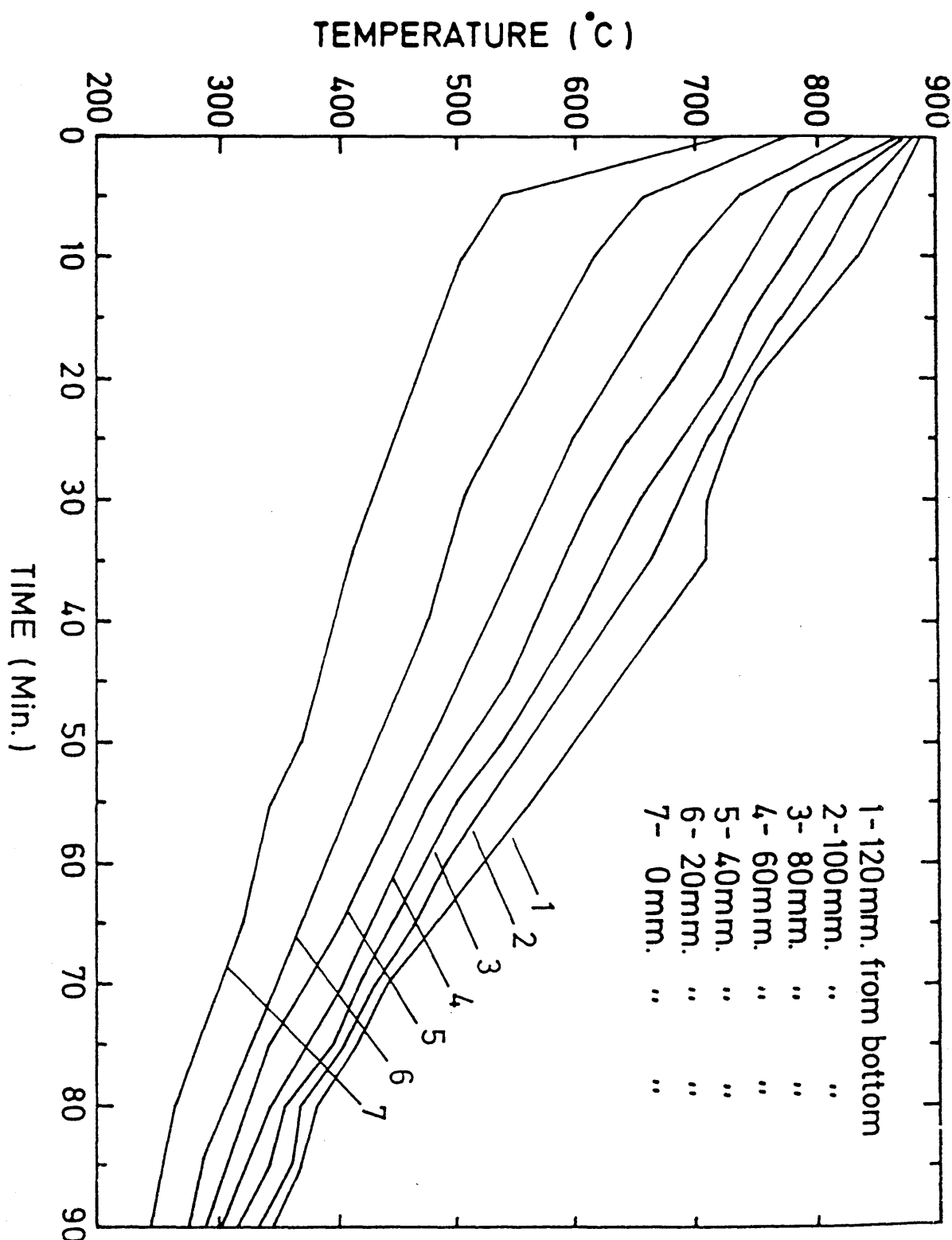


Figure 13 Temperature changes with time during air changes at 37.4 litres/s (incomplete insulation during preheat).

TIME (min)	DISTANCE FROM COOLED BASE (mm)							
	0	20	40	60	80	100	120	
00	731	780	830	870	875	880	886	
05	544	662	727	769	800	820	858	
10	509	620	697	750	784	812	843	
15	491	591	668	721	755	784	806	
20	468	568	632	383	723	757	774	
25	450	544	608	659	697	721	745	
30	438	521	579	626	669	703	721	
35	421	491	556	603	644	680	703	
40	409	485	542	573	617	656	680	
45	391	468	521	562	591	626	662	

TABLE 16

Temperatures of axial thermocouples at different times
during transformation

Cooling Air Flow = 32.3 litres/s

Preheat Insulation: Incomplete

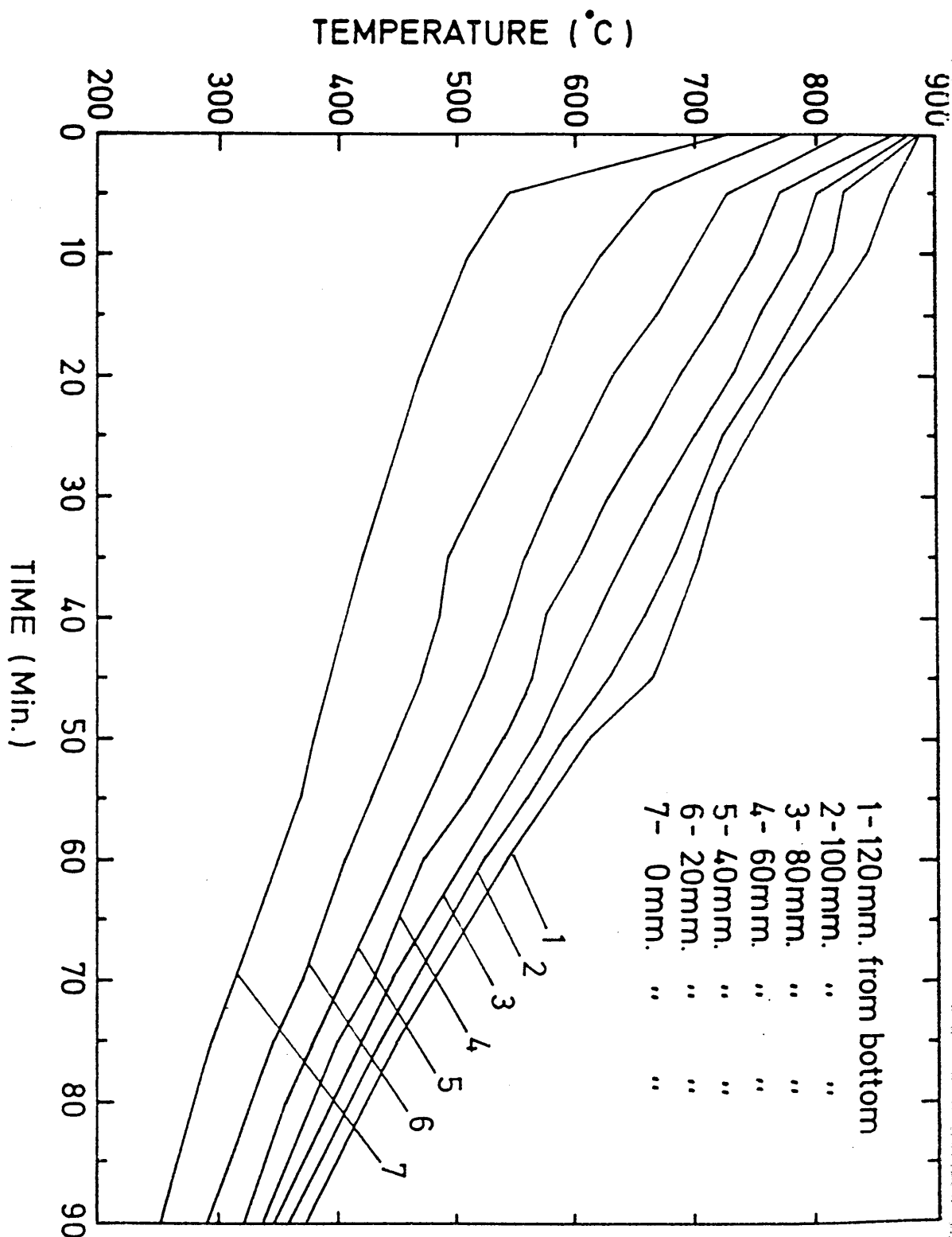


Figure 14 Temperature changes with time during air changes at 32.3 litres/s (incomplete insulation during preheat).

TIME (min)	DISTANCE FROM COOLED BASE (mm)							
	0	20	40	60	80	100	120	
00	731	780	830	870	875	880	886	
05	568	674	736	769	808	828	840	
10	538	638	697	750	788	800	837	
15	515	608	681	733	765	776	818	
20	497	585	657	703	739	762	789	
25	480	568	629	680	715	739	769	
30	462	550	605	650	694	709	733	
35	444	527	579	626	662	691	709	
40	438	503	562	603	638	674	697	
45	427	493	550	585	620	656	688	

TABLE 17

Temperatures of axial thermocouples at different times
during transformation

Cooling Air Flow = 26.4 litres/s

Preheat Insulation: Incomplete

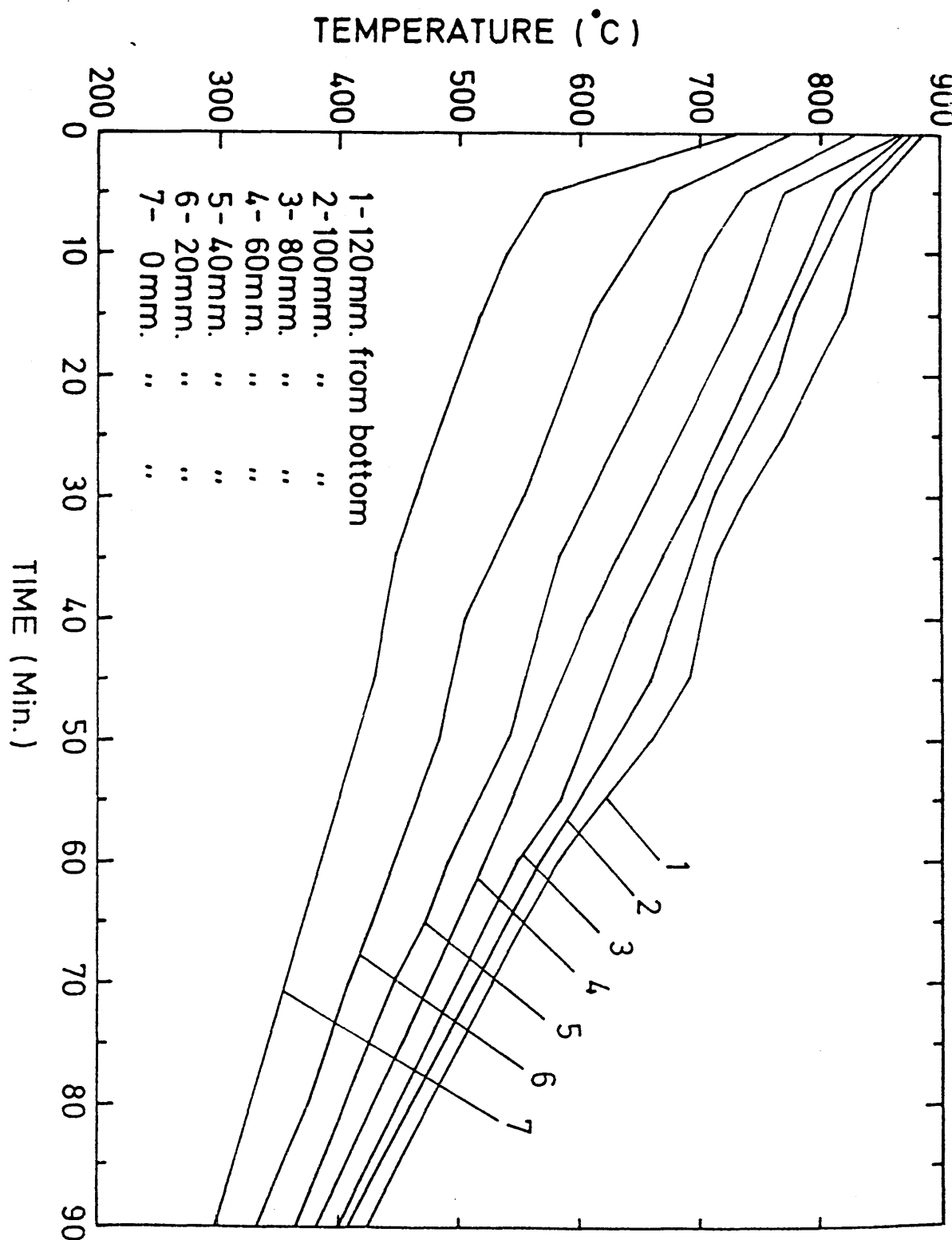


Figure 15 Temperature changes with time during air cooling at 26.4 litres/s (incomplete insulation during preheat).

TIME (min)	DISTANCE FROM COOLED BASE (mm)							
	0	20	40	60	80	100	120	
00	731	780	830	870	875	880	886	
05	579	680	745	784	818	837	861	
10	556	650	709	757	794	806	843	
15	546	638	897	745	782	794	830	
20	538	619	680	721	751	769	800	
25	527	603	662	703	733	751	776	
30	515	591	644	688	715	733	757	
35	503	579	626	668	700	721	739	
40	491	570	615	650	686	709	727	
45	480	665	591	631	664	686	715	
50	407	541	579	615	650	674	709	
55	462	527	568	603	632	659	697	

TABLE 18

Temperature of axial thermocouples at different times
during transformation

Cooling Air Flow = 18.7 litres/s

Preheat Insulation: Incomplete

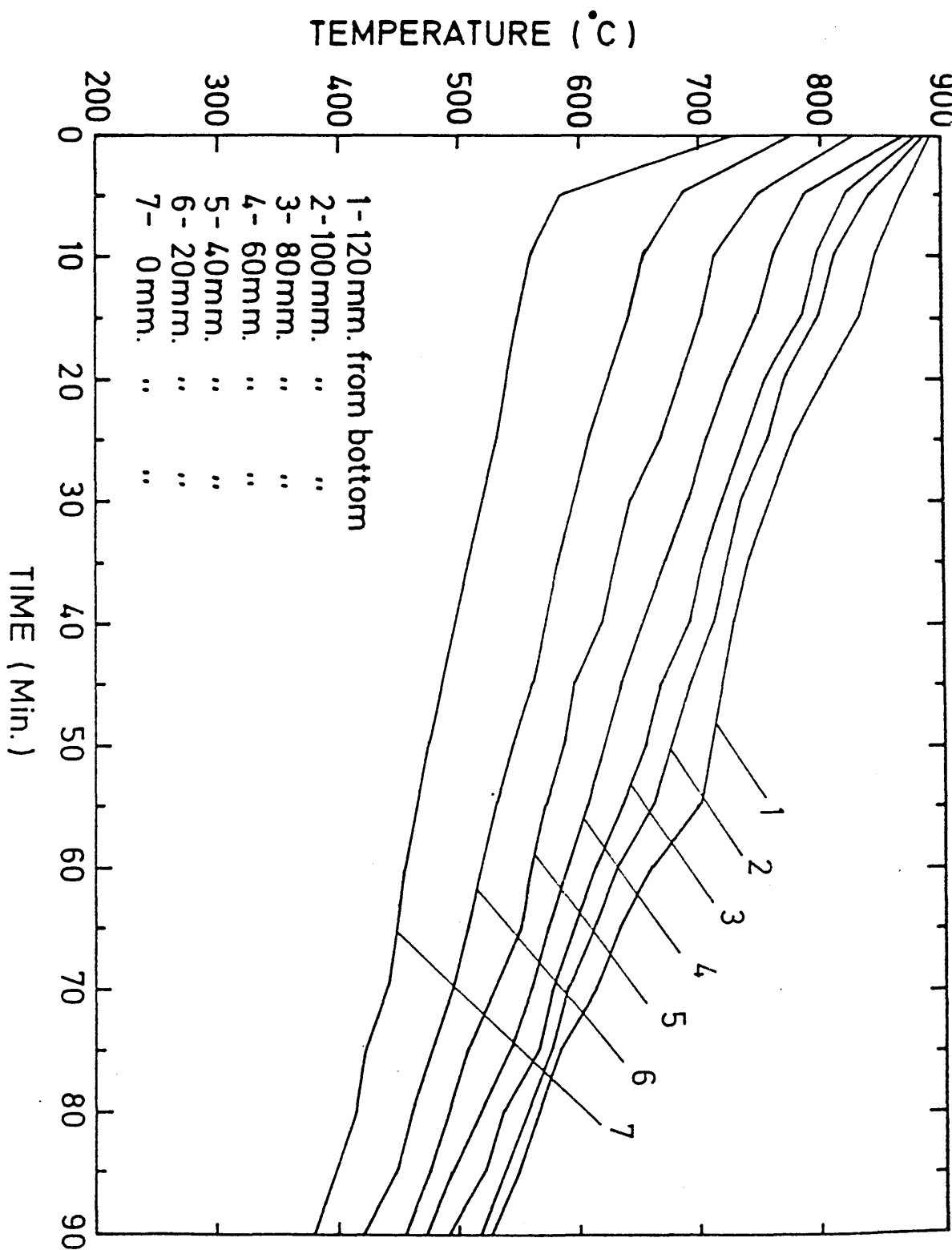


Figure 16 Temperature changes with time during air cooling at 18.7 litres/s (incomplete insulation during preheat).

TIME (min)	DISTANCE FROM COOLED BASE (mm)							
	0	20	40	60	80	100	120	
00	834	840	845	849	855	859	859	
05	508	725	775	810	830	852	852	
10	487	700	755	785	805	828	828	
15	473	685	735	760	780	803	803	
20	459	665	710	740	760	778	778	
25	443	642	690	720	740	754	754	
30	433	624	665	700	715	730	730	
35	421	601	650	675	700	718	718	
40	414	589	625	660	685	710	710	
45	402	579	610	645	670	694	710	
50	389	560	590	615	650	670	683	
55	384	549	570	595	625	646	646	
60	372	531	655	575	595	611	611	

TABLE 19

Temperatures of axial thermocouples at different times
during transformation

Cooling Air Flow = 37.4 litres/s Preheat Insulation: complete

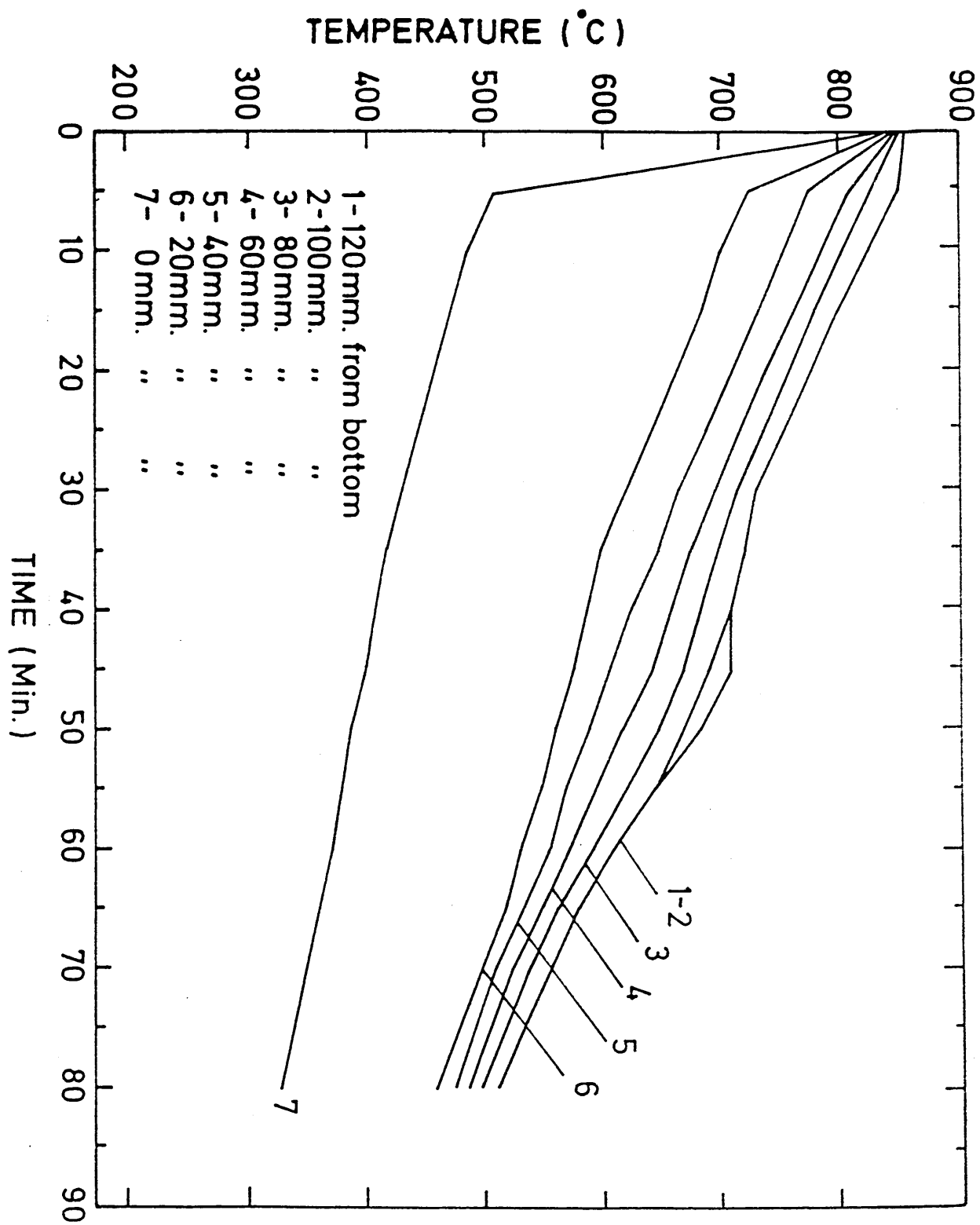


Figure 17 Temperature changes with time during air cooling at 37.4 litres/s (complete insulation during preheat).

TIME (min)	DISTANCE FROM COOLED BASE (mm)							
	0	20	40	60	80	100	120	
00	853	855	857	859	862	873	873	
05	508	746	806	835	842	869	869	
10	487	714	762	799	816	850	850	
15	473	685	732	767	787	820	820	
25	443	642	689	719	737	764	764	
30	433	624	673	707	719	740	740	
35	421	601	649	690	707	721	721	
40	414	589	637	673	696	712	712	
45	402	579	613	653	679	698	712	
48	459	663	707	744	759	795	795	
50	389	560	601	637	666	680	698	
55	384	549	584	613	643	662	662	

TABLE 20

Temperatures of axial thermocouples at different times during transformation

Cooling Air Flow = 37.4 litres

Preheat Insulation: Complete

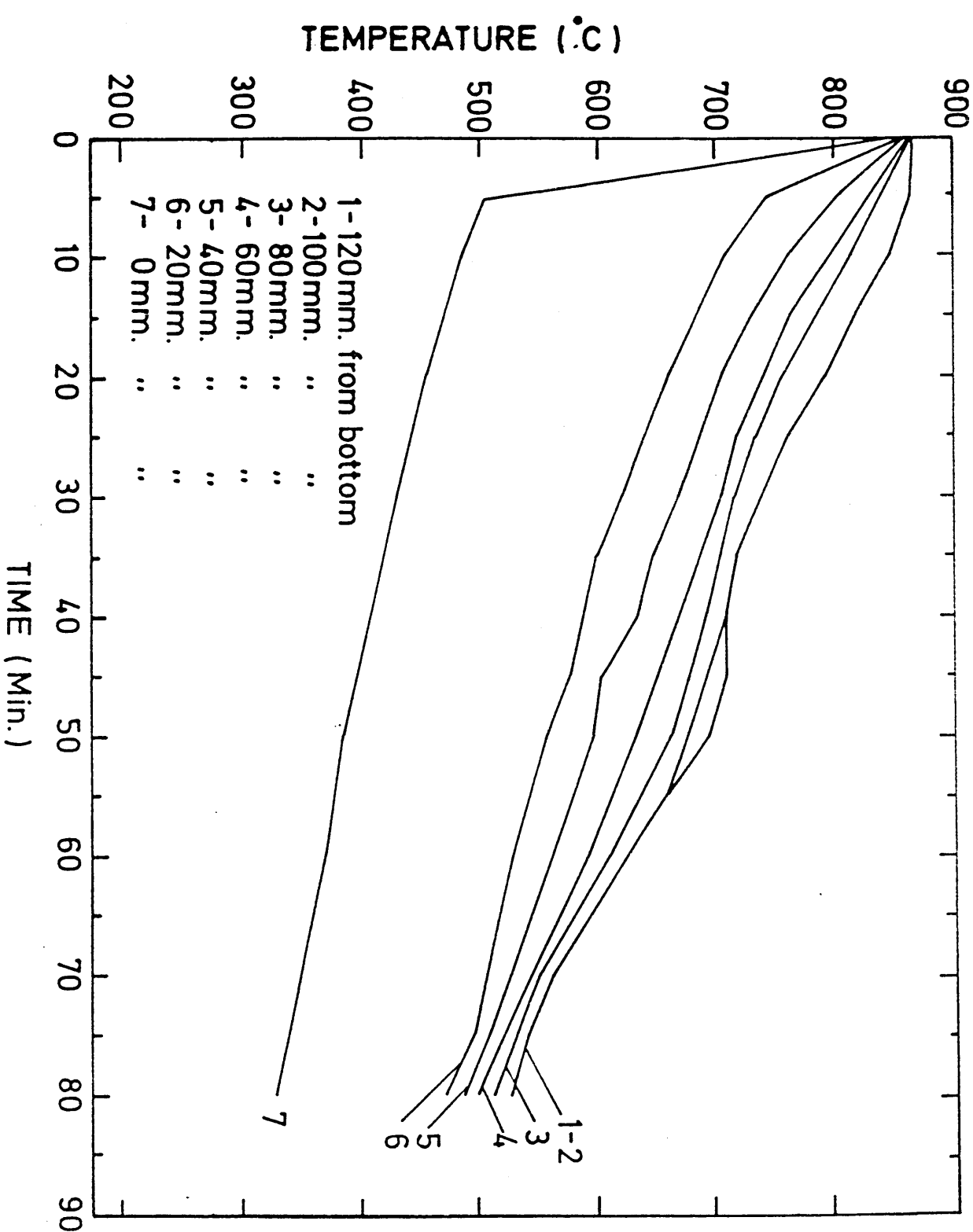


Figure 18 Temperature changes with time during air cooling at 37.4 litres/s (complete insulation during preheat).

TIME (min)	DISTANCE FROM COOLED BASE (mm)							
	0	20	40	60	80	100	120	
00	854	858	860	862	864	866	866	
05	508	747	806	835	842	865	865	
10	487	714	762	699	816	841	841	
15	473	685	732	767	790	814	814	
20	459	663	707	744	759	785	785	
25	443	652	689	719	737	761	761	
30	431	624	673	707	719	738	738	
35	421	601	649	690	740	719	719	
40	414	589	637	673	696	711	711	
45	402	579	613	653	679	702	711	
50	389	560	601	637	666	689	707	
55	384	549	584	613	643	671	691	
60	372	531	567	596	613	664	664	

TABLE 21

Temperatures of axial thermocouples at different times
during transformation

Cooling Air Flow = 37.4 litres/s

Preheat Insulation: Complete

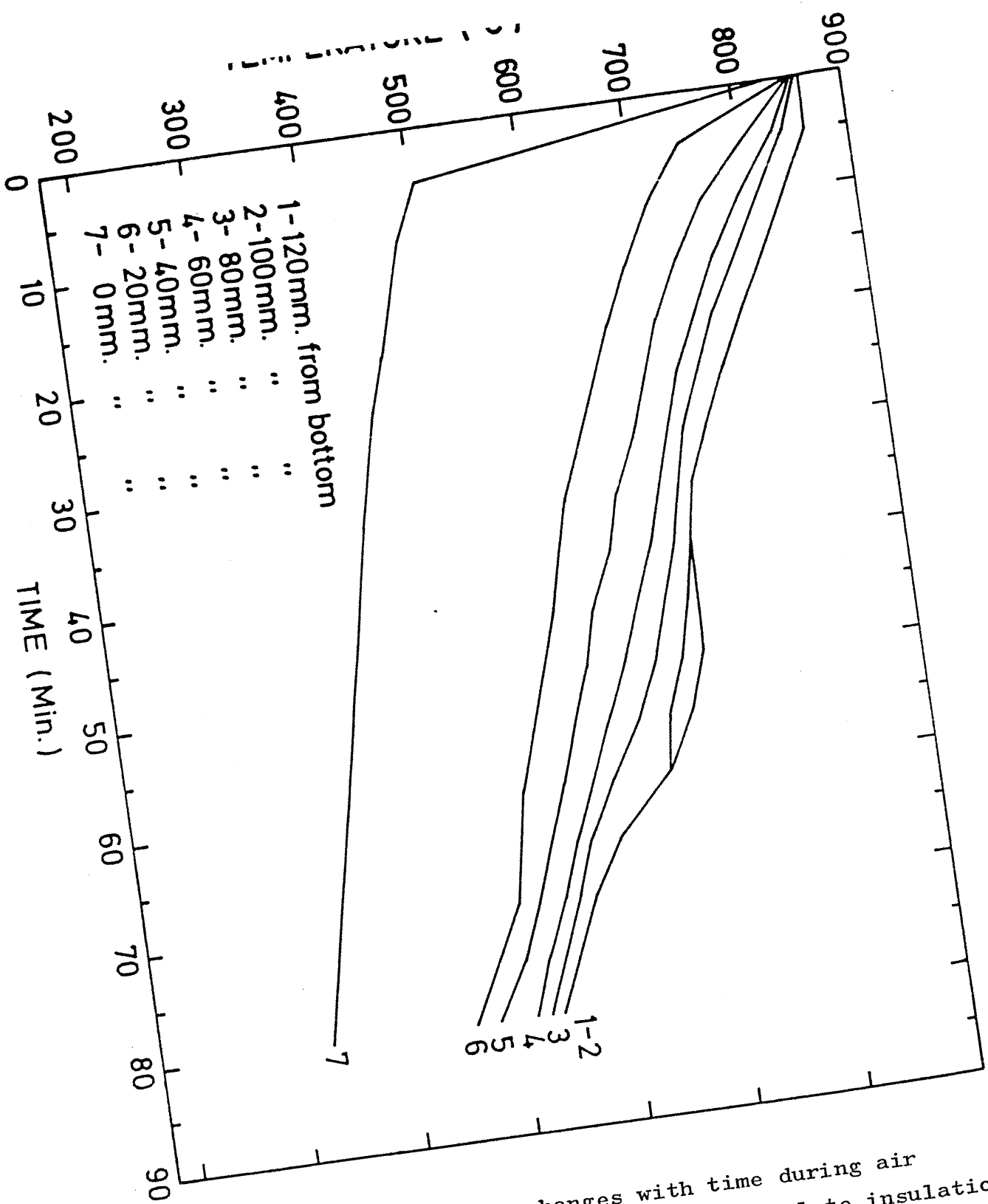


Figure 19 Temperature changes with time during air cooling at 37.4 litres/s, (complete insulation during preheat).

TABLE 22

Temperatures of axial thermocouples at different times
during transformation

Cooling Air Flow = 18.7 litres/s

Preheat Insulation: Complete

TIME (min)	DISTANCE FROM COOLED BASE (mm)							
	0	20	40	60	80	100	120	
00	842	854	856	858	861	865	873	
05	550	750	795	825	840	857	865	
10	540	720	765	800	820	851	857	
15	530	690	735	775	800	832	851	
20	520	665	715	755	785	813	826	
25	515	653	695	740	765	795	807	
30	505	630	680	725	750	777	789	
35	500	620	665	710	735	759	770	
40	490	610	655	695	720	740	752	
45	480	600	645	685	710	728	740	
50	475	595	635	675	695	721	725	
55	470	586	625	665	690	721	721	
60	460	580	610	650	680	710	716	
65	450	575	600	640	665	698	716	
70	445	570	590	625	650	686	704	
75	435	565	585	615	635	662	674	
80	425	560	575	600	620	638	650	

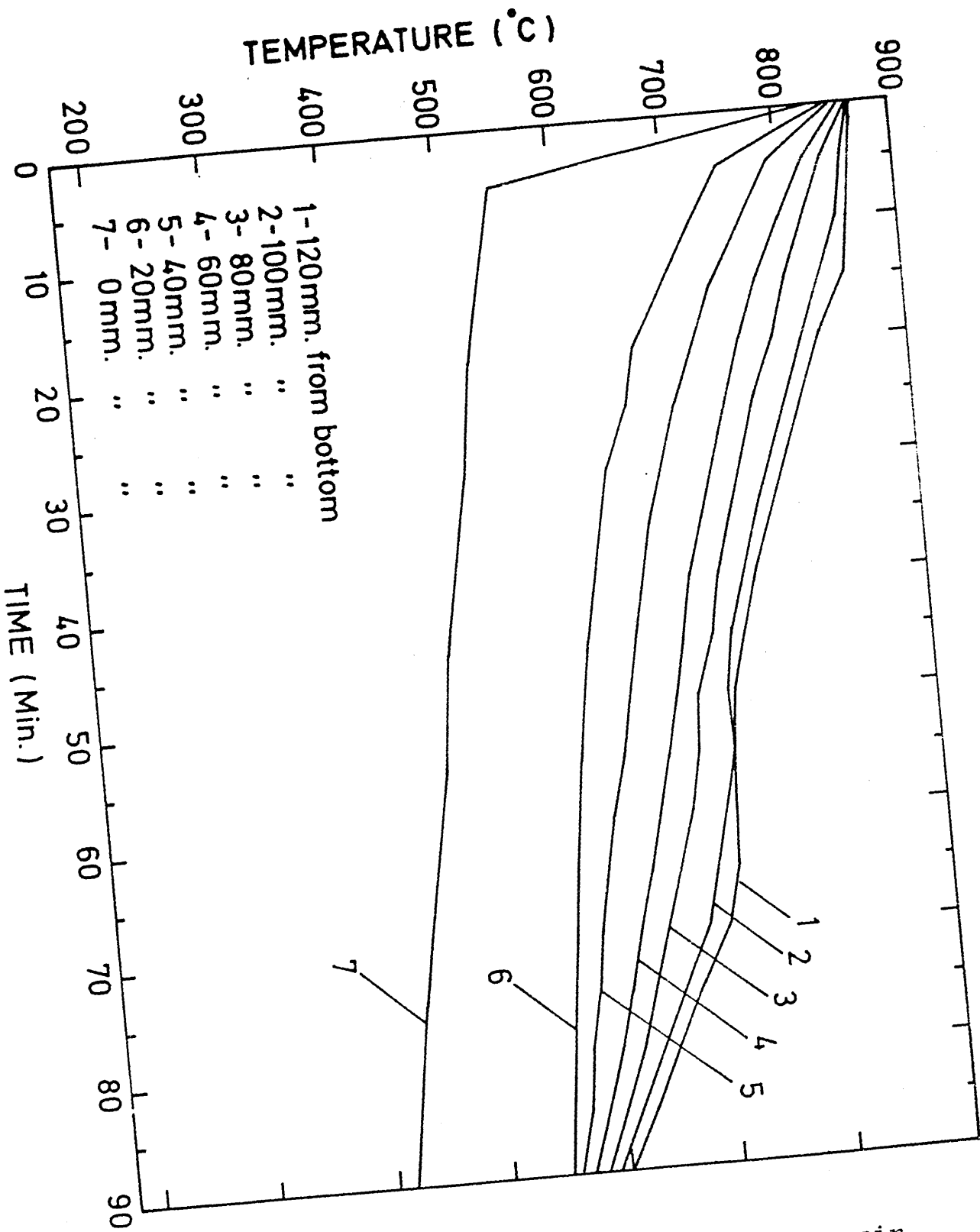


Figure 20 Temperature changes with time during air cooling at 18.7 litres/s (complete insulation during preheat).

TABLE 23 Temperatures of axial thermocouples at different times during transformation

Cooling Air Flow = 13.2 Litre/s

Preheat Insulation : Complete

TIME (min)	DISTANCE FROM COOLED BASE (mm)						
	0	20	40	60	80	100	120
00	853	856	859	862	866	870	875
05	580	760	805	835	850	865	870
10	570	730	775	810	830	853	865
15	560	700	745	785	810	841	853
20	553	675	720	765	795	823	835
25	545	660	705	750	775	804	819
30	535	640	690	735	760	791	804
35	525	630	680	720	745	779	791
40	515	620	665	705	730	761	773
45	505	610	655	695	720	755	767
50	495	605	650	685	715	743	755
55	490	600	645	680	710	737	743
60	480	595	640	675	705	725	731
65	475	590	635	670	700	726	726
70	470	585	625	660	695	719	723
75	465	580	620	655	690	719	731
80	460	575	615	645	675	707	719
85	455	570	610	635	665	695	707
90	450	565	600	625	645	671	683

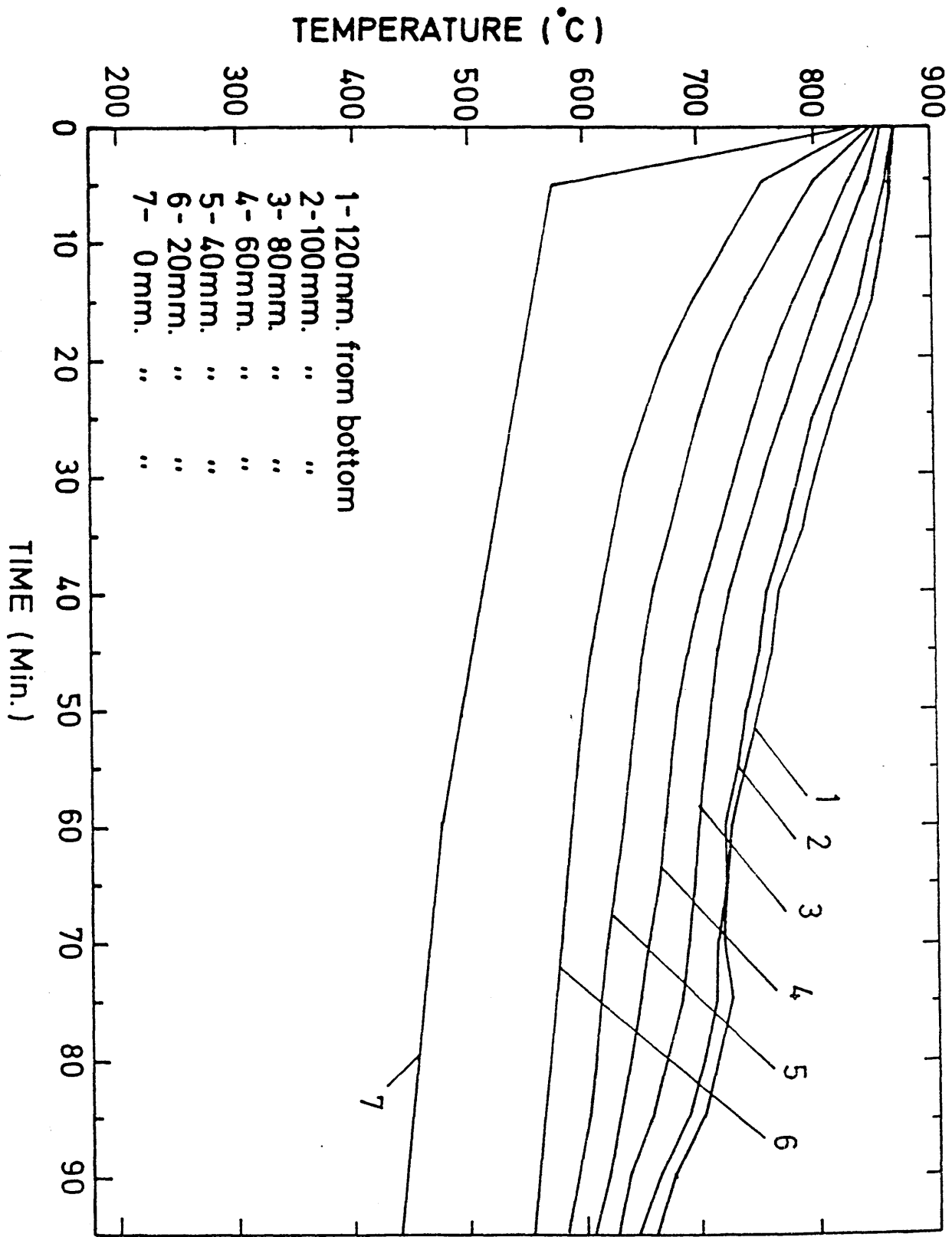


Figure 21 Temperature changes with time during air cooling at 13.2 litres/s (complete insulation during preheat).

5.5 TEMPERATURE OF TRANSFORMATION

The temperatures of transformation were taken from the Figures 17, 18, 19, 20 and 21 at different air cooling flow rates. The transformation temperature was assumed to be the temperature of arrest indicated for by the thermocouples at 10 and 12 cm from the base. The values obtained are shown in Table 24, together with the average velocity of the transformation front determined as described in the next section.

EXP. NO.	AIR COOLING FLOW RATE (litres/s)	AVERAGE FRONT VELOCITY (mm/min)	TRANSFORMATION TEMPERATURE (°C)
5	37.4	2.2	709
6	37.4	2.2	709
7	37.4	2.2	709
8	18.7	1.7	715
9	13.2	1.5	725

TABLE No. 24

Temperature of transformation at different air
cooling rates.

5.6 PROGRESS_OF_TRANSFORMATION_FRONT

The progress of the transformation front was determined taking the temperature of transformation as the arrest point in the curves of the thermocouple positioned twelve centimeters from the base. The times at which the steel around the other thermocouples transformed was then taken as the time when each thermocouple had been cooled to this temperature.

Table 25 presents the results for all the cooling conditions investigated. The second to fifth columns present results for the experiments in which the billet sample was not completely insulated during the preheating period. The last three columns present the results for the experiments in which the base of the sample was insulated during the preheating period by the insertion of the refractory insulating block.

The data is also presented graphically in figures 21 to 28. The transformation front velocities presented in Table 24 were obtained as the average slope of the graphs presented in these figures. Individual values of the slope were determined to each point and it is the average of these values that is presented in Table 24 for each set of cooling conditions.

Table No. 25

Transformation times at different thermocouple positions

Distance from base (cm)	Transformation times (min) with different cooling									
	Air cooling flow rate (litre/s)									
	37.4	32.3	26.4	18.7	37.4*	37.4*	37.4*	18.7*	13.2*	
0	0.0	0.3	0.4	0.5	2.0	2.0	2.0	2.3	2.4	
2	2.0	3.0	3.2	6.5	8.5	10.0	10.5	10.0	11.0	
4	6.0	8.0	8.5	9.0	20.5	19.0	19.5	18.0	20.0	
6	15.5	16.0	19.0	21.0	27.0	28.4	28.0	32.0	33.5	
8	19.5	22.0	27.0	30.0	32.0	33.0	34.0	40.0	42.5	
10	22.0	26.5	29.0	36.5	40.0	40.0	41.0	55.0	70.0	
12	25.0	30.0	35.0	45.0	45.5	45.5	47.0	60.0	75.0	

* Results obtained with complete insulation of the sample billet during the preheat period.

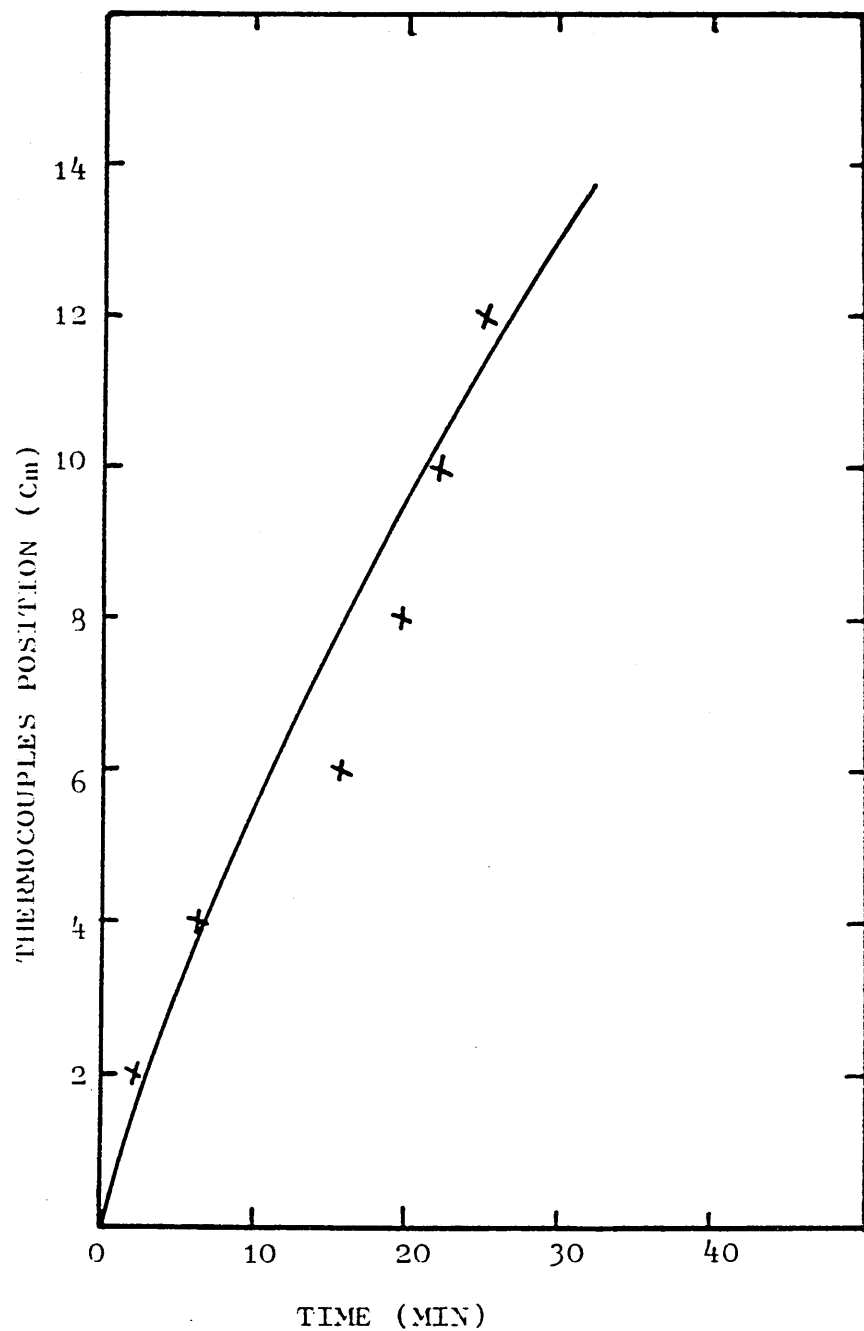


Figure 22 Progress of the transition front with air cooling at 37.4 litres/s (incomplete insulation during preheat).

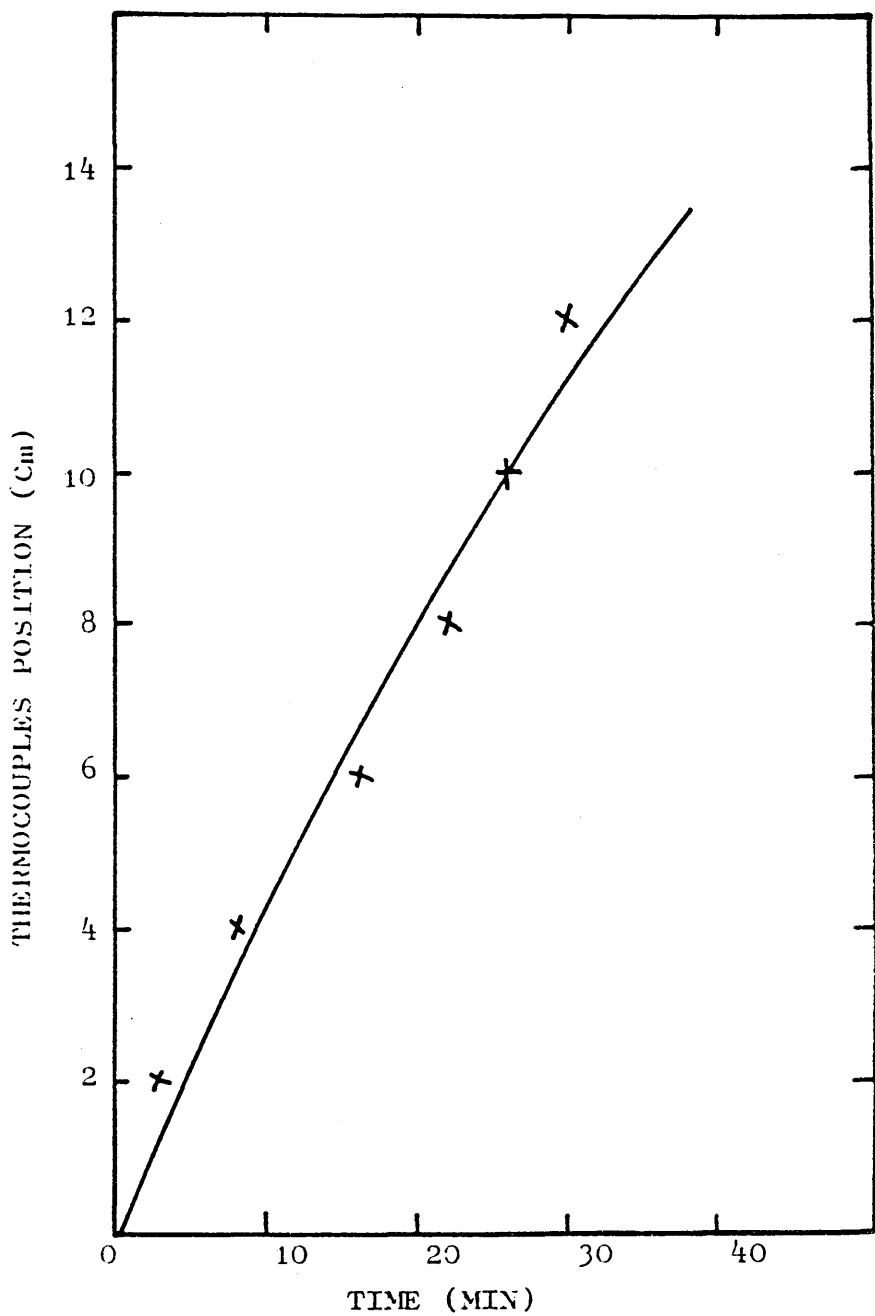


Figure 23 Progress of the transition front with air cooling at 32.3 litres/s (incomplete insulation during preheat).

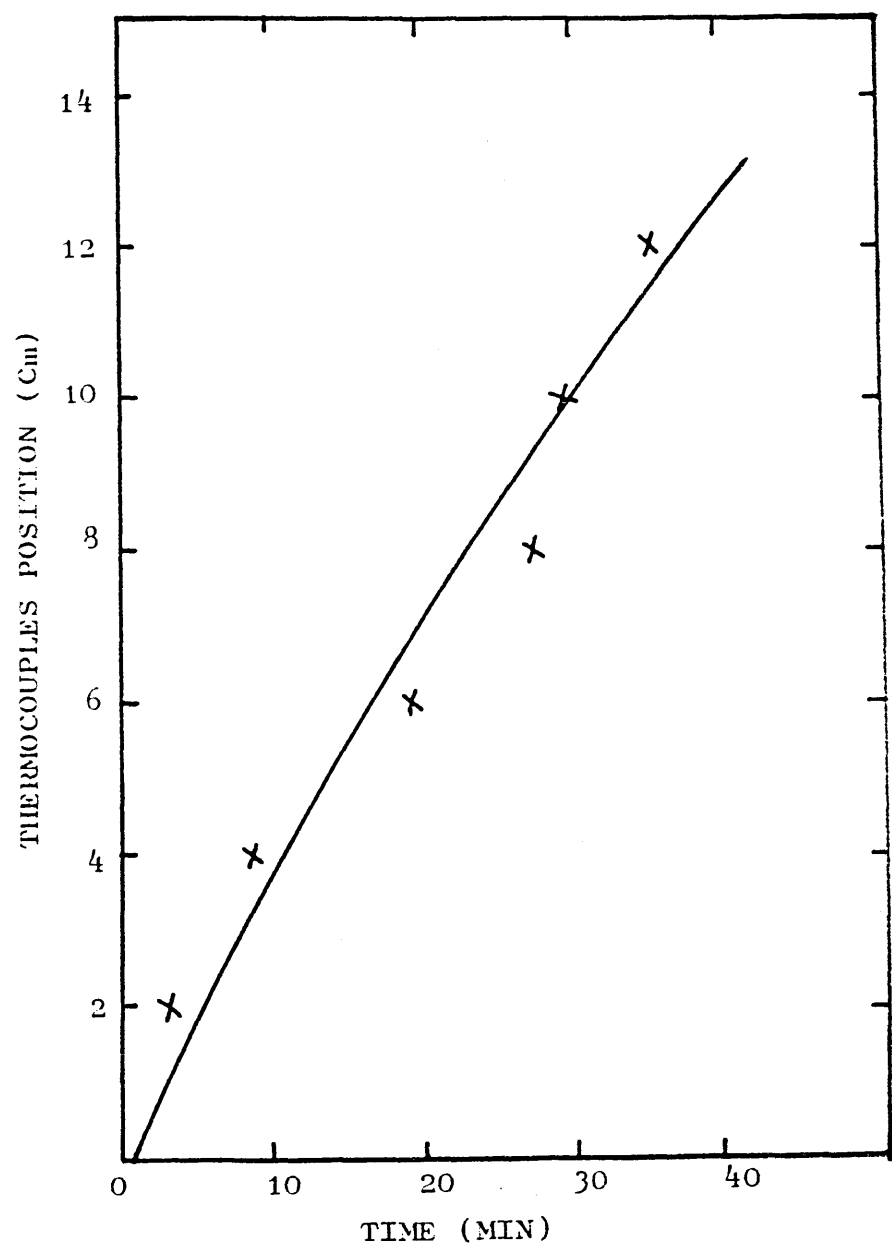


Figure 24 Progress of the transition front with air cooling at 26.4 litres/s (incomplete insulation during preheat).

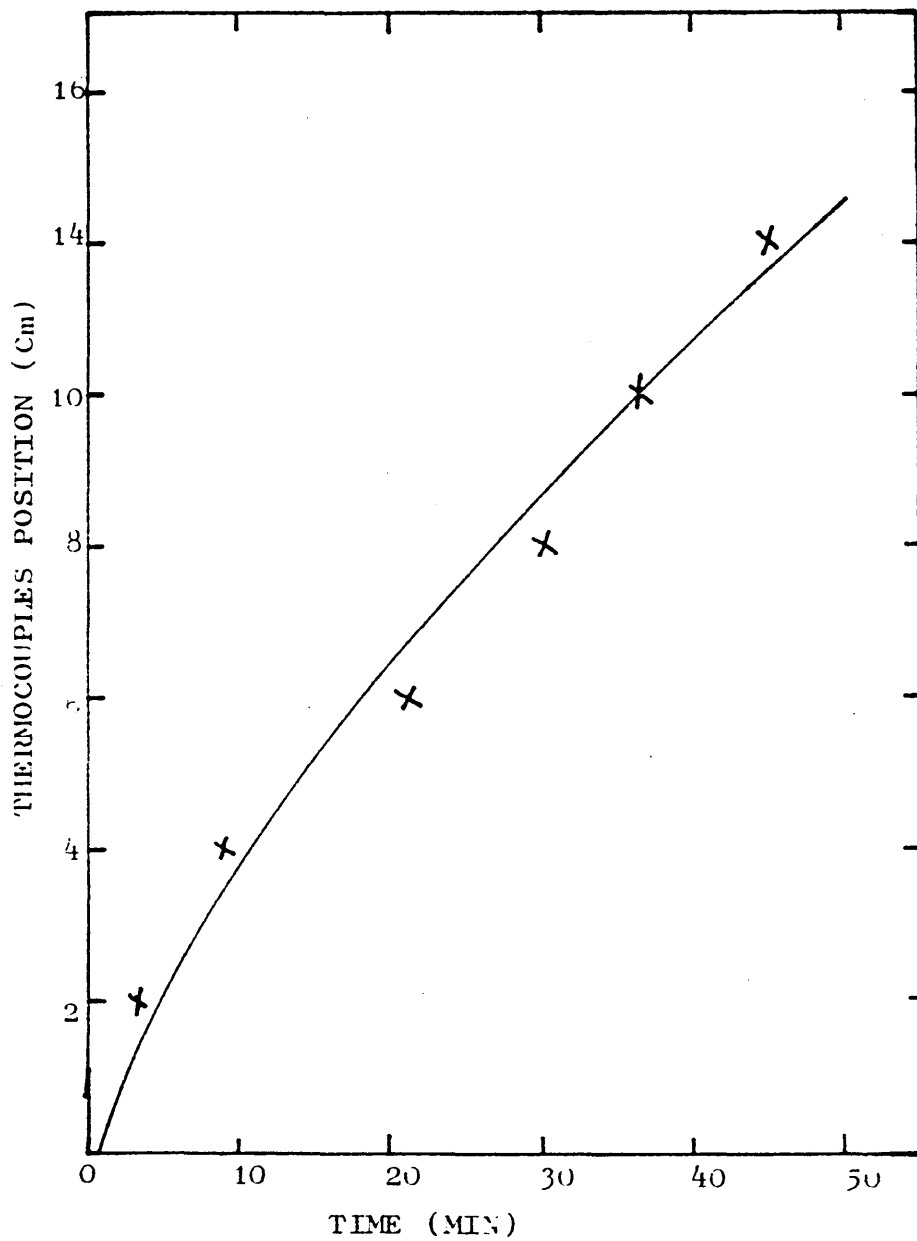


Figure 25 Progress of the transition front with air cooling at 18.7 litres/s (incomplete insulation during preheat).

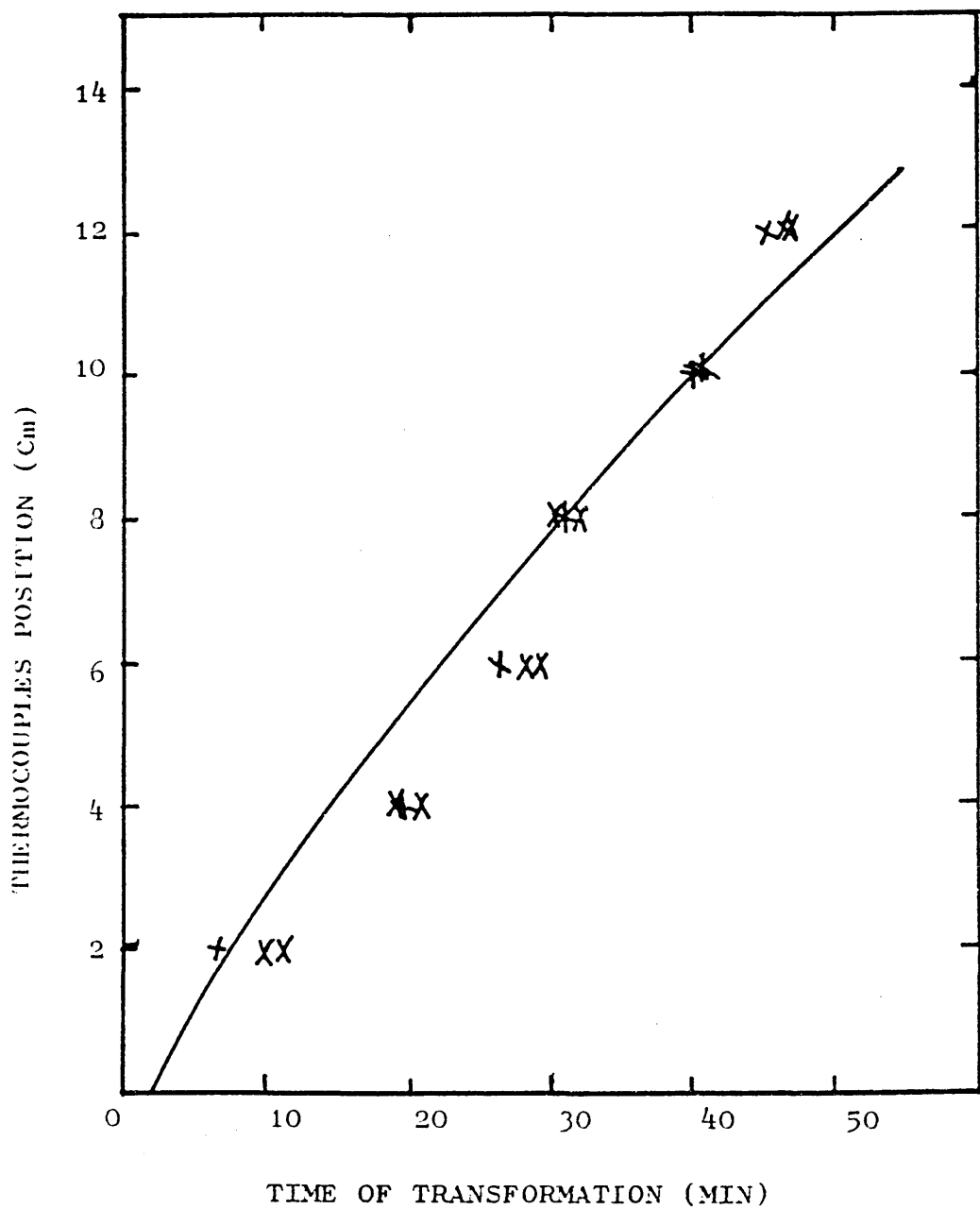


Figure 26 Progress of the transition front with air cooling at 37.4 litres/s (complete insulation during preheat).

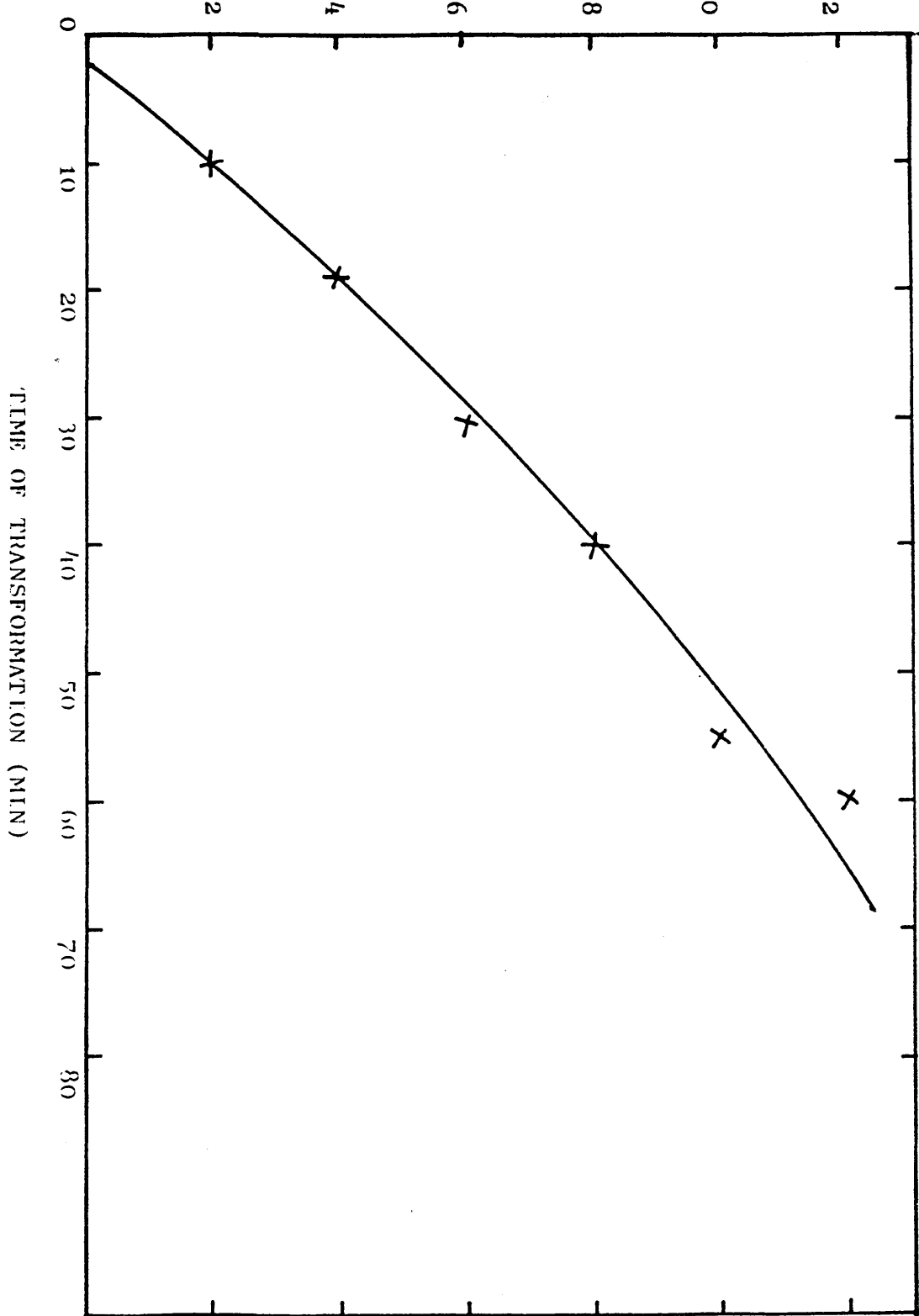


Figure 27 Progress of the transition front with air cooling at 18.7 litres/s (complete insulation during preheat).

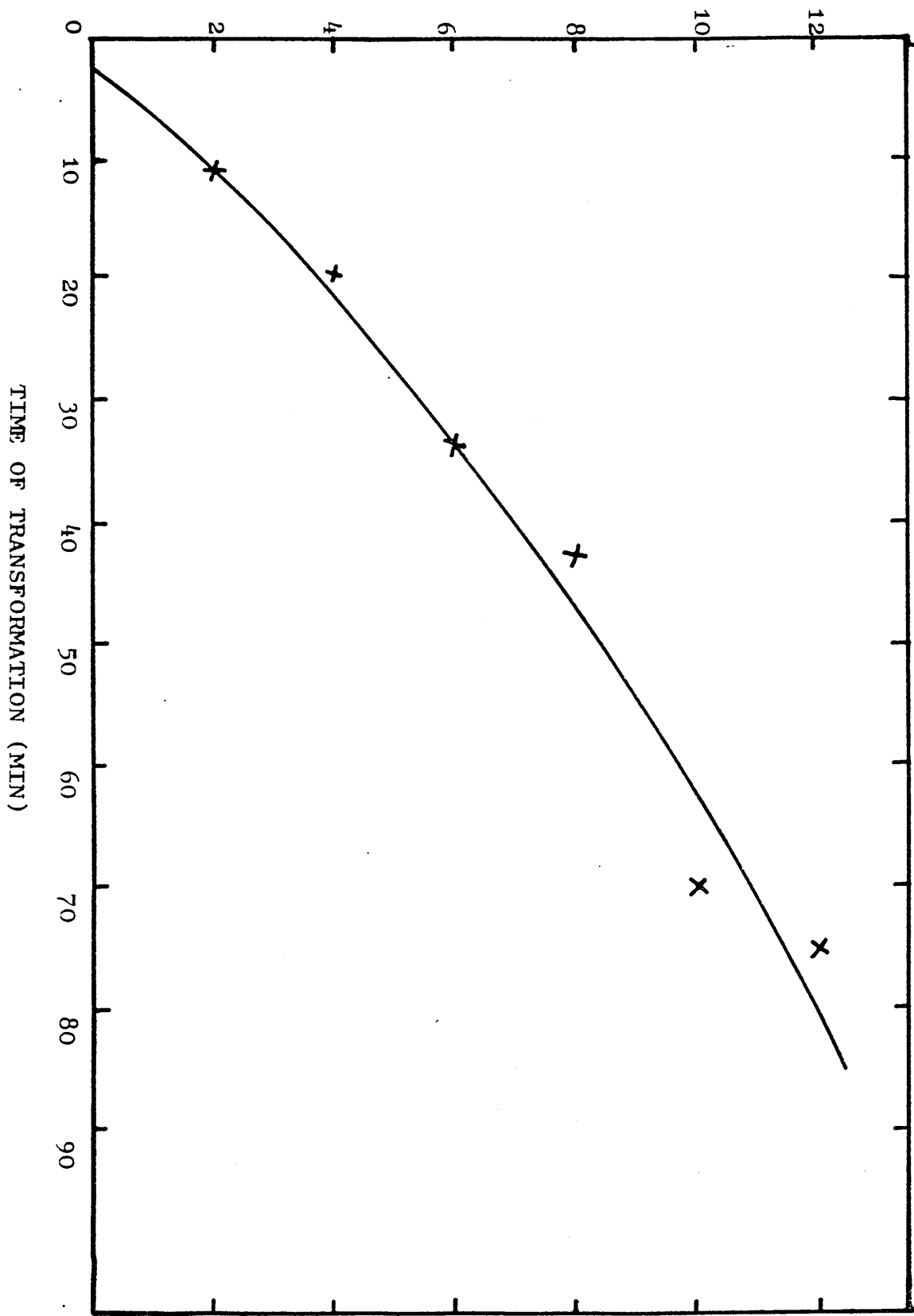


Figure 28 Progress of the transition front with air cooling at 13.2 litres/s (complete insulation during preheat).

5.7 HEAT BALANCE ON THE BILLET IN THE ABSENCE OF TRANSFORMATION

One of the experiments in which the billet was cooled from an initial temperature below the transformation temperature using an air flow of 37.4 litre/s was used as the basis for a heat balance. The heat lost by the billet was compared with the heat removed by the cooling air.

The heat removed by the billet was obtained by integrating the temperature distribution from the bottom to the top of the billet at the beginning and end of the cooling period. These temperatures are shown in Figure 29.

The temperature distribution was integrated as:-

$$\int_0^{15 \text{ cms}} \theta \, dx = \int_0^{12 \text{ cms}} \theta \, dx + \int_{12 \text{ cms}}^{15 \text{ cms}} \theta \, dx$$

The first integral on the right hand side of this equation was evaluated by Simpson's rule from the experimentally measured temperatures shown in Tables 26 and 27 and plotted in Figure 29. The second integral was evaluated by extrapolation from the other values. The following results were obtained:-

$$\text{At zero time: } \int_0^{15 \text{ cms}} \theta \, dx = 107^{\circ}\text{C.m}$$

equivalent to a mean temperature of 713°C

$$\text{After 90 minutes } \int_0^{15 \text{ cms}} \theta \, dx = 41.9^{\circ}\text{C.m}$$

equivalent to a mean temperature of 280°C

The cross sectional area of the billet is 0.0177 m^2 and its length is 0.15 m , so that its volume is $2.66 \times 10^{-3} \text{ m}^3$. The equation

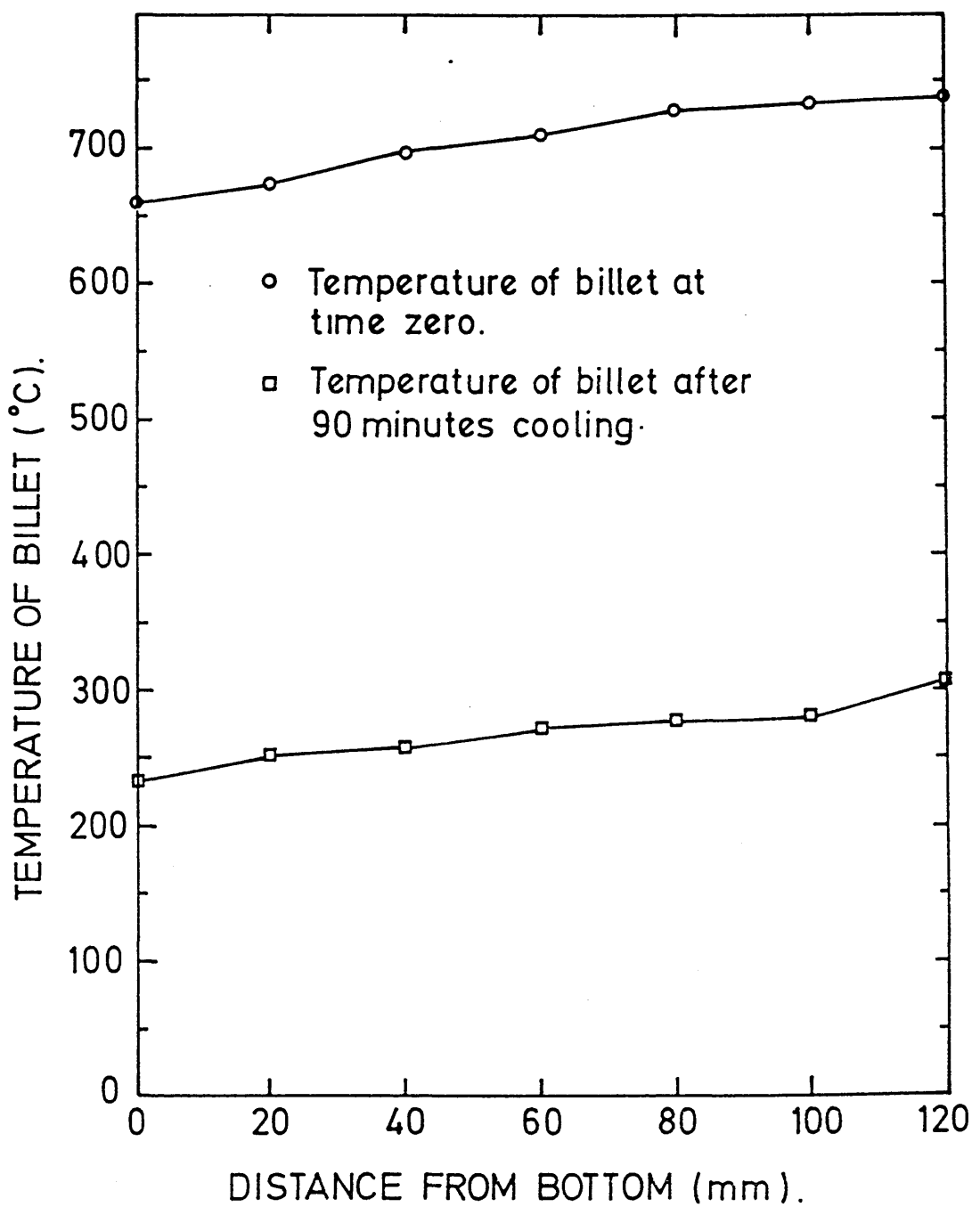


Figure 29 Measured temperatures within the billet at the start and finish of the cooling experiment without transformation.

TABLE 26 Temperatures at different distances
from bottom at the start of the cooling
experiment in the absence of transformation.

Temperature (°C)	Distance from bottom (mm)
662	0
674	20
697	40
709	60
729	80
733	100
738	120

TABLE 27 Temperatures at different distances
from bottom at the finish of the cooling
experiment in the absence of transformation.

Temperature (°C)	Distance from bottom (mm)
234	0
252	20
259	40
271	60
279	80
283	100
308	120

adopted in Appendix 1 shows that the mean specific heat over the temperature range involved in the heat balance experiment is 0.55 kJ/kg.K. Taking this value and the mean steel density specified in Appendix 1, gives the thermal capacity of the billet sample as 11.2 kJ/K and the heat lost by the billet in the cooling experiment as 4.9 MJ.

The heat removed from the block was determined as:-

$$q = A \int_0^{90 \text{ mins}} \theta h(\theta_0 - \theta_A) dt$$

The heat transfer coefficient is a function of temperature, as will be discussed later, so that it cannot be removed from within the integral sign. Values of the surface temperature were taken every 10 minutes from the temperature record of the cooling experiment and are shown in Table 28. Also in that table are the values of $q [= Ah(\theta_0 - \theta_A)]$ at these same times. These latter values have been calculated from the recorded surface temperature and from the heat transfer coefficient calculated as outlined in section 6.1.3.

Using Simpson's rule to evaluate the above integral gives:-

$$A \int_0^{90 \text{ mins}} \theta h(\theta_0 - \theta_A) dt = 6.9 \text{ MJ}$$

The discrepancy between these two values will be discussed in section 6.

TABLE 28

Surface temperatures and heat removal rates
from the billet base during the cooling
experiment in the absence of transformation

Time/min	$\theta_s/^\circ\text{C}$	\dot{q}/kw
0	662	2.75
5	544	2.11
10	484	1.82
15	450	1.66
20	427	1.55
25	415	1.50
30	391	1.39
35	379	1.34
40	367	1.29
45	344	1.19
40	332	1.14
50	332	1.14
55	320	1.09
60	295	0.99
65	283	0.94
70	271	0.89
75	259	0.84
80	247	0.79
85	240	0.76
90	234	0.74

5.8 INTERLAMELLA SPACING OF PEARLITE

After an experiment in which the sample billet was cooled with air at 13.2 litres/s, it was removed from the apparatus and sectioned to examine the microstructure so that the interlamella spacing of the pearlite could be determined.

Several samples were taken from the billet, at the heights of the six thermocouples and from its upper surface. After standard metallographic preparation and etching in Nital, the interlamella spacing was measured by Belaiew's method⁽²⁵⁾ in the scanning microscope. Average results are shown in Table 29.

Photographs of typical microstructures that were taken are shown in Figures 30 to 35.

Distance from billet base (mm)	Interlamella spacing (m)
150	0.37
120	0.35
100	0.33
80	0.31
60	0.28
40	0.19
20	0.17

TABLE 29

Interlamella spacing of pearlite as a
function of distance from the cooled base

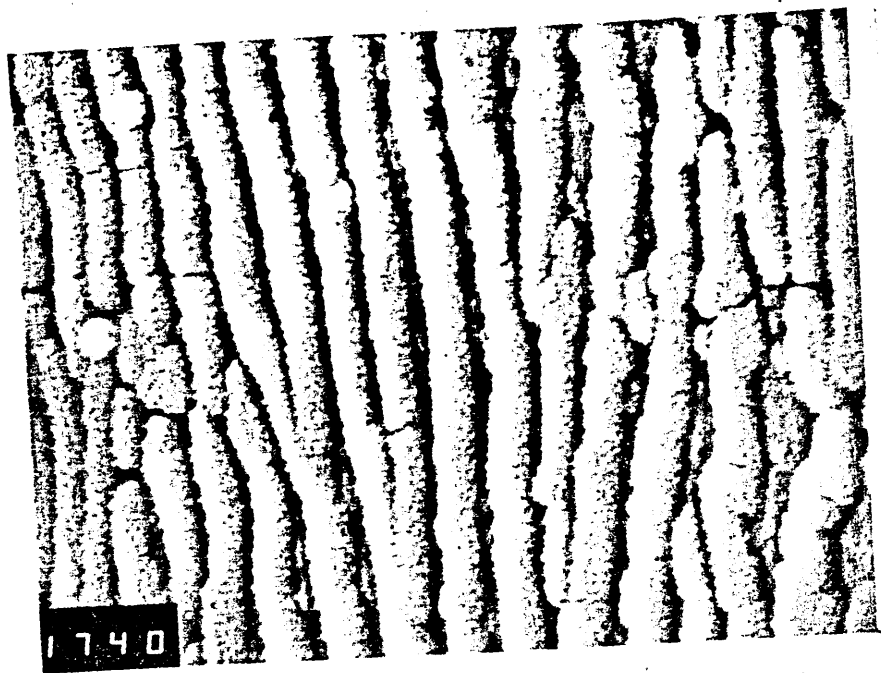


Figure 30 Pearlite spacing at 12 cm from the base of the steel sample. Magnification 26250X.

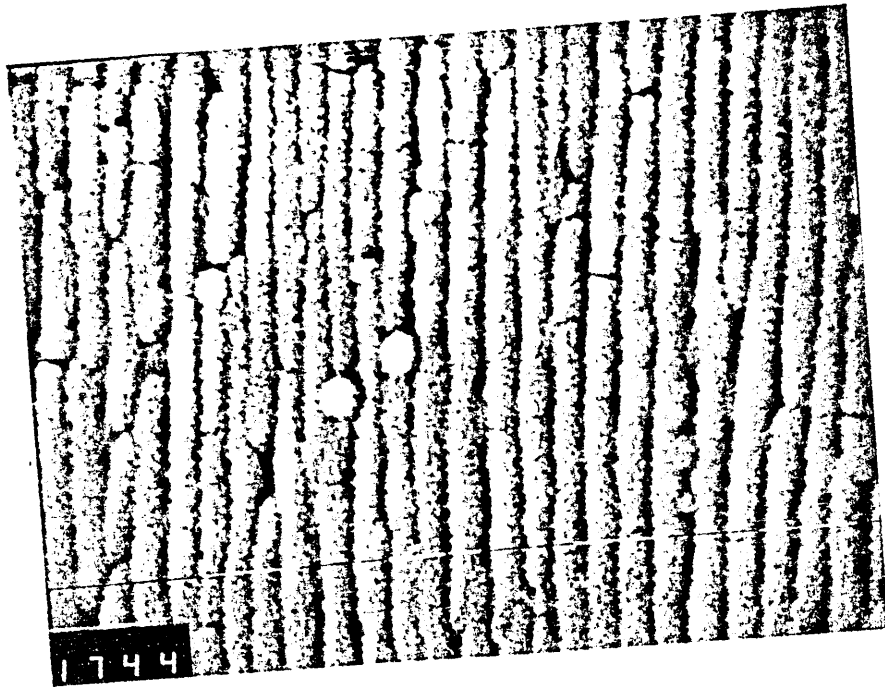


Figure 31 Pearlite spacing at 10 cm from the base of the steel sample. Magnification 26250X.

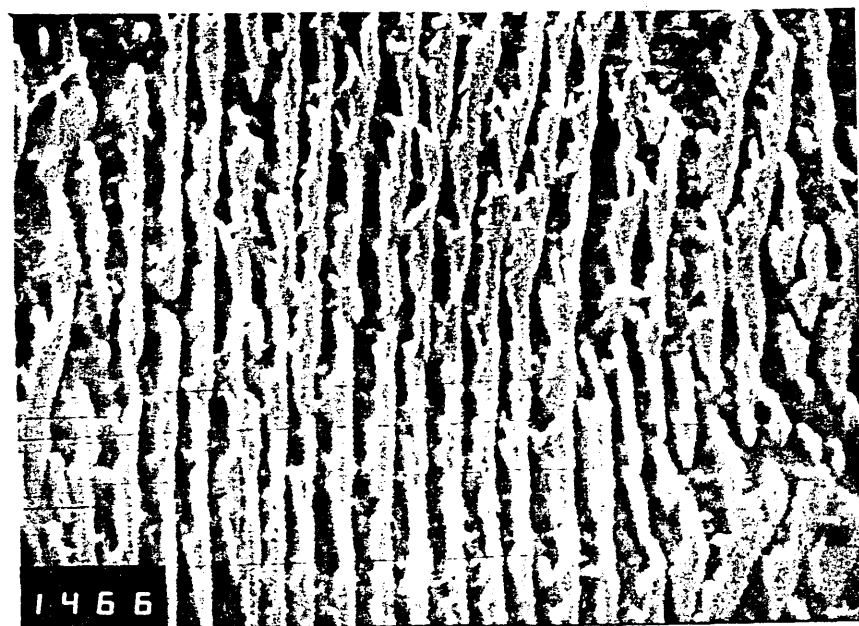


Figure 32 Pearlite spacing at 8 cm from the base of the steel sample. Magnification 26250X.

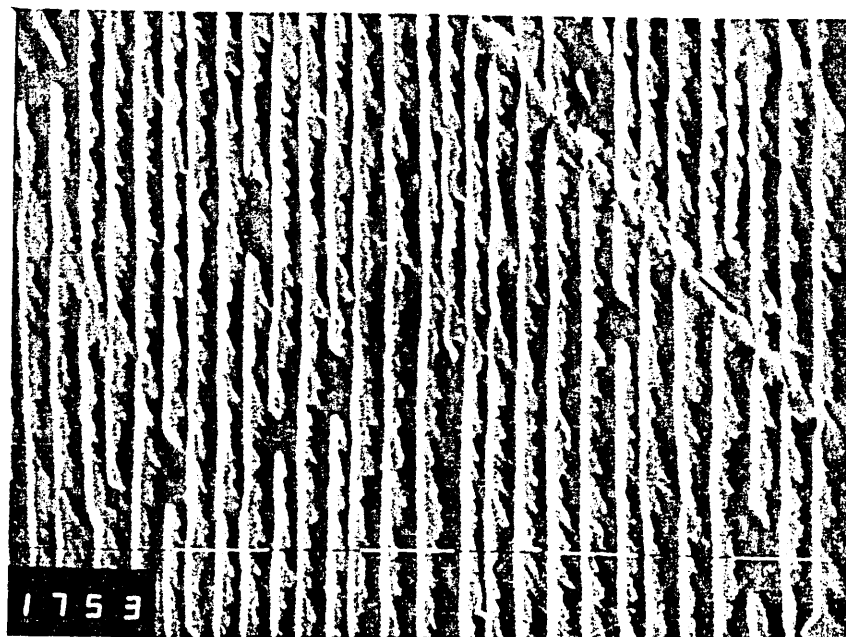


Figure 33 Pearlite spacing at 6 cm from the base of the steel sample. Magnification 26250X.

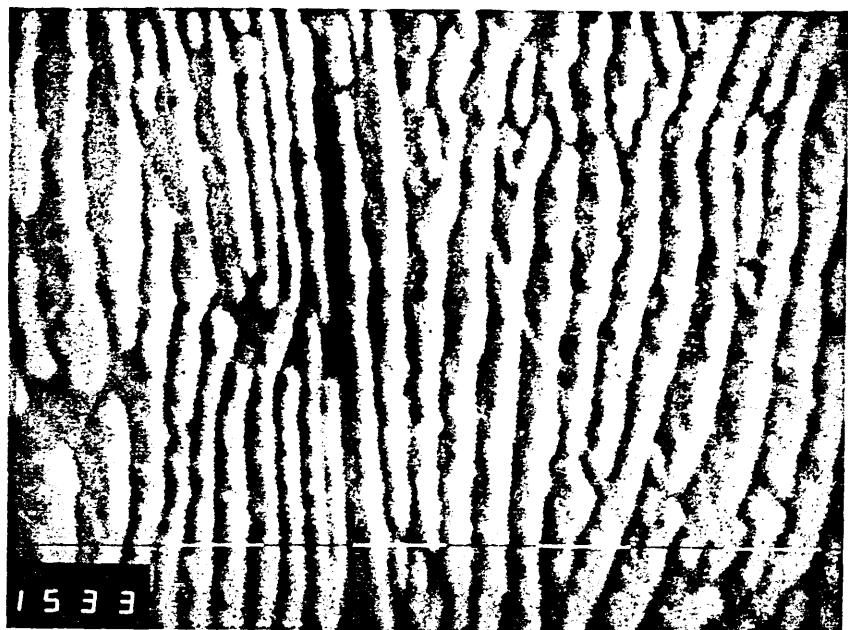


Figure 34 Pearlite spacing at 4 cm from the base of the steel sample. Magnification 26250X.

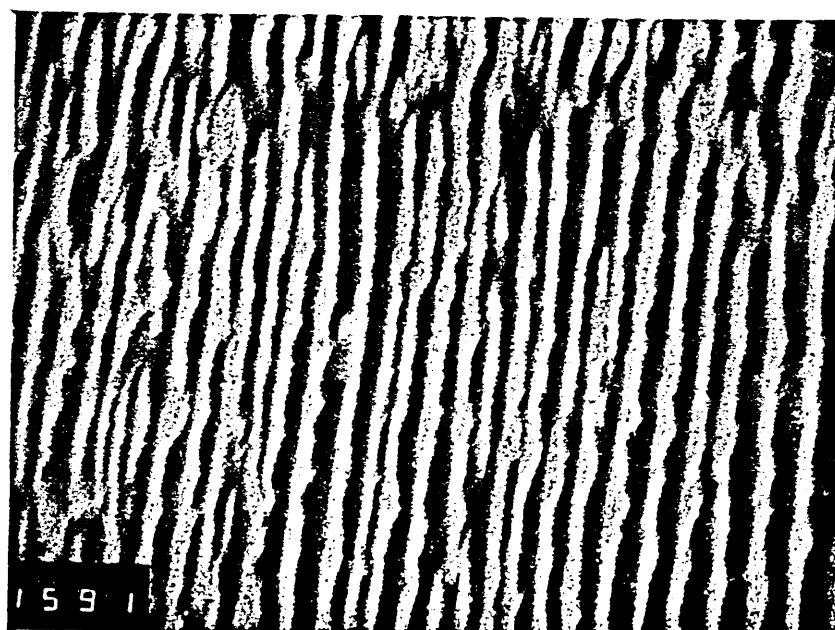


Figure 35 Pearlite spacing at 2 cm from the base of the steel sample. Magnification 26250X.

5.9 COMPUTER RESULTS

Tables 30 to 37 show results obtained from the computer programme listed in chapter 3.

The computer runs for which output is presented have been carried out for the conditions set out below:-

Run 53 - Cooling air flow = 37.4 litre/s giving a convective heat transfer coefficient of $203 \text{ W/m}^2\text{K}$, specific heat modified to include effect of thermal load of heater; property values otherwise as set out in Appendix 1; average surface temperature taken from Table 38, showing the results of the dynamic heat balance (see section 6.3.5), to be 603°C , giving a radiation contribution to the heat transfer coefficient of $37 \text{ W/m}^2\text{K}$.

Run 54 - Conditions identical to Run 53 except that a 50% of the latent heat of transformation is distributed over the temperature range around the transformation temperature.

Run 63 - Same conditions as Run 53 except that the cooling air flow rate is 18.7 liter/s giving a convective heat transfer coefficient of $120 \text{ W/m}^2\text{K}$; average surface temperature taken from Table 39, showing the results of the dynamic heat balance (see section 6.3.5), to be 608°C giving a radiation contribution to the heat transfer coefficient of $38 \text{ W/m}^2\text{K}$.

Run 73 - Same as conditions as Run 53 except that the cooling

air flow is 13.2 litre/s giving a convective heat transfer coefficient of $90 \text{ W/m}^2\text{K}$; average surface temperature taken from Table 40, showing the results of the dynamic heat balance (see section 6.3.5), be 599°C giving a radiation contribution to the heat transfer coefficient of $37 \text{ W/m}^2\text{K}$.

In each case, the actual parametric values used in the computer programme are tabulated in the heading section of the computer output.

The results obtained are discussed in section 6.

TABLE_30 THEORETICAL COMPUTER RESULTS FOR CONDITIONS SPECIFIED
AS RUN 53 - PREDICTED THICKNESSES

THEORETICAL CALCULATIONS FOR EXPERIMENTAL RUN NUMBER 53

DATA USED IN THE CALCULATIONS:-

LR/m	LD	COND/W.m-1K-1	DNSTY/kg.m-3	SPCFHT/J.kg-1K-1
,15	,144E+01	25.0	,774E+04	860.

LATENT/J.KG-1	THTRNS/C	THTAIR/C	LTNTD	THT1/C	THT1D	H/W.m-2K-1
,101E+06	709.0	40.0	,176E+00	861.0	1.227	240.0

CONVERSION FACTORS:- TIMCNV = ,482E+02, THKCNV = ,104E+03

TIME/MIN	THICKNESSES/MM		TEMPERATURES/C		DIMENSLSS VARIABL(*100)				
	TNSD	COOLD	SURFCE	INSLTD	KSI	TX	TCX	TH0*	TH10*
0.0	0.	.	861.	861.	000.	000.	000.	123.	123.
1.5	0.	47.	709.	861.	3.	000.	45.	100.	123.
2.0	,	57.	706.	861.	4.	.	55.	100.	123.
2.6	2.	66.	696.	861.	5.	2.	63.	93.	123.
3.2	4.	72.	685.	861.	7.	4.	69.	96.	123.
4.5	9.	82.	663.	861.	9.	8.	79.	93.	123.
9.5	23.	108.	601.	861.	20.	22.	103.	84.	123.
12.4	31.	119.	575.	861.	26.	30.	114.	80.	123.
14.5	37.	113.	559.	840.	30.	35.	114.	78.	120.
19.5	50.	100.	527.	795.	40.	48.	114.	73.	113.
24.5	64.	86.	499.	758.	51.	62.	114.	69.	107.
29.5	80.	70.	476.	732.	61.	77.	114.	65.	103.
34.5	97.	53.	456.	716.	72.	93.	114.	62.	101.
35.7	101.	49.	452.	714.	74.	97.	114.	62.	101.
37.0	105.	45.	447.	712.	77.	101.	114.	61.	100.
38.2	110.	40.	443.	711.	79.	105.	114.	60.	100.
39.5	114.	36.	439.	710.	82.	110.	114.	60.	100.
40.7	119.	31.	435.	709.	85.	114.	114.	59.	100.
42.0	123.	27.	431.	709.	87.	118.	114.	58.	100.
43.2	128.	22.	427.	709.	90.	123.	114.	58.	100.
44.5	132.	18.	424.	709.	92.	127.	114.	57.	100.
45.7	136.	14.	420.	709.	95.	131.	114.	57.	100.
46.4	138.	12.	419.	709.	96.	133.	114.	57.	100.
51.4	155.	-5.	406.	709.	107.	149.	114.	55.	100.

TABLE_31 THEORETICAL COMPUTER RESULTS FOR CONDITIONS SPECIFIED
AS RUN 53 - PREDICTED TEMPERATURES

THEORETICAL CALCULATIONS FOR EXPERIMENTAL RUN NUMBER 53

DATA USED IN THE CALCULATIONS:-

LR/m	LD	COND/W.m-1K-1	DNSTY/kg.m-3	SPCFHT/J.kg-1K-1
,15	,144E+01	25.0	,774E+04	860.

LATENT/J.KG-1	THTRNS/C	THTAIR/C	LTNTD	THT1/C	THT1D	H/W.m-2K-1
,101E+06	709.0	40.0	,176E+00	861.0	1.227	240.0

CONVERSION FACTORS:- TIMCNV = ,482E+02, THKCNV = ,104E+03

TIME/MIN	THERMOCOUPLE TEMPERATRURES					
	1(120,MM)	2(100,MM)	3(80,MM)	4(60,MM)	5(40,MM)	6(20,MM)

0.	861.	861.	861.	861.	861.	861.
2.	861.	861.	861.	861.	857.	810.
2.	861.	861.	861.	861.	847.	795.
3.	861.	861.	861.	859.	834.	780.
3.	861.	861.	861.	853.	823.	769.
4.	861.	861.	859.	841.	804.	750.
9.	859.	849.	827.	795.	753.	697.
12.	851.	834.	808.	774.	731.	670.
14.	831.	814.	790.	758.	717.	653.
19.	787.	773.	753.	725.	684.	616.
24.	752.	742.	725.	701.	653.	586.
29.	728.	720.	709.	676.	626.	559.
34.	714.	710.	690.	653.	602.	536.
36.	712.	708.	685.	648.	597.	531.
37.	711.	705.	681.	643.	591.	526.
38.	710.	702.	676.	638.	586.	521.
39.	709.	698.	672.	633.	581.	517.
41.	709.	695.	668.	629.	577.	512.
42.	708.	692.	664.	624.	572.	508.
43.	706.	689.	661.	620.	568.	503.
44.	704.	686.	657.	616.	563.	499.
46.	702.	683.	653.	612.	559.	495.
46.	701.	682.	651.	610.	557.	494.
51.	693.	671.	638.	595.	542.	479.

TABLE_32 THEORETICAL COMPUTER RESULTS FOR CONDITIONS SPECIFIED
AS RUN 54 - PREDICTED THICKNESSES

THEORETICAL CALCULATIONS FOR EXPERIMENTAL RUN NUMBER 54

DATA USED IN THE CALCULATIONS:-

LR/M	LD	COND/W.M-1K-1	DNSTY/kg.m-3	SFCFHT/J.kg-1K-1
,15	,144E+01	25.0	,774E+04	1030.

LATENT/J.KG-1	THTRNS/C	THTAIR/C	LTNTD	THT1/C	THT1D	H/W.M-2K-1
,510E+05	709.0	40.0	,740E-01	861.0	1.227	240.0

CONVERSION FACTORS:- TIMCNV = ,577E+02, THKCNV = ,104E+03

TIME/MIN	THICKNESS/MM		TEMPERATURES/C		DIMENSLSS VARIABL'S (*100)				
	TRNSD	COOLD	SURFCE	INSLTD	KSI	T*	TC*	TH0*	THI0*
0.0	0.	,	861.	861.	000.	000.	000.	123.	123.
1.9	0.	47.	709.	861.	3.	000.	45.	100.	123.
2.1	.	51.	709.	861.	4.	,	49.	100.	123.
2.4	1.	56.	703.	861.	4.	1.	53.	99.	123.
2.7	2.	59.	697.	861.	5.	2.	56.	98.	123.
3.3	4.	64.	684.	861.	6.	4.	61.	96.	123.
4.6	9.	71.	661.	861.	8.	8.	68.	93.	123.
9.6	24.	93.	599.	861.	17.	23.	89.	84.	123.
14.6	38.	108.	560.	861.	25.	37.	103.	78.	123.
15.3	40.	110.	555.	861.	27.	38.	105.	77.	123.
19.6	51.	99.	529.	818.	34.	49.	105.	73.	116.
24.6	67.	83.	503.	775.	43.	64.	105.	69.	110.
29.6	85.	65.	480.	740.	51.	81.	105.	66.	105.
30.9	90.	60.	475.	733.	53.	86.	105.	65.	104.
32.1	95.	55.	470.	727.	56.	91.	105.	64.	103.
33.3	100.	50.	465.	721.	58.	96.	105.	64.	102.
34.6	106.	44.	460.	717.	60.	102.	105.	63.	101.
35.8	112.	38.	455.	713.	62.	108.	105.	62.	101.
37.1	119.	31.	451.	711.	64.	114.	105.	61.	100.
37.7	122.	28.	448.	710.	65.	117.	105.	61.	100.
38.3	126.	24.	446.	710.	66.	120.	105.	61.	100.
38.9	129.	21.	444.	709.	68.	124.	105.	60.	100.
39.6	132.	18.	442.	709.	69.	127.	105.	60.	100.
40.2	136.	14.	439.	709.	70.	130.	105.	60.	100.
40.5	137.	13.	438.	709.	70.	132.	105.	60.	100.
40.8	139.	11.	437.	709.	71.	134.	105.	59.	100.

TABLE_33 THEORETICAL COMPUTER RESULTS FOR CONDITIONS SPECIFIED
AS RUN 63 -- PREDICTED THICKNESSES

THEORETICAL CALCULATIONS FOR EXPERIMENTAL RUN NUMBER 63

DATA USED IN THE CALCULATIONS:-

LR/M	LD	COND/W.M-1K-1	DNSTY/kg.m-3	SPCFHT/J.kg-1K-1		
.15	.948E+00	25.0	.774E+04	860.		
LATENT/J.KG-1	THTRNS/C	THTAIR/C	LTNTD	THT1/C	THT1D	H/W.M-2K-1
.101E+06	715.0	40.0	.174E+00	860.0	1.215	158.0

CONVERSION FACTORS:- TIMCNV = .111E+03, THKCNV = .158E+03

TIME/MIN	THICKNESSES/MM		TEMPERATURES/C		DIMENSNLSS VARIABLSS(*100)				
	TRNSD	COOLD	SURFCE	INSLTD	KSI	T*	TC*	TH0*	TH10*
0.0	0.	.	860.	860.	000.	000.	000.	121.	121.
3.2	0.	68.	715.	860.	3.	000.	43.	100.	121.
5.0	2.	92.	706.	860.	5.	1.	58.	99.	121.
6.2	5.	101.	696.	860.	6.	3.	64.	97.	121.
11.2	16.	127.	658.	860.	10.	10.	80.	92.	121.
12.4	18.	132.	650.	860.	11.	11.	83.	90.	121.
16.3	26.	124.	627.	831.	15.	17.	83.	87.	117.
21.3	38.	112.	601.	798.	19.	24.	83.	83.	112.
26.3	49.	101.	578.	770.	24.	31.	83.	80.	108.
31.3	62.	88.	558.	748.	28.	39.	83.	77.	105.
36.2	75.	75.	540.	732.	33.	47.	83.	74.	102.
41.2	89.	61.	524.	722.	37.	56.	83.	72.	101.
46.2	103.	47.	509.	717.	42.	65.	83.	70.	100.
47.5	107.	43.	503.	716.	43.	67.	83.	69.	100.
48.7	110.	40.	503.	716.	44.	70.	83.	69.	100.
50.0	114.	36.	500.	715.	45.	72.	83.	68.	100.
51.3	117.	33.	497.	715.	46.	74.	83.	68.	100.
52.5	121.	29.	494.	715.	47.	76.	83.	67.	100.
53.8	124.	26.	491.	715.	48.	79.	83.	67.	100.
55.0	128.	22.	488.	715.	50.	81.	83.	66.	100.
56.3	131.	19.	485.	715.	51.	83.	83.	66.	100.
57.5	135.	15.	483.	715.	52.	85.	83.	66.	100.
62.5	148.	2.	473.	715.	56.	94.	83.	64.	100.
67.5	161.	-11.	463.	715.	61.	102.	83.	63.	100.

TABLE_34 THEORETICAL COMPUTER RESULTS FOR CONDITIONS SPECIFIED
AS RUN 63 - PREDICTED TEMPERATURES

THEORETICAL CALCULATIONS FOR EXPERIMENTAL RUN NUMBER 63

DATA USED IN THE CALCULATIONS:-

LR/M	LD	COND/W.m-1K-1	DNSTY/kg.m-3	SPCFHT/J.kg-1K-1
.15	,948E+00	25.0	,774E+04	860.

LATENT/J.KG-1	THTRNS/C	THTAIR/C	LTNTD	THT1/C	THT1D	H/W.m-2K-1
,101E+06	715.0	40.0	,174E+00	860.0	1.215	158.0

CONVERSION FACTORS:- TIMCNV = ,111E+03, THKCNV = ,158E+03

TIME/MIN	THERMOCOUPLE TEMPERATRURES					
	1(120,MM)	2(100,MM)	3(80,MM)	4(60,MM)	5(40,MM)	6(20,MM)

0.	860.	860.	860.	860.	860.	860.
3.	860.	860.	860.	858.	835.	788.
5.	860.	860.	857.	840.	810.	766.
6.	860.	859.	850.	830.	798.	755.
11.	855.	844.	825.	798.	765.	725.
12.	852.	839.	819.	792.	759.	719.
16.	824.	812.	794.	769.	739.	697.
21.	792.	781.	766.	745.	718.	669.
26.	765.	756.	743.	726.	696.	644.
31.	744.	737.	727.	712.	674.	622.
36.	729.	724.	717.	693.	653.	602.
41.	720.	717.	705.	675.	635.	585.
46.	716.	713.	691.	660.	619.	569.
47.	716.	710.	688.	656.	615.	565.
49.	715.	707.	684.	653.	612.	562.
50.	715.	704.	681.	649.	608.	558.
51.	715.	702.	678.	646.	605.	555.
53.	715.	699.	675.	642.	601.	552.
54.	713.	697.	672.	639.	598.	549.
55.	711.	694.	669.	636.	595.	546.
56.	709.	692.	666.	633.	592.	543.
58.	707.	689.	664.	630.	589.	540.
63.	700.	680.	653.	619.	577.	529.
67.	693.	671.	643.	609.	567.	519.

TABLE_35 THEORETICAL COMPUTER RESULTS FOR CONDITIONS SPECIFIED
AS RUN 73 - PREDICTED THICKNESSES

THEORETICAL CALCULATIONS FOR EXPERIMENTAL RUN NUMBER 73
DATA USED IN THE CALCULATIONS:-

LR/m	LD	COND/W.m-1K-1	DNSTY/kg.m-3	SPCFHT/J.kg-1K-1
,15	,762E+00	25.0	,774E+04	860.

LATENT/J.KG-1	THTRNS/C	THTAIR/C	LTNTD	THT1/C	THT1D	H/W.m-2K-1
,101E+06	725.0	40.0	,171E+00	863.0	1.201	127.0

CONVERSION FACTORS:- TIMCNV = ,172E+03, THKCNV = ,197E+03

TIME/MIN	THCKNSSES/MM		TEMPERATURES/C		DIMENSNLSS VARIABL\$(*100)				
	TRNSD	COOLD	SURFCE	INSLTD	KSI	T*	TC*	TH0*	TH10*
0.0	0.	,	863.	863.	000.	000.	000.	120.	120.
4.4	0.	79.	725.	863.	3.	000.	40.	100.	120.
5.0	,	89.	724.	863.	3.	,	45.	100.	120.
10.0	8.	127.	699.	863.	6.	4.	64.	96.	120.
12.3	12.	138.	686.	863.	7.	6.	70.	94.	120.
15.0	17.	133.	673.	845.	9.	9.	70.	92.	118.
20.0	27.	123.	649.	815.	12.	14.	70.	89.	113.
25.0	38.	112.	628.	790.	15.	19.	70.	86.	109.
30.0	48.	102.	609.	769.	17.	25.	70.	83.	106.
35.0	60.	90.	591.	752.	20.	30.	70.	80.	104.
40.0	72.	78.	576.	739.	23.	37.	70.	78.	102.
45.0	85.	65.	562.	731.	26.	43.	70.	76.	101.
50.0	97.	53.	549.	727.	29.	50.	70.	74.	100.
55.0	110.	40.	537.	725.	32.	56.	70.	73.	100.
60.0	123.	27.	527.	725.	35.	62.	70.	71.	100.
61.3	126.	24.	524.	725.	36.	64.	70.	71.	100.
62.5	129.	21.	522.	725.	36.	66.	70.	70.	100.
63.8	132.	18.	520.	725.	37.	67.	70.	70.	100.
65.0	135.	15.	517.	725.	38.	69.	70.	70.	100.
70.0	147.	3.	509.	725.	41.	75.	70.	68.	100.
75.0	159.	-9.	501.	725.	44.	81.	70.	67.	100.

TABLE_36 THEORETICAL COMPUTER RESULTS FOR CONDITIONS SPECIFIED
AS RUN 73 - PREDICTED TEMPERATURES

THEORETICAL CALCULATIONS FOR EXPERIMENTAL RUN NUMBER 73

DATA USED IN THE CALCULATIONS:-

LR/M	LD	COND/W.M-1K-1	DNSTY/kg.m-3	SPCFHT/J.kg-1K-1
.15	.762E+00	25.0	.774E+04	860.

LATENT/J.KG-1	THTRNS/C	THTAIR/C	LTNTD	THT1/C	THT1D	H/W.M-2K-1
.101E+06	725.0	40.0	.171E+00	863.0	1.201	127.0

CONVERSION FACTORS:- TIMCNV = .172E+03, THKCNV = .197E+03

TIME/MIN	THERMOCOUPLE TEMPERATRURES					
	1(120.MM)	2(100.MM)	3(80.MM)	4(60.MM)	5(40.MM)	6(20.MM)
0.	863.	863.	863.	863.	863.	863.
4.	863.	863.	863.	855.	829.	786.
5.	863.	863.	862.	848.	821.	780.
10.	861.	853.	837.	815.	796.	750.
12.	856.	845.	827.	804.	775.	740.
15.	839.	828.	812.	790.	762.	730.
20.	810.	800.	786.	767.	743.	708.
25.	785.	777.	765.	748.	728.	685.
30.	765.	758.	748.	734.	710.	665.
35.	749.	743.	736.	725.	691.	646.
40.	737.	733.	728.	709.	674.	629.
45.	730.	728.	720.	693.	658.	614.
50.	726.	725.	707.	680.	644.	600.
55.	725.	717.	696.	667.	631.	588.
60.	723.	708.	685.	656.	620.	577.
61.	722.	706.	683.	653.	617.	574.
63.	720.	704.	681.	651.	615.	572.
64.	718.	701.	678.	648.	612.	569.
65.	716.	699.	676.	646.	609.	567.
70.	710.	691.	667.	636.	600.	557.
75.	703.	684.	658.	628.	591.	549.

6.1 HEAT_TRANSFER_MEASUREMENTS

6.1.1 Effect of radiation

Heat transfer coefficients from the bottom of the billet have been determined in steady state heat transfer experiments, in which a heated copper plate simulates the bottom of the billet, and in analogous mass transfer measurements involving the sublimation of naphthalene.

Heat is actually removed from the bottom of the billet by the combination of convective heat transfer into the cooling air and by radiation loss to the multiple jet nozzle and to the surroundings.

The rate at which heat is transferred from unit area of the base of the billet can thus be written in the form:-

$$q'' = h_C(\theta_S - \theta_A) + \sigma\epsilon(\theta_S^4 - \theta_A^4) \quad (6.1)$$

where ϵ is the emissivity of the surface losing heat.

Dividing equation (6.1) by $(\theta_S - \theta_A)$ allows a combined heat transfer coefficient from the surface to be defined:-

$$h_T = h_C + \sigma\epsilon(\theta_S^2 + \theta_A^2)(\theta_S + \theta_A) \quad (6.2)$$

The mass transfer coefficients measured in the mass transfer experiments are analogous to h_C . On the other hand, it is the value of h_T that is measured in the steady state heat transfer coefficients and applies in the transformation experiments. Even here, it might not apply precisely because of differences between the emissivities of the steel and copper surfaces. It is thus necessary to elucidate the relative combinations made by

convection and radiation to heat transfer in the steady state experiments.

Overall heat transfer coefficients were measured in the steady state heat transfer experiments at a range of different air flow rates and at different surface temperatures. The result for the four air flow rates used are plotted in figure 36 against the value of $\sigma(\theta_S^2 + \theta_A^2)(\theta_S + \theta_A)$. It can be seen that the results for the separate flow rates fall on separate straight lines all with the same slope. This result confirms the appropriateness of equation (6.2).

For each flow rate, the intercept on the heat transfer axis in the graph in figure 36 represents the convective heat transfer coefficient with which the mass transfer is analogous. The variation of this coefficient with air flow rate and its comparison with the analogous mass transfer results and with the results of other workers are discussed in the next section. The actual values of the convective heat transfer coefficient obtained by extrapolation are, however, listed in table 37.

Further confirmation for the accuracy of this analysis of the effect of thermal radiation is provided by the slope of the lines in figure 36. All the lines are parallel and their slope is 0.8. The copper plate used in the steady state heat transfer experiments was heavily oxidised. In his exhaustive compilation of surface emissivities, McAdams⁽⁴⁸⁾ gives the emissivity of oxidised copper as 0.8 - the identical value to that determined from figure 36.

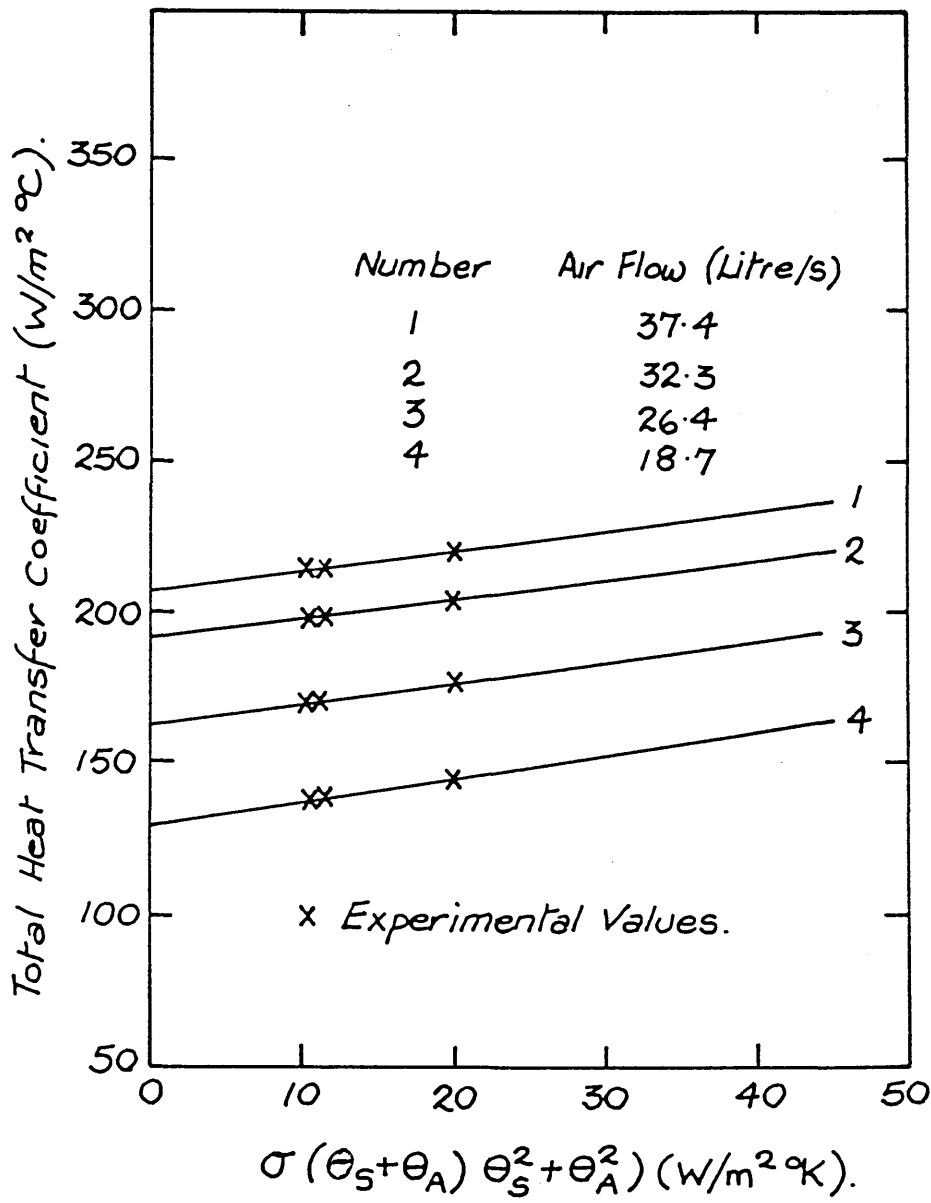


Figure 36 Heat transfer coefficients measured
in the steady state heat flow experiments
plotted against the radiation contribution.

Air flow rate litre/s	Convective heat transfer coefficient by extrapolation in Figure 36 (W/m ² .K)
37.4	206
32.3	190
26.4	163
18.7	130

TABLE_37

HEAT_TRANSFER_COEFFICIENTS_OBTAINED_BY_EXTRAPOLATION_FROM_THE
STEADY_STATE_HEAT_TRANSFER_EXPERIMENTS

6.1.2 Comparison with the mass transfer experiments and with Moore's research (47)

Convective heat transfer coefficients in forced convection are normally correlated by equations of the form:-

$$\text{Nu} = ax\text{Re}^{0.8} \times \text{Pr}^{1/3} \quad (6.3)$$

where Nu is the Nusselt number ($= h d / k$), Re is the Reynold's number ($= vpd/\mu$) and Pr is the Prandtl number ($= \mu C_p / k$).

Experimental data has not been determined that will allow the complete applicability of this correlation to be examined for the results obtained in this work. Some indication of its validity can be obtained, however, by plotting the convective heat transfer coefficients obtained by extrapolation from the steady state heat transfer experiments (Table 37) and by the mass transfer analogy (Table 9) against the air flow rate raised to the 0.8 power.

This plot is presented in figure 37 together with some data obtained by Moore for a similar nozzle.

The agreement achieved between the two methods of measuring the heat transfer coefficient in this work is extremely good indeed. Except for the mass transfer result at the lowest flow, the extrapolated and analogue values of the convective heat transfer coefficient agree to better than 3%. Moreover, the plot against the flow rate raised to the 0.8 power is a respectable straight line.

The results that Moore obtained using the mass transfer analogy on a similar multiple hole nozzle also fall on a straight line

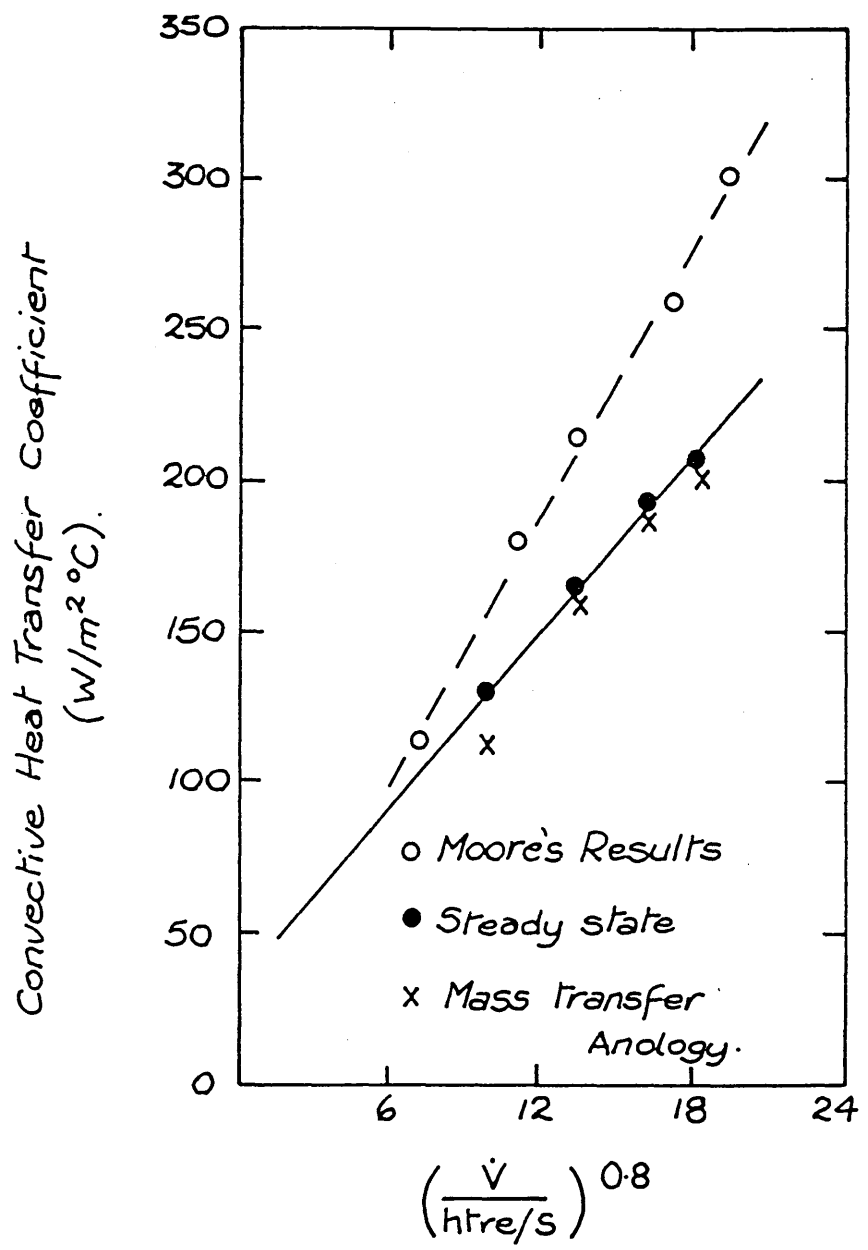


Figure 37 Values of the convective heat transfer coefficient from the heat transfer and mass transfer experiments against the air flow rate to the 0.8 power (also with Moore's results).

but are considerably higher. This is to be expected because the multiple jet in Moore's work was playing on a circular surface of 112.5 mm in diameter. It was, moreover, constrained to operate within a cylindrical tube of this diameter so that the entire air flow was constrained to impinge on the cooled surface. In contrast, the surface cooled in this work was 150 mm and the air was not constrained by an outer tube.

6.1.3 Extrapolation to higher temperatures

The discussion in the previous two sections suggests that the convective heat transfer coefficient is known in the apparatus to a high degree of accuracy. The heat transfer coefficients measured in the steady state experiments cannot, however, be used exactly in analysing the transformation experiments. The emissivities of steel and copper differ and the temperature of the cooled surface of the billet in the transformation experiments is higher than that of the cooled surface of the copper disc used in the steady state heat transfer experiments.

McAdams gives the emissivity of oxidised steel plate as 0.65, and this surface condition is that closest to the condition of the surface of the steel billet. Using the tabulated value of the Stefan-Boltzmann constant, σ , and this emissivity, gives the radiation contribution to the overall heat transfer coefficient defined by equation (6.2) for the billet as:

$$0.037 \times [\theta_S / 100K + 5.86] \times [(\theta_S / 100K + 2.73)^2 + 9.80] \text{ W.m}^{-2}\text{K}^{-1}.$$

The heat transfer coefficient to be used in analysing the experiments involving the steel billet is thus the value of the convective heat transfer coefficient appropriate to the flow rate used, as tabulated in section 6.1.2, plus the value of the above radiation contribution.

The heat transfer coefficient that was used in analysing the results of the heat balance, see section 5.7, has been determined in this way as a function of the surface temperature. The theoretical method outlined in chapter 3, however, assumes a constant value of the heat transfer coefficient. Thus the computer results presented in 5.9 have been calculated using an average value of the heat transfer coefficient calculated for a surface temperature some half-way through the experiment being analysed. The value used is specified in the computer print-out.

6.2 PERFORMANCE OF THE TRANSFORMATION APPARATUS.

6.2.1 Uniformity of initial temperatures

In those industrial processes for which the influence of solid state transformation on heat transfer is important, steel articles are normally heated to a uniform temperature above the transformation temperature and held there for some time. The transformation is then started by allowing the article to cool through the transformation regime.

For this reason, as well as for mathematical convenience, the theoretical analysis developed in this work assumes that the billet is uniformly heated to a constant temperature before it is cooled. In order, then, to make meaningful comparisons

between the theoretical predictions and the experimental results, it was necessary to ensure that the apparatus could heat the sample billet to a constant temperature before cooling was started.

Initially, this criterion could not be met. Tables 15 to 18 and their accompanying figures, pages 5/23 to 5/30, show that the initial temperature difference was of the order to $\pm 80^{\circ}\text{C}$, or $\pm 10\%$. This figure was far too large to allow accurate measurements of the transformation front velocity to be made, especially as the variation represented a much larger fractional variation of the temperature above the transformation point.

Once the bottom of the sample billet was insulated during preheating by the insertion of a refractory block, however, a much more uniform temperature could be achieved. Table 20, on page 5/53, for example, shows that the initial temperature of the billet is $887^{\circ}\text{C} \pm 7^{\circ}\text{C}$, a uniformity better than $\pm 1\%$. Even smaller fractional variations are achieved for the initial conditions in some of the other experiments in which the refractory block was used.

These conclusions are also born out by the experiment reported in section 5.3, commencing on page 5/17. Axial and radial temperature distributions were examined in these experiments, the results being presented in Tables 12 and 13 and their accompanying Figures. Table 12 shows that the axial variation is preheat temperature is certainly less than 2% and Table 13 shows the radial variation is less than 1%. Clearly, the apparatus is

able to preheat the sample billet to a uniformity of temperature better than 2%.

6.2.2 Measurement of surface temperature

The measurement of the temperature of a surface being vigorously cooled is extremely difficult. A thermocouple attached to the surface with leads in the cooling medium will always give an erroneously low reading. Heat loss from the thermocouple leads to the cooling medium itself will be intense. This loss must be compensated for by heat transferred to the thermocouple bead from the local surface in the region of the bead. There is thus an additional cooling effect at the point where the measurement is being made. Anything but the most perfect of thermal contacts between the bead and the surface will lead to a further significant temperature difference being established in order to sustain the heat flow necessary to compensate for the losses from the leads.

For this reason, the thermocouple used to measure the surface temperature was embedded in a slot cut in the surface. It was hoped that the thermocouple leads would not be cooled additionally and the temperature errors would therefore be absent. As will be discussed below, this device appears to have been only partly successful.

An alternative method used to measure surface temperatures involves the measurement of temperatures at a range of different positions within the material followed by extrapolation back to the surface. In effect this method was also used in this work

since temperatures have been determined at a number of different positions within the billet. Comparison can thus be made of the two methods in order to evaluate the success of the direct measurement technique attempted in this work.

During the heat balance experiment, the temperature curves shown in figure 29 indicate that the surface temperatures measured directly and by extrapolation agree extremely well. The direct measurement appears to be working satisfactorily.

This is not the case, however, during the final transformation experiments in which the base of the billet was insulated during preheat. The variations of the surface and internal temperatures with time during these experiments are shown in figures 17 to 21. Temperatures are not plotted against distance from the surface in these figures but figure 38 shows four such plot made at different times during a typical transformation experiments involving cooling at the maximum air flow rate. This figure shows that the surface temperature measurement is erroneously low. Indeed, the separation between the lines in figures 17 to 21 which show the surface and internal temperatures indicate that similar errors have occurred in all the transformation experiments involving complete insulation during preheat.

Internal temperatures measured during the transformation experiments carried out without full insulation of the billet during preheating are shown in figures 13 to 16. As well as showing that the billet was not isothermal at the start of these experiments, the figures suggest that extrapolated and measured

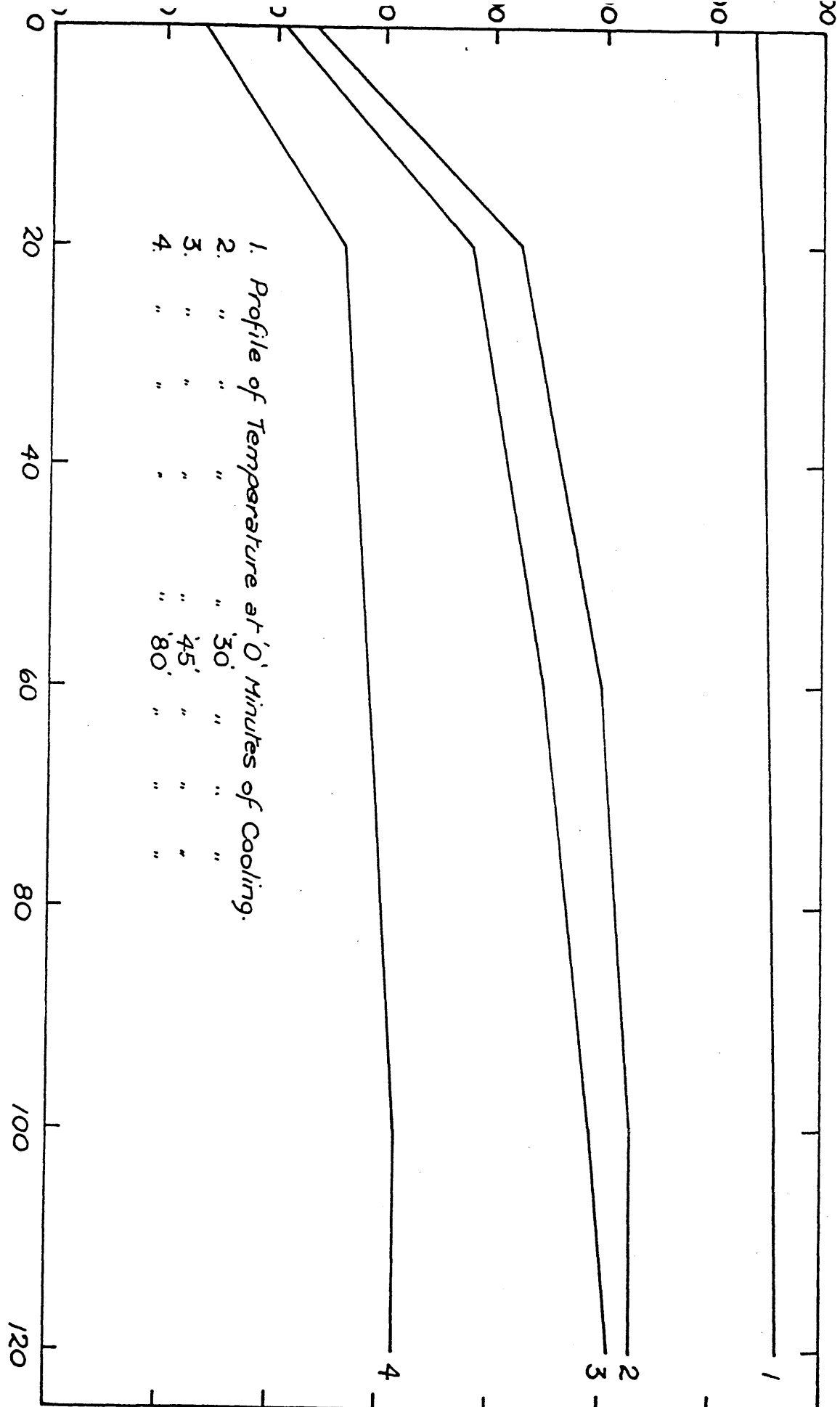


Figure 38 Profile of temperature at different cooling times. Cooling air flow 37.4 litres/s.

surface temperatures would agree during these experiments. Thus the direct measurement of the surface temperature appears satisfactory in these experiments.

As previously reported, an insulating block was inserted between the bottom of the billet and the multiple air jet system during the preheating period in the final transformation experiments. It is possible that the insertion of this block or its removal at the start of an experiment disturbed the thermocouple leads so that they became exposed to direct cooling in the air jet.

In addition, it is possible that oxidation occurring during the duration of the experiments lessened the thermal contact between the thermocouple and the lower billet surface leading to further thermometric error.

Thus it appears that the surface temperatures measured during the heat balance experiment were accurate but that those measured during the final transformation experiments were far too low.

5.2.3 Thermal load of the heater

Whereas the apparatus was designed to place a low thermal load on the billet during cooling, this had not proved possible for the heater. In order to obtain consistent and reliable heater performance at the high temperatures involved in the transformation experiments, it was been found necessary to use a substantial refractory heater manufactured by Litherland Elements Ltd. The thermal load of this heater has a major influence on the experimental results.

The heater is a cylinder 203 mm in height, of 203 mm internal diameter and 248 mm outer diameter, was constructed of oxide materials - primarily 75% Al_2O_3 , 16.5% SiO_2 and 7.7% CaO - and has a porosity of 28%.

The volume of the heater is $3.24 \times 10^{-3} \text{ m}^3$ and, using the densities and specific heats set out in Appendix 1, the thermal capacity of the heater can be shown to be 5.7 kJ.K^{-1} .

As determined in section 5.7, concerned with the heat balance, the volume of the steel billet sample is $2.66 \times 10^{-3} \text{ m}^3$ and its density is 7.74 Mg/m^3 . The mean temperature of the billet in the transformation experiments is some 700°C so that the mean value of the specific heat relevant to these experiments is 0.57 kJ/kg.K (see Appendix 1) so that the thermal capacity of the billet sample during these experiments is 11.5 kJ/K . The thermal capacity of the heater is thus some 50% of the thermal capacity of the steel billet neglecting the heat of transformation.

6.2.4 Overall heat balance in the absence of transformation

Section 5.7 on page 5/52 presents the results of the heat balance that was carried out for the cooling of the billet from a temperature below the transformation temperature and at an air flow rate of 37.4 litre/s.

Table 28 in that section presents the measured base temperature and the heat loss rate from the base calculated using the equation:-

$$\dot{q} = Axh_T \times (\theta_S - 40^\circ\text{C}) \quad (6.4)$$

where h_T is the total heat transfer coefficient as elucidated in section 6.1. Thus the value of h_T used in calculating the values of q in Table 28 is given by the equation:-

$$h_T = \left\{ 203 + 0.037 \times [\theta_S / 100K + 5.86] \times [(\theta_S / 100K + 2.73)^2 + 9.80] \right\} W.m^{-2}K^{-1}$$
(6.5)

A short programme in BASIC was written to carry out these calculations on a Microcomputer, together with the Simpson's rule integration, and is presented in Appendix 2.

Since it has been established in section 6.2.2 that the measured surface temperatures in the heat balance experiment appear accurate, the heat loss rates can be regarded with some confidence.

The results obtained in the heat balance show that the billet liberated some 4.9 MJ in cooling from an average temperature of 713°C to an average temperature of 280°C . On the other hand, the air cooling system removed some 6.9 MJ of heat from the base of the billet. The difference between these two quantities represents the heat transferred from the heater to the cooling billet and then through the billet to the cooling air - some 2.0 MJ. This corresponds to a fall in the temperature of the billet of some $(2.0 \text{ MJ}) / (5.7 \text{ kJ.K}^{-1}) = 350 \text{ K}$.

At the start of the cooling experiment, the heater and the billet were at 713°C so that the temperature of the heater at the end of the cooling experiment is about 360°C , by which time the temperature of the billet had dropped to an average value of 280°C .

The heat lost from the heater has to be transferred by radiation across the annular space between the heater and the billet. Almost all the radiation leaving the heater will eventually be absorbed by the sample, so that we can write the radiation transfer across the space as:-

$$q = A_1 \sigma (\theta_1^4 - \theta_2^4) \quad (6.6)$$

which is equivalent to a radiation transfer coefficient given by:-

$$h_{R,H} = \sigma (\theta_1 + \theta_2) \times (\theta_1^2 + \theta_2^2) \quad (6.7)$$

Thus the rate of radiation transfer at the end of the cooling period is given by:-

$$\begin{aligned} q_{12} &= \pi \times (0.15m)^2 \times 5.67 \times 10^{-8} (W/m^2 K^4) \times [(360+273)^4 - (280+273)^4] K^4 \\ &= 270 W. \end{aligned} \quad (6.8)$$

(equivalent to a heat transfer coefficient of $48 W/m^2 K^2$)

Similarly, the mean temperatures of the heater and billet are $537^\circ C$ and $497^\circ C$ respectively so that the mean heat radiation flux between the heater and the billet is:-

$$\begin{aligned} q_{12} &= \pi \times (0.15m)^2 \times 5.67 \times 10^{-8} (W/m^2 K^4) \times [(537+273)^4 - (497+273)^4] K^4 \\ &= 316 W \end{aligned} \quad (6.9)$$

(equivalent to a heat transfer coefficient of $112 W/m^2 K^2$)

The heat balance showed that 2 MJ of heat were transferred in 90 minutes giving a mean rate of heat transfer of $2MJ/(90 \times 60s)$
 $= 370 W.$

The closeness of the heat transfer rates calculated from radiation transfer considerations and from the heat balance confirms that the excess heat in the heat balance was heat liberated as the heater cooled and that this heat was transferred

by radiation across the annular space between the heater and the sample.

6.3 TRANSFORMATION EXPERIMENTS

6.3.1 Importance of initial temperature uniformity

As stated previously, special precautions were taken to ensure that the billet was uniformly heated before the transformation experiments were commenced since a uniform initial temperature was the time boundary condition for which the theoretical calculations were carried out.

The results in section 5.4 show how important these precautions are. Figures 17 to 21 present the temperatures measured in the billet during the transformation experiments carried out without complete insulation during preheat. The transformation temperature, as indicated by the thermocouple most remote from the cooled surface, is about 735°C and it is doubtful if the surface layers of the billet were preheated sufficiently above this temperature for them to have been transformed to austenite. In any case, the amount of heat that must be removed from the surface layers before they can be cooled below the apparent transformation temperature is very much less than it would be had the billet been preheated to a uniform temperature well within the austenite region. On both these counts, then, the 725°C isothermal would be expected to penetrate more rapidly into the billet than it would after uniform preheat.

The results obtained in section 5.4 demonstrate that this is the case. Table 25 on page 5/44 shows how the apparent transformation isothermal penetrates into the billet. The speed of penetration in those experiments where the billet was not insulated completely during preheat is about twice as fast, for any given cooling condition, as the speed when the billet was completely insulated. Clearly the use of the refractory block to insulate the billet base during preheat was extremely important.

6.3.2 Reproducibility of measurements

In order to examine the reproducibility of the measurements, three transformation experiments were carried out under identical cooling conditions and from the same nominal preheat temperature. The cooling conditions chosen were those established by a cooling air flow of 37.4 litre/s.

The measured temperatures are set out in Tables 19, 20 and 21. These Tables show that the actual average preheat temperatures obtained were 850°C , 862° and 861°C respectively and that the greatest difference between temperatures measured at the same point and at the same nominal time in different experiments was 30°C in some 800°C , a fractional variation less than 4%. This variation was principally due to the low preheat temperature that had been established in one of the experiments. Even so, values of temperature variation as high as 30°C occur relatively rarely in the measured temperatures, more usual variances are less than half this value.

A further test of the reproducibility of the results is provided by the transformation times determined from the cooling curves obtained for each of the thermocouples. These transformation times are presented in Table 25 and plotted in Figure 26 for the three runs obtained with a cooling air flow rate of 37.4 litre/s.

The Figure illustrates a high degree of reproducibility in the transformation times that were determined. Although there are only three times determined for each thermocouple position for the repeated cooling conditions, the standard deviations of the values in Table 25 can also be used to demonstrate the reproducibility of the results obtained.

The largest variation occurs for the transformation time at the thermocouple positioned 2 cm from the cooled base, where the standard deviation is 0.8 mins in 9.7 min - a fractional variation of 9%. This variation is, once again, principally due to the low preheat temperature in one experiment and occurs at the embedded thermocouple closest to the cooled surface and thus corresponds to the largest temperature variation referred to above.

In the main, the results obtained have a high degree of reproducibility, of the order of 5% or better. The accuracy of the thermocouple measurements, about $\pm 2^{\circ}\text{C}$, is considerably better than this so that the errors in this work are no more than the 5% reproducibility.

6.3.3 Influence of the heater - effective specific heat

It has already been established that the thermal capacity of the heater is some 50% of that of the billet, neglecting the latent heat of transformation, and that the transfer of heat from the

heater to the cooling billet is controlled by radiation. This transfer will occur much more rapidly in the transformation experiments than it did in the relatively low temperature experiment for which the heat balance was carried out. The radiation heat transfer coefficient between the billet and the heater in that experiment at the end of the cooling period has been shown to be $48 \text{ W/m}^2\text{K}$. The radiation transfer coefficient in the transformation experiment can be estimated in a similar way from the average temperature of the billet.

Table 20 on page 5/33 presents a typical set of temperatures during a transformation experiment, these temperatures being plotted in figure 18. This figure shows that the transformation front passes the final thermocouple after some 45 minutes. The temperature distribution along the axis of the billet at that time given in Table 20 shows the average temperature of the billet to be 680°C . The average temperature of the heater at the same time will not be less than this figure, so we can say that the minimum value of the radiation transfer coefficient will be:-

$$h_R = 5.67 \times 10^{-8} (\text{W/m}^2\text{K}) \times 4 \times (680 + 273)^3 \text{K}^3 = 470 \text{ W/m}^2\text{K} \quad (6.10)$$

This value is 10 times greater than the corresponding value in the low temperature heat balance experiment. Thus we can conclude that the temperature difference between the heater and the billet at the end of a transformation experiment will be about a tenth of that existing at the end of the low temperature heat balance experiment, or some 8°C . To all intents and purposes, then, the heater liberates all its sensible heat to the billet during the transformation experiments.

The effect of this transferred heat is to increase the effective specific heat of the billet by some 0.28 kJ/kg.K during the transformation experiments.

6.3.4 Estimation of surface temperature

It has already been shown that the temperatures measured directly at the exposed surface of the billet are erroneously low. The temperatures there must be known, however, in order to estimate the heat transfer conditions. This has been done by extrapolation from the temperatures measured inside the billet by fitting a cubic temperature profile to the temperatures measured at 20, 40 and 60 mm from the base. This gives the following formula for the surface temperature:-

$$\theta = 3(\theta_{20\text{cms}} - \theta_{40\text{cms}}) + \theta_{60\text{cms}} \quad (6.11)$$

Application of this formula to the experimental results shows that the average surface temperature during the transformation experiments in which the billet was completely insulated during preheat is some 630°C . The extrapolation formula will also be used subsequently to determine an overall heat balance on the billet.

6.3.5 Dynamic heat balance during transformation

Surface temperatures estimated as described in the previous section were used to obtain a dynamic heat balance during the transformation experiments. The rate of heat removal from the surface was determined using the convective heat transfer coefficient averaged from the data set out in Tables 9 and 37 and augmented by the radiation contribution evaluated in section 6.1.3

In obtaining the heat balance, the rate of heat removal from the surface was determined using the convective heat transfer coefficient averaged from the data set out in Tables 9 and 37 and augmented by the radiation contribution evaluated in section 6.1.3. Simpson's rule was then used to determine the total heat removed from the billet over 10 minute periods.

The total heat that had been lost by the billet was also determined at each 10 minute interval. Simpson's rule was used to determine the average temperature in the billet and this was then multiplied by the density and thermal capacity values for the billet, as set out in Appendix 1, in order to determine the sensible heat content. To this was added the heat of transformation of the untransformed layer, the thickness of transformed steel being read from the appropriate graph of figures 26 to 28. The temperatures used to determine the surface temperature and the average temperature in the billet are those set out in Tables 19, 22 and 23.

A 'BASIC' programme was written to carry out these calculations and is listed in Appendix 2. The results are set out in Tables 38, 39 and 40.

TABLE_38

Dynamic Heat Balance on Ingot Heated Above Transition Temperature

Table of Surface Temperatures and Heat Removal Rates for Run 53
(Billet specific heat augmented to account for heater)

Convective heat transfer coefficient taken as 203 W/m².K

Time (min)	TS (°C)	Qdot (kW)	Heat(MJ) Trnsfred (°C)	Tav (°C)	Heat(MJ) Lost
0	834	3.81			
5	660	2.70			
10	620	2.48	1.71	780	1.74
15	610	2.43			
20	605	2.40	3.17	736	2.94
25	576	2.25			
30	577	2.25	4.53	692	4.09
35	528	2.01			
40	552	2.12	5.77	663	4.94
45	552	2.12			
50	525	1.99	7.03	629	5.82

Initial Average Temperature = 851 Deg-C

Initial Heat Content = 17.04 MJ

TABLE_39

Dynamic Heat Balance on Ingot Heated Above Transition Temperature

Table of Surface Temperatures and Heat Removal Rates for Run 63
 (Billet specific heat augmented to account for heater)

Convective heat transfer coefficient taken as 120 W/m².K

Time (min)	TS (oC)	Qdot (kW)	Heat(MJ) Trnsfred	Tav (oC)	Heat(MJ) Lost
0	852	2.75			
5	690	1.93			
10	665	1.82	1.23	801	1.43
15	640	1.71			
20	605	1.57	2.25	759	2.53
25	614	1.61			
30	575	1.46	3.20	725	3.46
35	575	1.46			
40	560	1.41	4.07	694	4.28
45	550	1.37			
50	555	1.39	4.90	674	4.89
55	548	1.36			
60	560	1.41	5.72	659	5.36
65	565	1.42			
70	565	1.42	6.57	642	5.86

Initial Average Temperature = 862 Deg-C

Initial Heat Content = 17.25 MJ

TABLE 40

Dynamic Heat Balance on Ingot Heated Above Transition Temperature

Table of Surface Temperatures and Heat Removal Rates for Run 73
 (Billet specific heat augmented to account for heater)

Convective heat transfer coefficient taken as 90 W/m².K

Time	TS	Qdot	Heat(MJ)	Tav	Heat(MJ)	
(min)	(oC)	(kW)	Trnsfred	(oC)	Lost	
0	853	2.33				
5	700	1.62				
10	675	1.53	1.03	810	1.31	
15	650	1.43				
20	630	1.36	1.90	769	2.34	
25	615	1.31				
30	585	1.21	2.68	736	3.19	
35	570	1.16				
40	570	1.16	3.38	709	3.92	
45	560	1.13				
50	550	1.10	4.06	692	4.44	
55	545	1.09				
60	540	1.07	4.71	677	4.89	
65	535	1.06				
70	540	1.07	5.35	667	5.22	
75	535	1.06				
80	525	1.03	5.98	656	5.57	

Initial Average Temperature = 865 Deg-C

Initial Heat Content = 17.31 MJ

6.4 COMPARISON BETWEEN THEORETICAL AND EXPERIMENTAL RESULTS

6.4.1 Progression of the Transformation Front

The principal purpose of this investigation is to discover whether the assumptions made in establishing the theoretical method provided a basis for predicting the rates at which steel transformation reactions take place in large steel components. The theoretical method assumes that the rate of the transformation is controlled by the rate of cooling and hence by the rates at which heat is transferred from the cooling steel component. The rate of transformation can thus be predicted by solving the heat transfer equation. The theory developed in Chapter 3 ignores any interaction between the kinetics of the transformation and the heat transfer process. The reaction is assumed to take place over so narrow a range of temperature that the latent heat of the reaction can be assumed to be liberated at a single unique temperature.

The method then used to solve the heat transfer equation, and hence to predict the transformation rates, is the integral-profile method. This is an approximate method that uses assumed quadratic temperature profiles within the transformed and untransformed steel in order to obtain average solutions to the heat transfer equation in the two regions.

The method has been shown to solve a number of unsteady state heat transfer problems to an accuracy well within engineering requirements.

The accuracy of the theoretical predictions is to be judged from

comparisons between them and the results of five particular experiments in which the block was completely insulated during the preheat period. The results of these experiments are presented in Tables 19 to 23 and in Figures 17 to 21 and Figures 26, 27 and 28.

The results have also been plotted in a slightly different way in figures 38A to 43 together with predictions from the computer programme set out in Tables 38 to 40.

Moderately good agreement has been obtained between the theoretical curves and the experimental measurements.

The most consistent relationship is shown in Figure 38A in which the results of computer run 53 are compared with the results of one of the experiments at a cooling air flow of 37.4 litre/s. The theoretical transformation curve in this figure lies some 12% above virtually all the experimental measurements that were made. The theoretical transformation front is advancing more rapidly into the material than the measured front.

In order to find out whether this is due to the theoretical treatment afforded to the release of latent heat, a second computer run was undertaken for identical cooling conditions but with a different pattern for the release of latent heat. Instead of all the latent heat being released at the transformation temperature, half was assumed to be released over a range of temperature on either side of the transformation temperature. This was most conveniently done in the theory by halving the value of the latent heat of transformation and enhancing the

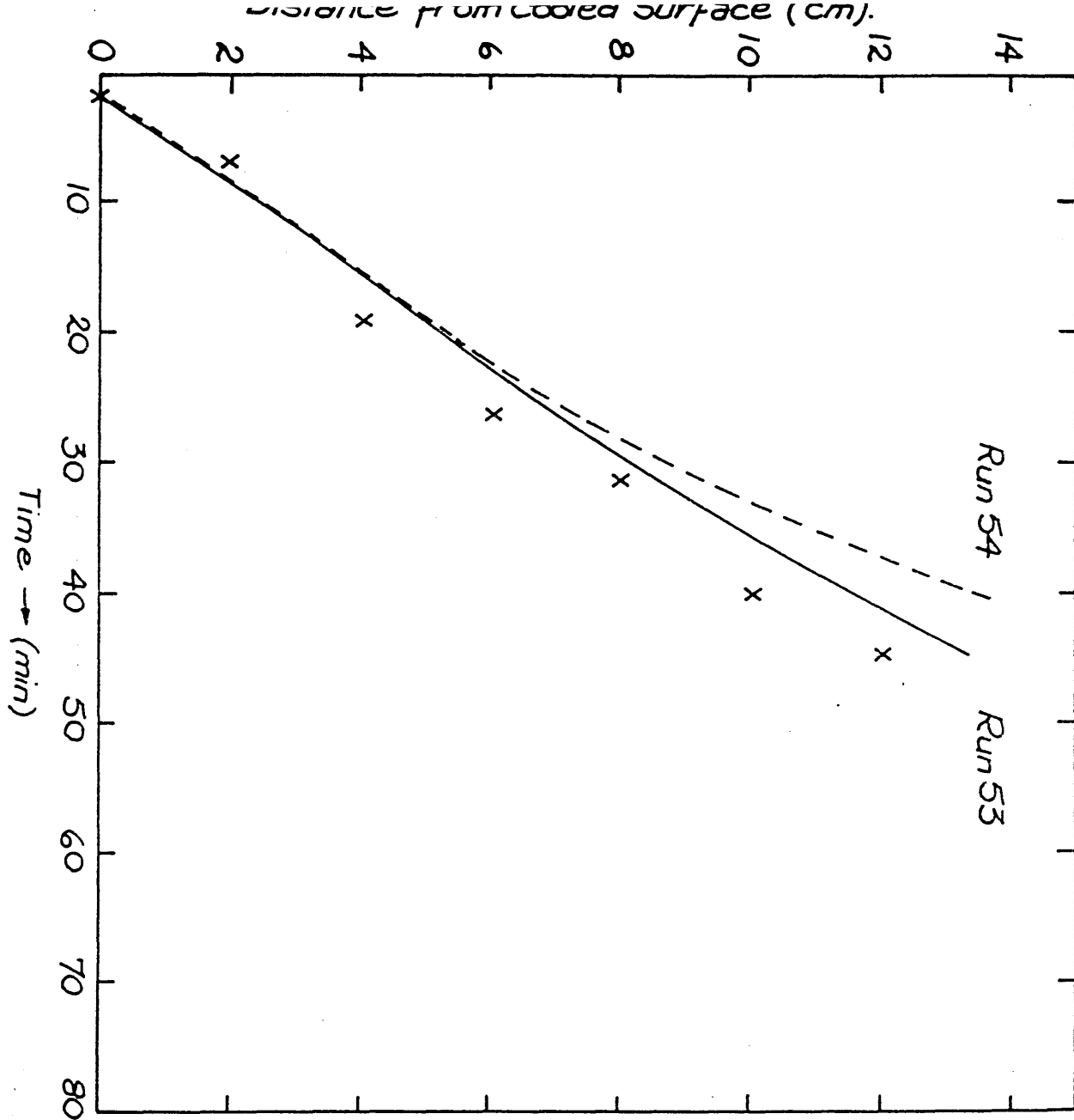


Figure 38A Theoretical and experimental positions of the transformation front - cooling air flow = 37.4 litres/s.

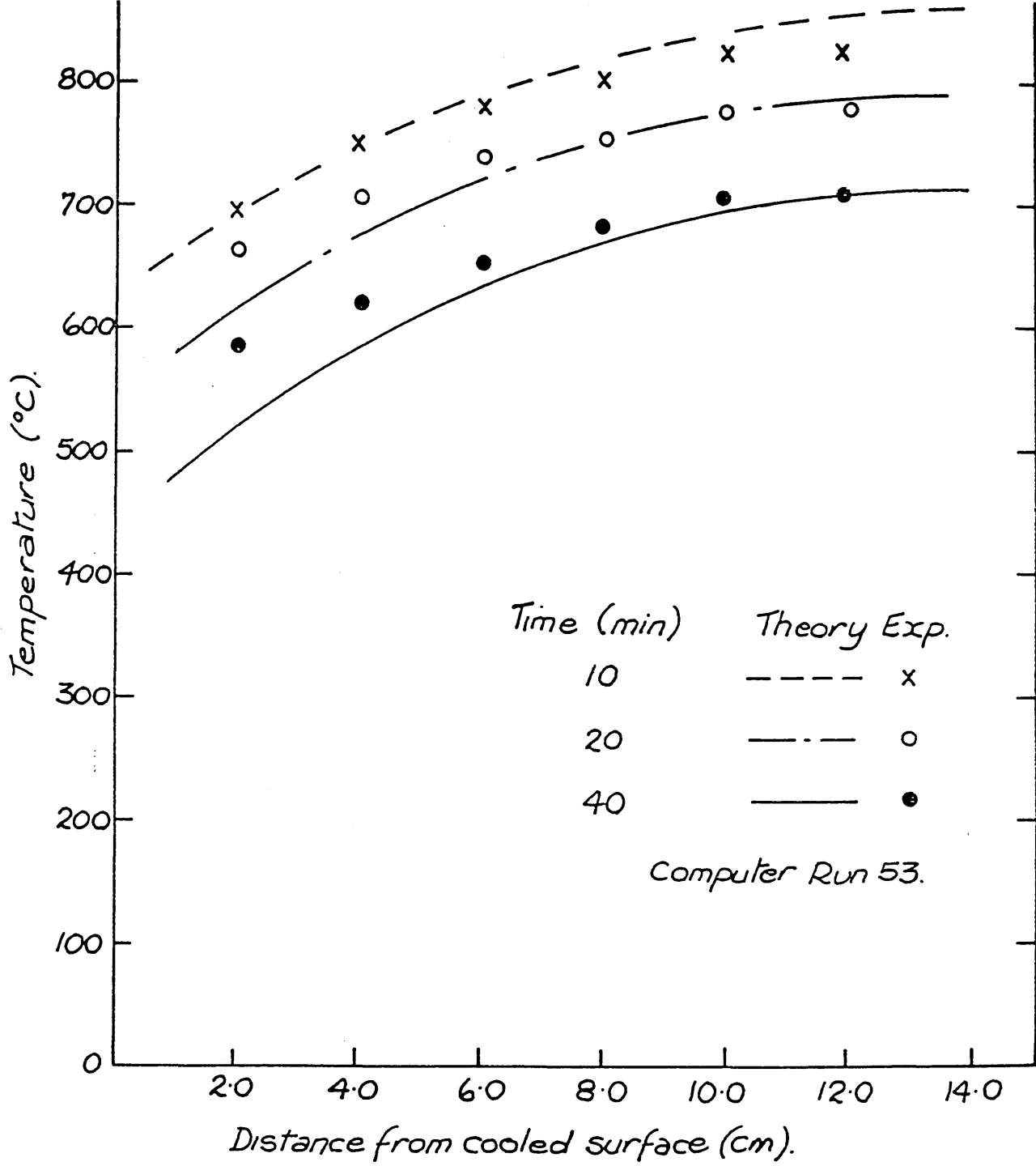


Figure 39 Theoretical and experimental temperature distributions at different times - cooling air flow is 37.4 litres/s.

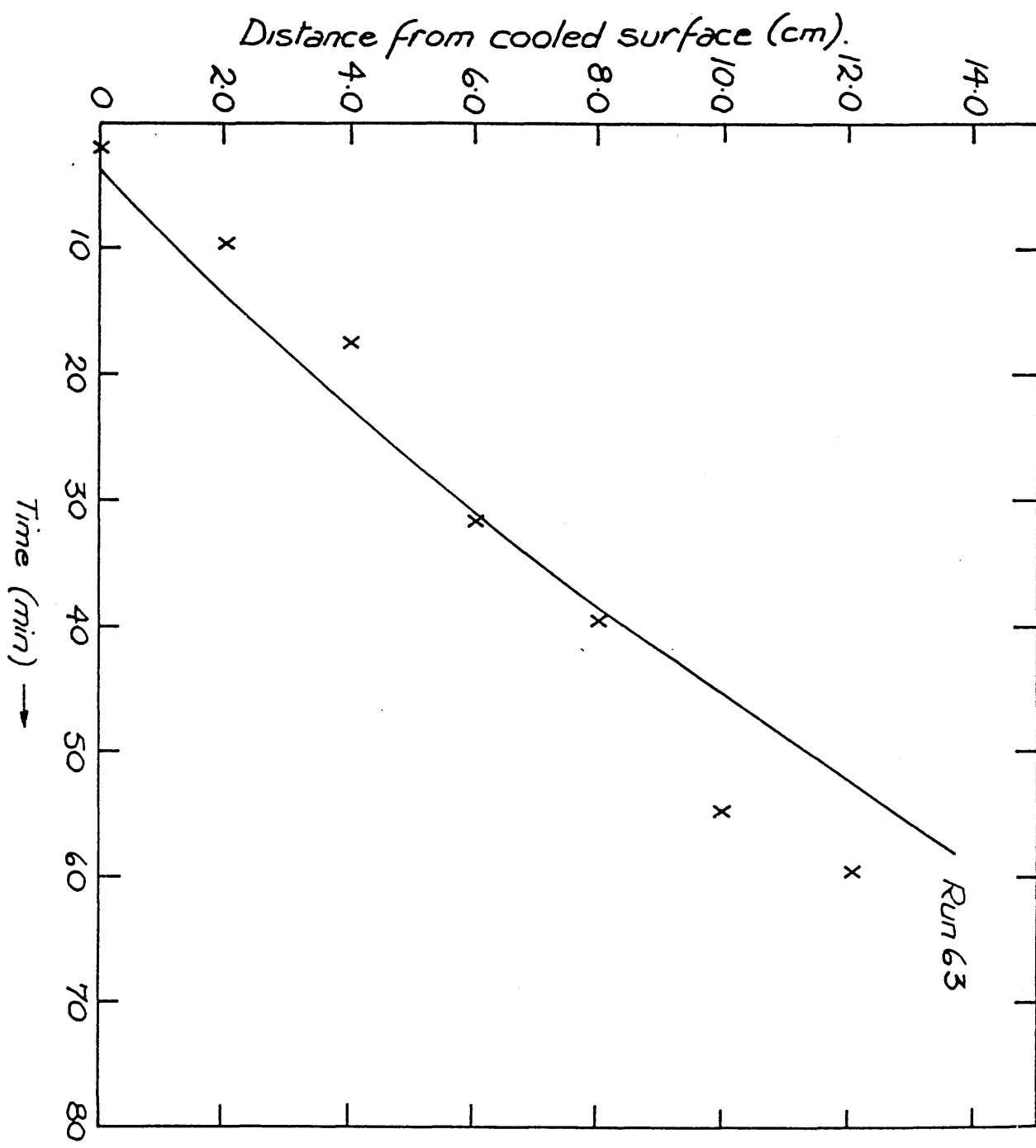


Figure 40 Theoretical and experimental positions of the transformation front - cooling air flow rate 18.7 litres/s.

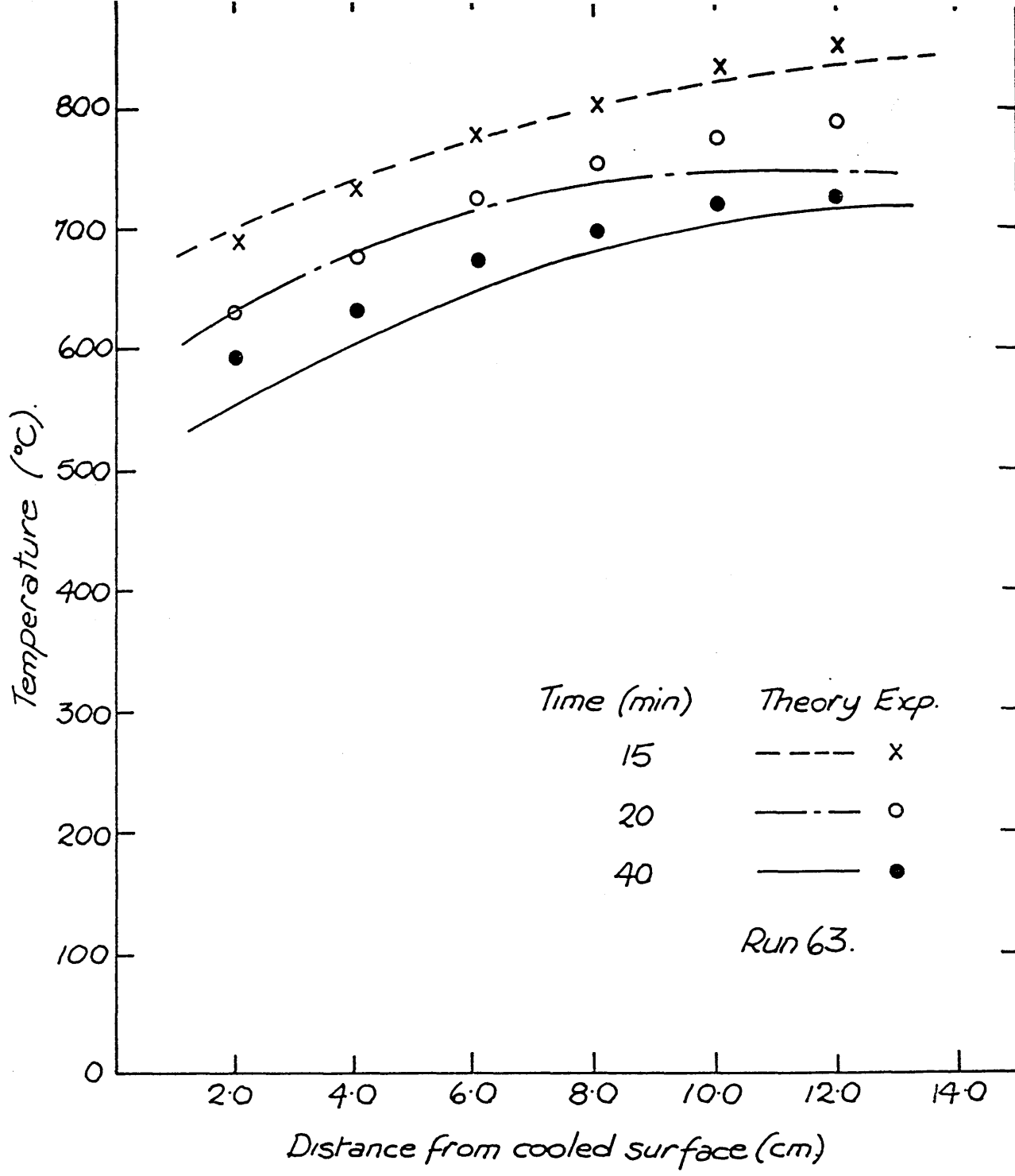


Figure 41 Theoretical and experimental temperature distributions at different times - cooling air flow is 18.7 litres/s.

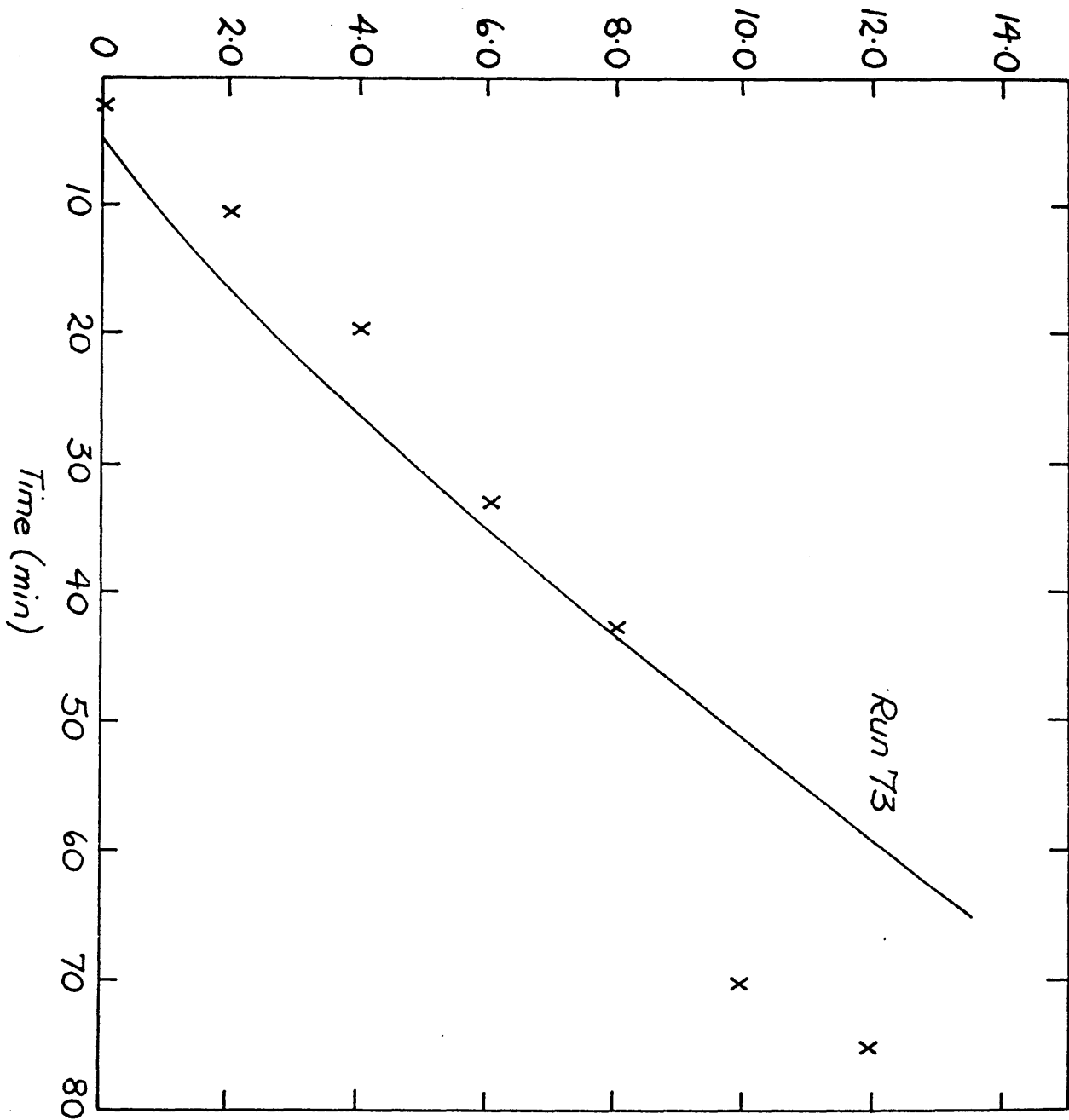


Figure 42 Theoretical and experimental positions of the transformation front - cooling air flow rate = 13.2 litres/s.

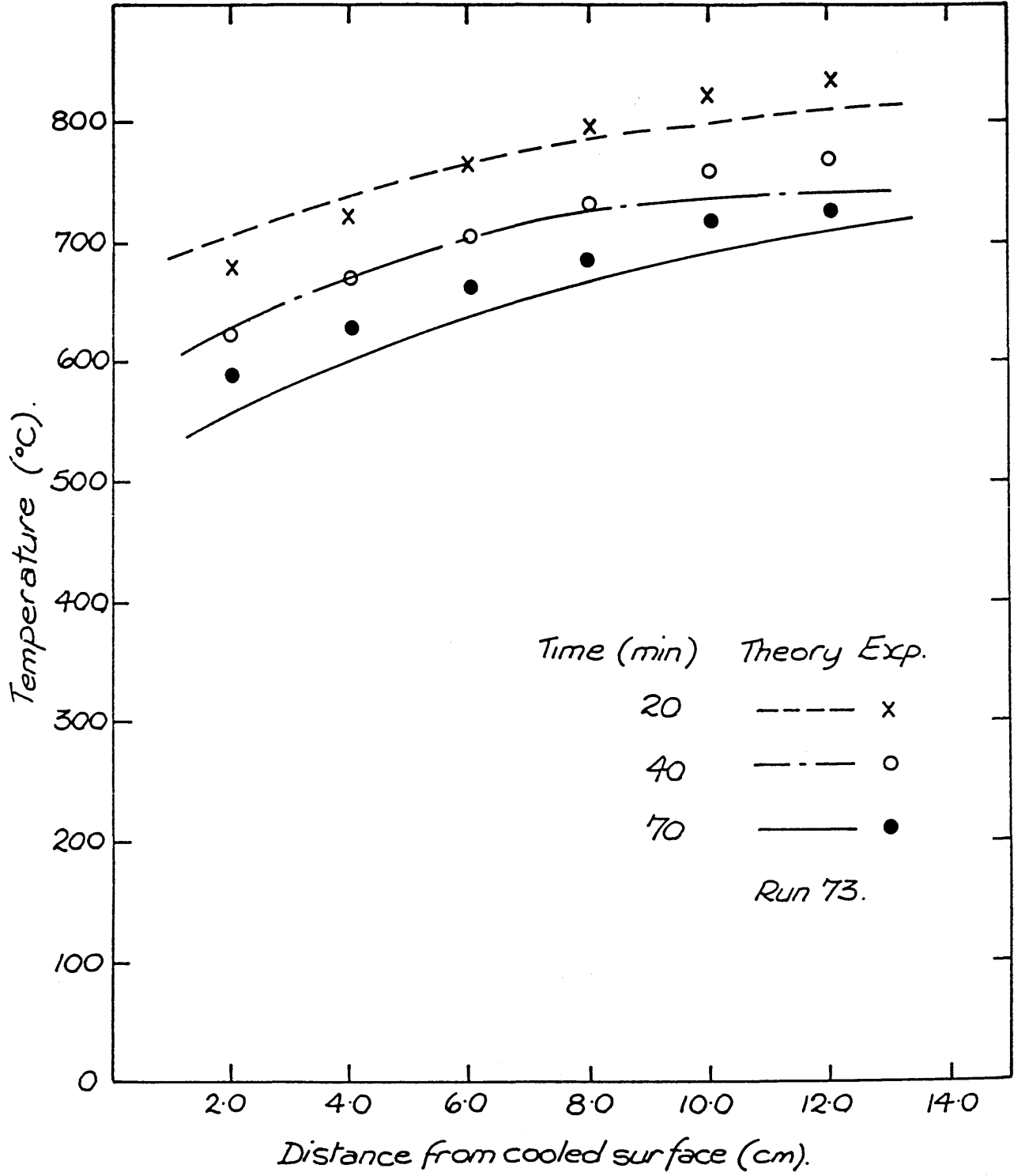


Figure 43 Theoretical and experimental temperature distributions at different times - cooling air flow is 13.2 litres/s.

specific heat to compensate. The resulting curve for the position of the transformation front is shown as a dotted curve in figure 38A- the result of computer run number 54.

This curve advances more rapidly into the billet and is further away from the experimental results. This is only to be expected. In the original theoretical assumption, all latent heat must be conducted away from a layer of untransformed billet before the transformation front temperature can cross it. Delay of the release of a proportion of this heat due to transformation kinetics lessens the amount of heat that must be removed from the layer before the transformation temperature can cross it. Were the transformation to take place over an appreciable range of temperatures, then, the 'start of transformation front' would be able to move into the material more rapidly.

It is thus possible to conclude that the discrepancy between the experimental and theoretical results shown in Figure 38A is not due to the assumption that all the latent heat is released over a negligible temperatures range.

Similar conclusions can be drawn from Figures 40 and 42 corresponding, respectively, to the experiments at air cooling flow rates of 18.7 and 13.2 litre/s. In both these curves, the agreement between theory and experiment is better than in Figure 38A for some 2/3 rds of the transformation process. In the upper third of the billet, however, the measured transformation rates are considerably slower than those predicted theoretically.

Some clue to the reasons for the discrepancy is provided by the

temperature profile curves plotted in Figures 39, 41 and 43. Tolerably good agreement is achieved between the theoretical and experimental curves except that the experimental profile in the untransformed material is much steeper than the theoretical profile especially during the middle stages of the transformation process - see particularly Figures 41 and 43. It appears that more heat is being conducted radially down the billet in the experimental apparatus than is accounted for in the theory.

This proposition is supported by the dynamic heat balances detailed in Tables 38 to 40. In the early stages of the experiments, the heat balances are fairly well in balance. However, as the experiments proceed more heat is removed by the cooling air than is liberated by the billet.

In calculating the heat balances, the heat transferred from the heater has been included in the same way as in the theoretical treatment. The mean specific heat of the steel, as indicated by the equation in Appendix 2, has been augmented by the 0.28 kJ/kg.K deduced from the low temperature heat balance. That the heat balances are even so still not in balance indicates that a further heat release mechanism is involved. The thermal mass of the support rods above the billet and of the insulation there is a possible source of this additional heat. This would certainly be consistent with the steeper temperature profile above the transformation front. It would also be consistent with the late stage in each experimental run when the additional heat appears. At this stage, the sensible heat will have been removed from the metal above the transformation front. An axial temperature

gradient can thus be established above the transformation front giving rise to the transfer of further heat from the furnace structure above the billet. This source of heat was not considered in the low temperature heat balance.

The conclusion that can be drawn is that the theory developed in this work predicts the progress of the transformation reaction to an accuracy of something better than 12%.

6.4.2 Internal Temperatures

Comparisons between the theoretical and experimental temperatures inside the billet are shown in Figure 39, 41 and 43. Once again the agreement is good although the theoretical method shows consistently steeper profiles close the billet's surface than are measured experimentally.

This is most probably due to the assumptions made in the theory that the thermal conductivity of the steel and the heat transfer coefficient from the surface are constant. Below the transformation front, the thermal conductivity of carbon and low alloy steels can rise steeply. Indeed, for low alloy steels of the type used in this study, tabulated values of the thermal conductivity⁽⁴³⁾ double between the transformation temperature and 100°C. The heat flux near the surface of a billet undergoing transformation is augmented by the heat released as the surface layers cool. If the thermal conductivity is assumed constant, this augmentation must result in the steepening of the temperature gradient near the surface shown in the theoretical

curves.

However, if the thermal conductivity increases as the temperature drops, the temperature gradient need not steepen in order to account for the increased heat flux.

In addition, the theoretical treatment assumes a constant heat transfer coefficient. The small contribution made by thermal radiation to the heat transfer coefficient in the experimental apparatus means that the heat transfer coefficient will drop in actuality. Although the effect will be small, it would result in a slightly smaller temperature gradient in the later stages of the experiment, further lessening the heat flux and hence the temperature gradient in the surface layers.

Thus it can be concluded that the theory predicts temperatures in the transforming billet fairly well, the principal discrepancies being due to real variations in the thermal conductivity that are not reproduced in the theoretical treatment presented in this work.

6.4.3 Constancy of the Transformation Front Temperature

The assumption made in the theory that the transformation interface remains at a constant temperature during any one of the transformation experiments cannot be examined directly. It is only the cooling curves of the two thermocouples most remote from the cooled surface that show an arrest temperature and these two curves show the same arrest temperature. This does not necessarily mean that material around thermocouples closer to the

cooled surface is transforming at the same temperature.

Some indication of the extent to which the transformation temperature varies can be obtained, however, from the pearlite spacing measured after the transformation experiment at 13.2 litre/s. The work of Razik, Lorimer and Ridley⁽⁶⁸⁾ is useful here. They carried out an extensive investigation into the transformation of eutectoid steels containing manganese. Included in the investigation was a study of the relationship between the pearlite spacing and transformation temperature for a range of steels of different composition. They were able to study this relationship because their samples were small enough to be considered of uniform temperature during cooling through the transformation region.

They found that the reciprocal of the spacing varied linearly with temperature, lines for different compositions being more or less parallel. Indeed, their work can be represented by a family of equations of the form:-

$$\frac{10 \text{ } \mu\text{m}}{s} = A - 1.50 \theta_T / \text{K} \quad (6.12)$$

where s is the pearlite spacing and A is a constant that varies with the actual composition of the steel.

The spacing variation found in this work, see table 29 on page 5/58, is from 0.17 μm at 20 mm from the cooled surface to 0.37 μm at 120 mm from the surface. Using equation (6.12), this can be shown to correspond to a transformation temperature variation of some 20°C. Since this is of the same order as the temperature

reproducibility found in this work, the variation is not thought to have a significant influence on the conclusions reached.

The general order of agreement between the spacings determined in this work and those quoted by Razik, Lorimer and Ridley is also of interest. A precise comparison is not possible because they studied the transformation of highly pure iron/carbon/manganese alloys whereas a commercial steel was used in this work and, moreover, the carbon and manganese contents of their steels differed from those in the commercial steel. A general comparison does, however, confirm the relevance of their results to the analysis of this work.

For a manganese free steel, Razik, Lorimer and Ridley showed that a pearlite spacing of $0.37 \mu\text{m}$ would correspond to a transformation temperature of some 720°C compared with the value of 725°C measured in this work. The actual relationship between the spacing and temperature is most strongly influenced by the changes in the equilibrium eutectoid temperature produced by changes in the steel compositions. The effect of manganese content on its own is to reduce the eutectoid temperature and hence the temperature at which any given pearlite spacing results. The composition of the steel used in this work is much more complex, see section 4.7, and it is difficult to predict the effect that the various solute species present would have on its equilibrium eutectoid temperature. However, it is apparent that the pearlite spacings determined in the two investigations are sufficiently close for the results of Razik, Lorimer and Ridley to throw light on the validity of the present work.

6.5 COMPARISON WITH OTHER WORKERS

As stated in the literature survey, a number of other authors have recently advanced theoretical methods for predicting rates of steel transformation under known heat transfer conditions. These methods differ from the work used here because the finite difference method is used to solve the heat transfer equations, because the transformation reaction is assumed to occur over a range of temperatures and because the absence of steady state heat transfer coefficient measurements does not allow independent heat balances to be made.

The principal theoretical assumption that differs between this work and the work of Agarwal and Brimacombe⁽⁶²⁾ or Fernandes, Deins and Simon⁽⁶⁵⁾, for example, concerns the release of latent heat of transformation. The latent heat is assumed in this work to be released at a single unique temperature, or at least over a negligibly small range of temperatures. The other workers assume that the transformation takes place over a range of temperatures so that its latent heat is released over a range of temperatures. The validity of these assumptions is related to the size of steel component and to the cooling rates under which the transformation takes place. As stated in the literature study, the slowest cooling rate considered in the work of Agarwal and Brimacombe was 7°C/s.

The cooling rate under which transformation occurs in this work is not immediately apparent because a large component is being studied. The cooling rate can, however, be deduced from the

velocity of the transformation interface and the latent heat of transformation. Equation (20) in the theoretical section, Chapter 3 on page 3/12, relates the rate of cooling in material immediately behind the transformation interface to the rate at which the interface moves:-

$$\left[\frac{\partial \theta}{\partial \tau} \right]_t = - \frac{dt}{d\tau} \left\{ \frac{\rho H}{k} \frac{dt}{d\tau} - \frac{q''}{k} t \right\} \quad (6.13)$$

Measured average interface velocities are tabulated in this work in Table 24. The highest value is 2.2 mm/min for experiments in which 33.7 litre/s of cooling air were used. The heat flux from the untransformed layer can be estimated from equation (43) in the theoretical section, page 3/18, using cooled layer thicknesses determined theoretically. For experiments in which the billet is cooled by 37.4 litre/s of air, an average value of the heat flux from the untransformed material is:-

$$\begin{aligned} q'' &= - 2x(25W/m.K)x(795 - 709)/(0.10 m) \\ &= - 43 \text{ kW/m}^2\text{K} \end{aligned} \quad (6.14)$$

Substituting into equation (6.13) gives:-

$$\begin{aligned} \left[\frac{\partial \theta}{\partial \tau} \right]_t &= \frac{2.2 \times 10^{-3} \text{ m}}{60 \text{ s}} \left\{ \frac{7.74 \times 10^3 \text{ kg/m}^3 \times 1.01 \times 10^5 \text{ J/kg.K}}{25 \text{ W/m.K}} \times \frac{2.2 \times 10^{-3} \text{ m}}{60 \text{ s}} \right. \\ &\quad \left. + \frac{43 \text{ kW/m}^2\text{K}}{25 \text{ W/m.K}} \right\} \\ &= 0.1 \text{ K/s} \end{aligned} \quad (6.15)$$

This cooling rate is very much smaller than the values considered by the previous workers.

The relevance of this fact can be appreciated from the shape of TTT curves for eutectoid steels even though such curves refer to

isothermal transformations. A typical curve is shown in Figure 44 taken from the paper of Razik, Lorimer and Ridley.⁽⁶⁸⁾

Superimposed on that figure is the line AA which shows approximately the temperature variation that would correspond to cooling through the transformation region at a rate of 0.1 C/s. It can be seen that the start and end of transformation are separated by no more than some 3°C. Thus it is legitimate in this work to consider that the transformation heat is liberated over a negligible temperature range because the cooling rate in the large sample used is relatively slow. The line BB superimposed on the figure corresponds, approximately for example, to the slowest cooling considered by Agarwal and Brimacombe. It is seen that the transformation takes place over a much larger range of temperatures.

The effect of the rate of cooling explains another difference between this work and that of other workers investigating the transformation in small samples. Most of these workers found a recalescence effect, the temperature rising to a greater or lesser extent once the transformation temperature had been passed. This effect is due to the onset of transformation being delayed by rapid cooling and then starting so quickly that the local rate of heat generation exceeds the rate of heat removal. No evidence of recalescence was apparent from any of the temperature curves determined in this work and it is apparent that this is due to the very much slower rates of cooling operating. At a cooling rate of 0.1 C/s or less, the onset of transformation was not delayed to any perceptable extent.

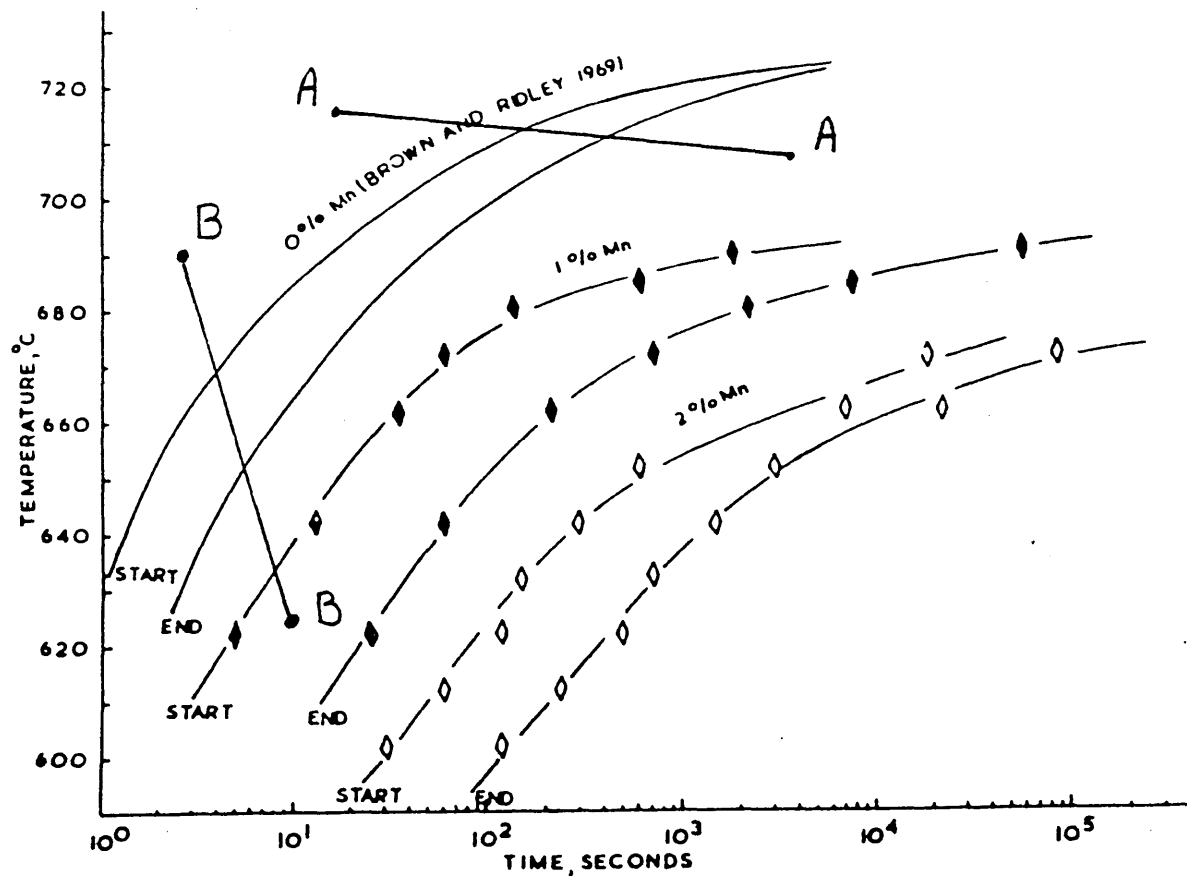


Figure 44 Isothermal transformation diagram taken from the work of Razik, Lorimer and Ridley.

7.1 CONCLUSIONS

A comprehensive range of experimental results has been obtained for the temperatures at certain known points inside the large samples of steel whilst they are undergoing transformation from austenite to pearlite. The transformation process has been carried out under a range of controlled cooling conditions, the cooling being provided by a specially designed air jet system. The results have not indicated the occurrence of any recalescence phenomena but have indicated a definite temperature arrest in regions of the sample remote from the cooled surface. The temperature of this arrest has been found to vary very little over the range of cooling rates experienced by the sample. The experimental results obtained are relevant to cooling rates significantly lower than those involved in most previous investigations.

In addition to the experimental work, a theoretical method has been developed from the integral profile method capable of predicting the progress of the transformation front and of predicting temperature histories throughout the sample. A computer programme has been produced from this method and used to obtain theoretical results.

In general the experimental results for the eutectoid transformation reaction of the steel used in this work are in good agreement with the integral profile

112

solutions obtained in the theoretical method for the experiments in which the steel sample was completely insulated during the preheat period. The discrepancy between the experimental and the theoretical results shown in Figure 38A at air cooling flow rate of 37.4 litres/s is not due to the assumption that all the latent heat is released over a negligible temperature range.

Similar conclusions can be drawn from Figures 40 to 42 corresponding, respectively, to the experiments at air cooling flow rates of 18.7 and 13.2 litres/s.

The theory predicts temperatures in the transforming billet fairly well, the principal discrepancies being due to real variations in the thermal conductivity that are not reproduced in the theoretical treatment presented in this work.

The integral profile method and the thermal analysis technique are good methods to study the extent to which heat conduction within large steel samples (billets) influences and is influenced by solid state transformation reactions.

The results of this investigation extended our current knowledge concerning heat transfer during transformation in large steel components.

7.2 FURTHER WORK

It is necessary to continue working with large

steel components but increasing the rate of cooling and eliminating the air gap between the sample and the heater.

It would be convenient to carry out investigations with small steel samples.

In the investigations proposed above it is important in the theoretical treatment to include the interaction between the kinetics of the transformation and the heat transfer process and also the real variations in the thermal conductivity.

1. Pohlhausen, K., Zeitschrift fur Angewandle
Mathematic und Mechanik, (1921), 1, 252.
2. Schlichling, H., Boundary Layer Theory, (1955),
Pergamon Press London.
3. Curle, N., The Laminar Boundary Layer Equations,
(1962), The University Press, Oxford.
4. Hillert, M., Decomposition of Austenite by
Diffusional Processes AIME, (1962), 197.
5. Benedicks, C., J. Iron Steel Inst., (London),
(1935), 2, 352.
6. Mehl, R.F. and Smith, D.W., Trans. AIME (1934),
113, 203.
7. Mehl, R.F. and Smith, D.W., Trans. AIME (1935),
116, 330.
8. Smith, E.V. and Mehl, R.F., Trans. AIME (1942),
150, 211.
9. Hull, F.C. and Mehl, R.F., Trans. ASM (1942),
30, 381.
10. Duke, A., Trans. AIME (1948), 158, 286.
11. Arrowson, H.I., Trans. AIME (1954), 162, 346.
12. Modin, S., Trans. AIME (1951), 135, 169.
13. Hanemann, H. and Schrader, A., Atlas Metallographics,
(1933), Berlin.

14. Mehl, R.F. and Hagel, W.C., Progr. in Metal.
Phys. (1956), 6, 74.
15. Hillert, M., Varmlaudska Bergsm. (1958),
Forem. Ann.
16. Hultgren, A. and Ohlin, H., Jernkontorets Ann.,
144 (1960), 356.
17. Hultgren, A., Josefsson, A., Kula, E. and
Lagerberg, G., Jernkontorets Ann. (1958),
142, 165.
18. Hultgren, A. et al., Kgl. Svenska Velenskapsakad.
(1953), Hdn., Ser. 4., 4, No. 3.
19. Nicholson, M.E., J. Metals (1954), 6, 1077.
20. Cahn, J.W., J. Metals (1957), 9, 140.
21. Smith, C.S., Trans. ASM (1953), 45, 533.
22. Carpenter, H.C.H. and Robertson, J.M., J. Iron
Steel Inst. London (1932), 125, 309.
23. Whiteley, J.H., J. Iron Steel Inst., No. II (1929),
147.
24. Pellisier, G.E., Hawkes, M.F., Johnson, W.A. and
Mehl, R.F., Trans. ASM (1942), Vol. 30, 1049.
25. Belaiew, N.T., The Inner Structure of the Pearlite
Grain, Iron and Steel Inst. (1922), Vol. 105,
201.

26. Oknof, M., Concerning the Question of the Inner
Structure of Pearlitic Steels, Metallurgie
(1911), Vol. 8, 138.
27. Oknof, M., Concerning the Structure of Martensite
and Pearlite, Metallurgie (1911), Vol. 8, 539.
28. Forsman, O., Investigation of the Space Structure
of a Carbon Steel of Hypereutectoid Composition,
Jernkontorets Ann. (1918), 1, 1.
29. Greene, E.V., Some Characteristics of Pearlite in
Eutectoid Rail Steels, Trans. American Society
for Steel Treating (1929), Vol. 16, 57.
30. Gensamer, M., Pearsall, E.B. and Smith, G.V.,
The Mechanical Properties of the Isothermal
Decomposition Products of Austenite, Trans.
ASM (1940), Vol. 28, 380.
31. Gensamer, M., Pearsall, E.B., Pellini, W.S. and
Low, J.R., The Tensile Properties of Pearlite
Bainite and Spheroidite, Trans. ASM (1941),
No. 19.
32. Belaiew, N.T., Discussion to Reference 37, 255.
33. Melhl, R.F., The Physics of Hardenability of
Alloy Steels, Trans. ASM (1939), 30.
34. Rosenhain, S., The Discussion to Reference 25, 229.
35. Benedicks, C., The Discussion to Reference 25, 233.

36. Davenport, E.S. and Bain, E.C., Transformation
of Austenite at Constant Sub-Critical
Temperatures, Trans. AIME (1930), 117.
37. Vilella, J.R., Guellick, G.E. and Bain, E.C.,
On Naming the Aggregate Constituents in
Steel, Trans. ASM (1936), Vol. 24.
38. Barrett, C.S., The Stereographic Projection,
Trans. American Institute of Mining and
Metallurgical Engineers (IMD), Vol. 124, 29.
39. Scheil, E., Statische Gefugeuntersuchungen,
Zeit. Metallkunde (1935), Vol. 27, 199.
40. Brown, D. and Ridley, N., J. Iron Steel Inst.,
(1966), Vol. 204, 811.
41. Asundi, M.K. and West, D.R.F. J. Inst. Metals
(1966), Vol. 94, 19.
42. Huang, G.C., Trans. Amer. Soc. Mech. Engrs.,
Series C (1963), 237.
43. Geiger, G.H. and Poirier, D.R., Transport
Phenomena in Metallurgy, Addison-Wesley
Publishing Co., U.S.A. (1973), 128, 130.
44. Douglas, J.F., Fluid Mechanics, Pitman Press,
(1975), 100.
45. Danckwerts, P.V. and Anolick, C., Trans. Inst.
Chem. Engrs. (1962), 40, 1203.

46. Perry's Chemical Engineering Handbook,
McGraw Hill (1983).
47. Moore, M.R., Thesis submitted for the Degree of
Doctor of Philosophy in the University of
London, 1966.
48. McAdams, W.H. Heat Transmission, McGraw Hill
(1954), 175.
49. Fuller, E.N., Sheltler, P.D. and Giddings, J.G.,
Ind. Eng. Chem. (1966), 58, 18.
50. Austin, J.B. and Rickett, R.L., Trans. AIME (1939),
135, 396.
51. Johnson, W.A. and Mehl, R.F. Trans. AIME (1939),
135, 416.
52. Scheil, E., Arch. Eisenhuttenwes (1935), 12, 565.
53. Manning, G.K. and Lorig, C.H., Trans. AIME (1946),
167, 442.
54. Kiefer, J.M. and Grange, R.A. Trans. ASM (1941),
29, 85.
55. Liedholm, C.A., Met. Prog. (1944), 45, 94.
56. Pumphrey, W.I. and Jones, F.W., J. Iron Steel Inst.
(1948), 159, 137.
57. Cahn, J.W. Acta Metall. (1956), 4, 572.
58. Avrami, M. J. Chem. Phys. (1941), 9, 177.

59. Markowitz, L.M. and Richman, M.H., Trans. AIME (1967), 239, 131.
60. Lindblom, B.E., Hoglund, L. and Anderson, C., J. Iron Steel Inst. (1971), 209, 958.
61. Hildenwall, B. and Ericsson, T., Hardenability concepts with Application to Steel (ed. Doane, D.V. and Kirkaldy, J.S.) 579, Warrendale, Pa., The Metallurgical Society of AIME (1978).
62. Agarwal, P.K. and Brimacombe, J.K., Metall. Trans. 12B (1981), 121.
63. Umemoto, M., Komatsubara, N. and Tamura, I., J. Heat Treat (1980), 1, 57.
64. Umemoto, M., Horiuchi, K. and Tamura, I. Trans. Iron Steel Inst. J. (1982), 22, 854.
65. Fernandes, F.M.B., Denis, S. and Simon, A. Materials Science and Technology (1985), Vol. 1, 10, 838.
66. Hills, A.W.D., Trans. Met. Soc. AIME (1969), 245, 1471.
67. Arpaci, V.S., Conduction Heat Transfer, Addison-Wesley, New York, (1966).
68. Razik, N.A., Lorimer, G.W. and Ridley, N., Acta Metallurgica, Vol. 22, October 1974, 1249-1258.

APPENDIX 1PROPERTY_VALUES_USED_IN_THIS_WORK

Table A1 : Densities, conductivities and thermal capacities.

Material	Density/(Mg.m ⁻³)	Spec. Heat kJ/kg.K	Conductivity W/m.K
Steel	7.75(R2)	see below	25(R3)
Al ₂ O ₃	2.9(R3)	0.84(R3)	-
SiO ₂	2.9(R3)	0.80(R3)	-
CaO	2.8(R3)	0.91(R4)	-

The latent heat and specific heat of the steel in this work are difficult to determine from values in the literature. The specific heat of materials at high temperatures is measured by determining, using a calorimeter, either the heat liberated as the material being investigated is cooled or the heat absorbed as the material is heated. In each case, the heat effect that is measured includes not only the specific heat but also the latent heat of any solid state reactions occurring within the material. Since the rate at which this latent heat is released depends upon the kinetics of the reactions themselves and since the kinetics depend upon the rate of heating or cooling, the heat effect measured calorimetrically can vary with the heating rate.

Fig A-1 shows the apparent specific heat measured as part of an extensive investigation into the thermal properties of steels^(R5), this particular curve being measured for a low alloy steel containing 1.5% Mn - the steel composition closest to that used in this work. The curve clearly shows the latent heat

effect associated with the solid state transformation between austenite and ferrite and pearlite.

The assumption made in this work is that this latent heat is all liberated at the transformation temperature. In order, then, to evaluate the magnitude of this latent heat, the dashed straight line shown in the figure has been drawn and is assumed to represent the variation of the true specific heat with temperature. The entire heat effect above the dashed line is then the latent heat of transformation.

The equation for the dashed line in the figure is:-

$$c_p = [0.5 + 9.1 \times 10^{-5} \times (\theta / {}^\circ C)] \text{ kJ/kg.K}$$

where θ is measured from ${}^\circ C$.

The latent heat is then given by the area above this line which has been determined by graphical integration to give:-

$$\Delta H = 101 \text{ kJ/kg.}$$

- R2. Perry R.H. and Green D, "Perry's Chemical Engineering Handbook", McGraw-Hill, 1984
- R3 Geiger G.H. and Poirier D.R., "Transport Phenomena in Metallurgy", Addison-Wesley, 1973.
- R4 Kubashchevski, E.LL, Metallurgical Thermo-Chemistry, Pergamon Press, 1967, London.
- R5 BISRA "Physical Constants of some Commercial Steels", (London : Butterowrth's Scientific Publications), 1952

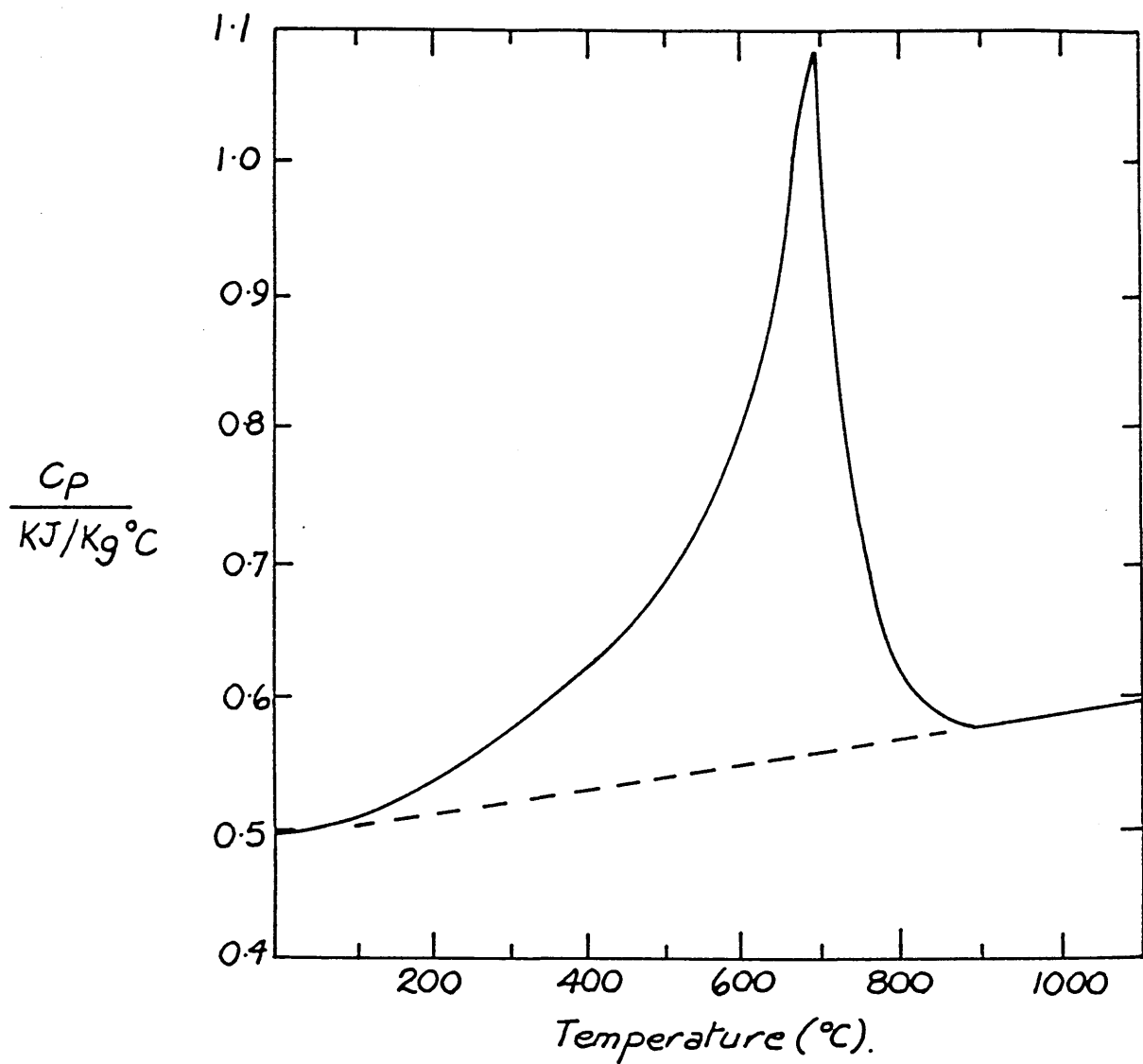


Figure A-1 Apparent specific heat of steels.

APPENDIX 2

'BASIC' COMPUTER PROGRAMMES USED IN HEAT BALANCE CALCULATIONS

A2.1 OVERALL HEAT BALANCE IN THE ABSENCE OF TRANSFORMATION

```
10 LPRINT "Heat balance in ingot heated below transition temperature"
12 LPRINT: LPRINT:
14 LPRINT "Table of surface temperatures and heat removal rates"
16 LPRINT: LPRINT:
20 LPRINT "-----"
40 LPRINT "! TIME: TS : QDOT:";LPRINT "-----"
50 SIG = 0: TT = -5
100 INPUT "THE FIRST SURFACE TEMPERATURE/DEG-C? ",TS
105 PRINT TS
150 GOSUB 20000
200 SIG = SIG + I
300 INPUT "THE NEXT EVEN TEMPERATURE/DEG-C? ",TS
305 PRINT ,TS,SIG
400 GOSUB 20000
500 SIG = SIG + 4*I
520 INPUT "PRESS RETURN FOR FURTHER INTEGRATION OF <E> TO END ",E0
550 IF E0<>"E" THEN GOTO 600
570 GOTO 900
600 INPUT "THE NEXT ODD TEMPERATURE/DEG-C? ",TS
605 PRINT TS
700 GOSUB 20000
800 SIG = SIG + 2*I
850 GOTO 300
900 INPUT "ENTER THE FINAL TEMPERATURE/DEG-C ",TS
1100 GOSUB 20000
1200 SIG = SIG + I
1205 PRINT ,TS
1220 QT = .0001*SIG
1230 LPRINT "-----"; LPRINT:LPRINT:
1240 LPRINT "Total Heat Removed = ";
1244 LPRINT USING "###";QT;
1248 LPRINT " MJ"
1500 END
20000 I = .0176*(206 + .037*(TS/100 + 5.86)*((TS/100+2.73)Q2 + 9.8))*(TS-40)
20020 TT = TT + 5
20030 LPRINT "; ";
20035 LPRINT USING "###";TT;
20040 LPRINT " ";
20050 LPRINT "; ";
20054 LPRINT USING "###";TS;
20058 LPRINT " ; ";
20062 LPRINT USING "###";I/1000;
20066 LPRINT " ;"
20100 RETURN
```

A2.2 DYNAMIC_HEAT_BALANCE_DURING_TRANSFORMATION

```
10 LPRINT , "Dynamic Heat Balance on Ingot Heated Above Transition Temperature"
12 LPRINT : LPRINT :
13 INPUT "RUN NUMBER? ", RON
14 LPRINT , "Table of Surface Temperatures and Heat Removal Rates for Run ";
15 LPRINT USING "##"; RON
16 LPRINT , "(Billet specific heat augmented to account for heater)": LPRINT
17 LPRINT
18 INPUT "WHAT IS THE CONVECTIVE HEAT TRANSFER COEFFICIENT TO USE? ", HCNV
20 LPRINT , "Conductive heat transfer coefficient taken as ";
22 LPRINT USING "###"; HCNV;
24 LPRINT " W/m2.K": LPRINT
38 LPRINT , -----
40 LPRINT , " Time: TS : Qdot :Heat(MJ); Tav :Heat(MJ);"
41 LPRINT , ":(min); (oC); (kW) :Trnsfred; (oC); Lost ;"
42 LPRINT , -----
50 SIG = 0: TT = -5
100 INPUT "FIRST TEMPERATURE AT 60 CMS? ", T60
101 INPUT "FIRST TEMPERATURE AT 40 CMS? ", T40
102 INPUT "FIRST TEMPERATURE AT 20 CMS? ", T20
103 TS = 3*(T20 - T40) + T60
105 PRINT TS
120 INPUT "NOW ENTER THE FIRST TEMPERATURE AT 80 CMS? ", T80
130 INPUT "NOW ENTER THE FIRST TEMPERATURE AT 100 CMS? ", T100
135 INPUT "NOW ENTER THE FIRST TEMPERATURE AT 120 CMS? ", T120
138 TAV = (TS + 4*T20 + 2*T40 + 4*T60 + 2*T80 + 4*T100 + T120)/18
140 TAV = (12*TAV + 3*T120)/15:TAV1 = TAV
142 GOSUB 40000
144 HTCNT1 = HTCNT
150 GOSUB 20000
200 SIG = SIG + I
300 INPUT "THE NEXT EVEN TEMPERATURE AT 60CMS? ", T60
301 INPUT "THE NEXT EVEN TEMPERATURE AT 40 CMS? ", T40
302 INPUT "THE NEXT EVEN TEMPERATURE AT 20 CMS? ", T20
303 TS = 3*(T20 - T40) + T60
305 PRINT , TS, SIG
400 GOSUB 20000
500 SIG = SIG + 4*I
520 INPUT "PRESS RETURN FOR FURTHER INTEGRATION OF <E> TO END ", E0
550 IF E0<>"E" THEN GOTO 600
570 GOTO 900
600 INPUT "THE NEXT ODD TEMPERATURE AT 60 CMS? ", T60
601 INPUT "THE NEXT ODD TEMPERATURE AT 40 CMS? ", T40
602 INPUT "THE NEXT ODD TEMPERATURE AT 20 CMS? ", T20
603 TS = 3*(T20 - T40) + T60
605 PRINT TS
610 INPUT "NOW ENTER THE NEXT ODD TEMPERATURE AT 80 CMS? ", T80
620 INPUT "NOW ENTER THE NEXT ODD TEMPERATURE AT 100 CMS? ", T100
630 INPUT "NOW ENTER THE NEXT ODD TEMPERATURE AT 120 CMS? ", T120
700 GOSUB 30000
800 SIG = SIG + I
850 GOTO 300
900 INPUT "ENTER THE FINAL TEMPERATURE AT 60 CMS? ", T60
901 INPUT "ENTER THE FINAL TEMPERATURE AT 40 CMS? ", T40
```

A2.2 DYNAMIC_HEAT_BALANCE_DURING_TRANSFORMATION (Cont.)

```

902 INPUT "ENTER THE FINAL TEMPERATURE AT 20 CMS? ",T20
903 TS = 3*(T20 - T40) + T60
910 INPUT "NOW ENTER THE NEXT ODD TEMPERATURE AT 80 CMS? ",T80
920 INPUT "NOW ENTER THE NEXT ODD TEMPERATURE AT 100 CMS? ",T100
930 INPUT "NOW ENTER THE NEXT ODD TEMPERATURE AT 120 CMS? ",T120
1100 GOSUB 30000
1205 PRINT ,TS
1220 QT = .0001*SIG
1230 LPRINT ,-----
1235 LPRINT
1240 LPRINT ,Initial Average Temperature = ;
1244 LPRINT USING "###";TAV1;
1245 LPRINT " Deg-C" : LPRINT
1250 LPRINT ,Initial Heat Content = ;
1255 LPRINT USING "##.##";HTCNT1;
1256 LPRINT " MJ"
1260 LPRINT
1500 END
20000 I = .0176*(HCNV + .037*(TS/100 + 5.86)*((TS/100+2.73)Q2 + 9.8))*(TS-40)
20020 TT = TT + 5
20030 LPRINT ,I ";
20035 LPRINT USING "##.#";TT;
20040 LPRINT " ";
20050 LPRINT "I ";
20054 LPRINT USING "##.#";TS;
20058 LPRINT "I ";
20062 LPRINT USING "##.##";I/1000;
20066 LPRINT "I"; "I" "I" "I" "I"
20100 RETURN
30000 I = .0176*(HCNV + .037*(TS/100 + 5.86)*((TS/100+2.73)Q2 + 9.8))*(TS-40)
30020 TT = TT + 5
30030 LPRINT ,I ";
30035 LPRINT USING "##.#";TT;
30040 LPRINT " ";
30050 LPRINT "I ";
30054 LPRINT USING "##.#";TS;
30058 LPRINT "I ";
30062 LPRINT USING "##.##";I/1000;
30063 SIG = SIG + I
30066 LPRINT "I";
30070 LPRINT USING "##.##.##";SIG/10000;
30072 LPRINT "I";
30075 TAV = (TS + 4*T20 + 2*T40 + 4*T60 + 2*T80 + 4*T100 + T120)/18
30080 TAV = (12*TAV + 3*T120)/15
30085 LPRINT USING "####";TAV;
30086 LPRINT "I";
30088 PRINT "HOW FAR HAS THE INTERFACE MOVED AFTER ";
30089 PRINT USING "##";TT;
30090 PRINT " MINUTES? ":INPUT "ENTER THICKNESS IN METRES ",THICK
30095 GOSUB 40000
30100 LPRINT USING "##.##.##";HTCNT1 - HTCNT;
30105 LPRINT "I"
30200 RETURN

```

A2.2 DYNAMIC HEAT BALANCE DURING TRANSFORMATION (Cont.)

```
40000 GAM = (.5 + .000091*TAV + .277)*7.74
40010 REM GAM IS IN MJ.M-3.K-1 AND IS AUGMENTED TO ACCOUNT FOR HEATER
40020 HTCNT = .00266*GAM*TAV + (.15 - THICK)*.0176*101*7.74
40030 REM HTCNT IS IN MJ
40300 RETURN
```